# FATIGUE AND FRACTURE OF THIN METALLIC FOILS WITH AEROSPACE APPLICATIONS

A Thesis
Presented to
The Academic Faculty

by

Leslie E. Lamberson

In Partial Fulfillment
of the Requirements for the Degree
Master of Science

School of Aerospace Engineering
Georgia Institute of Technology
May 2006

# FATIGUE AND FRACTURE OF THIN METALLIC FOILS WITH AEROSPACE APPLICATIONS

Approved by:

Dr. Erian A. Armanios, Advisor
School of Aerospace Engineering
*Georgia Institute of Technology*

Dr. David L. McDowell
School of Mechanical Engineering
*Georgia Institute of Technology*

Dr. Massimo Ruzzene
School of Aerospace Engineering
*Georgia Institute of Technology*

Date Approved: 03/31/2006

*To my dad*

# ACKNOWLEDGEMENTS

I extend my most sincere gratitude to the members of my thesis committee for their guidance and mentorship. Special thanks particularly to my thesis advisor, Dr. Erian Armanios, for his unconditional support of my research efforts, as well as Dr. Massimo Ruzzene and Dr. David McDowell for their patience, professionalism, and gracious assistance.

My deepest appreciation goes to my family: Mom, Dad, Aunt Jo Anne, and my brother, Jonathan. Special thanks to Professor Arthur Hoadley at Western Michigan University for introducing me to aeronautical engineering, as well as Professor Ann Marie Sastry at the University of Michigan for being an amazing role model and mentor throughout my studies. I also warmly acknowledge my Lockheed Martin Aeronautics mentors: Lee, Scott, Mike, Terry, and the rest of the Advanced Development Programs team in Forth Worth for their kind support of my graduate career. I extend a special heartfelt thank you to Amy, Adele, Lil, and Wendy, as well as Sandy and Mimi from WIE for helping me through some rough nights and stressful times; and to Frank for always being there to greet me at the door. Lastly, to the numerous artists who kept my creative side alive: Ms. Arthur, Mr. Estner, Peter, Judy, Christian, Gay, Margo, and Carol – thank you for the dance.

Generous financial support from the Georgia Institute of Technology NASA Space Grant Consortium and the Zonta International Amelia Earhart Fellowship are gratefully acknowledged.

The thesis topic suggestion and experimental configuration to test foils was supplied by Dr. John Holmes at the Georgia Institute of Technology.

# TABLE OF CONTENTS

# LIST OF TABLES

# LIST OF FIGURES

# NOMENCLATURE

## LIST OF SYMBOLS

| | |
|---|---|
| $\alpha$ | length ratio (half specimen width by half crack length) |
| C | Paris relation constant |
| $da/dN$ | cyclic crack growth rate |
| K | stress intensity factor |
| $K_{Ic}$ | fracture toughness (critical stress intensity factor) |
| $\Delta K$ | stress intensity factor range |
| $\Delta K_{th}$ | threshold region |
| $m$ | fatigue crack growth rate exponent |
| $N_T$ | cycles to failure |
| $r_y$ | cyclic plastic zone size |
| R | stress ratio (minimum/maximum) |
| $R^2$ | constant of correlation |
| $\sigma_{min}$ | minimum stress |
| $\sigma_{max}$ | maximum stress |
| $\sigma_y$ | yield strength |
| x | multiplying factor |
| X | magnifying factor |
| $Y$ | geometry correction factor |

# LIST OF ABBREVIATIONS

| | |
|---|---|
| AETB | alumina enhanced thermal barrier tiles |
| AFRSI | advanced flexible reusable surface insulation |
| AMHC | advanced metallic honeycomb |
| ARMOR | adaptable robust metallic operable reusable |
| C-9 | colloidal silica coating |
| C-C | carbon-carbon composite |
| CMC | carbon-matrix composite |
| CTOD | crack tip opening displacement |
| FEM | finite element method |
| LEO | low earth orbit |
| LVDT | linear variable displacement transducer |
| MEMS | micro-electro-mechanical system |
| MFR | magnetic fusion reactor |
| MTS | material testing system |
| PM2000 | iron base alloy |
| RCG | reaction-cured glass |
| RLV | reusable launch vehicle |
| RTV | room temperature vulcanizing adhesive |
| SA/HC | superalloy honeycomb |
| SA/HC2 | 2nd generation superalloy honeycomb |
| TABI | tailorable advanced blanket insulation |
| TI/HC | titanium honeycomb |
| TIMW | titanium multiwall |
| TPS | thermal protection system(s) |
| TUFI | toughened uni-piece fibrous insulation |

# SUMMARY

Metallic honeycomb structures are being studied as thermal protection systems for hypersonic vehicles, reusable launch vehicles, and as structural panels in other aerospace applications. One critical concern is the growth of fatigue cracks in the thin facesheets used for these structures. To address this concern, the effect of specimen thickness on fracture toughness and tensile fatigue behavior of aluminum-magnesium alloy foils was investigated. Experimental studies were conducted at ambient conditions on foils ranging from 30 μm to 250 μm in thickness. Constant amplitude fatigue tests were performed at a loading frequency of 10 Hz and a nominal stress ratio of 0.2. The Mode I fracture toughness of the foils was significantly low, ranging between approximately 13 MPa√m and 17 MPa√m for all thicknesses. For a fixed maximum fatigue stress level, the fatigue life of the 30 μm foils was approximately 40% lower than that observed for the 100 μm foils. In all cases, the cyclic crack growth data could be fit to a characteristic Paris relationship between crack growth rate and stress-intensity range. However, the values for the stress intensity exponent, $m$, were higher than what is typically found for the same material of greater thickness. For the foils examined in this study, the $m$ values averaged between 5 and 7. Details of the experimental technique as well as the fatigue and fracture toughness results are provided.

# CHAPTER 1

# INTRODUCTION

Aviation, as a science, can be described as a continuous desire to push the envelope of flight. The fascination with flying farther, faster, and higher provides fuel for advancements in the aerospace industry initiated by the Wright brothers over a century ago. Not surprisingly, one of the most difficult challenges inherent to this pursuit is accommodating the heating associated with supersonic and hypersonic flight regimes. In this respect, thermal protection systems (TPS) are imperative to viable flight of the future.

Spacecraft, next generation reusable launch vehicles, military reconnaissance and surveillance aircraft, supersonic aircraft, ballistic missiles, probes studying distant regions of space, communication satellites, and remote sensing spanning every country across the globe require TPS. These TPS must also remain robust in their ever-changing environment, withstanding not only large thermal gradients and mechanical loading profiles, but also dynamic and acoustic loading, aerodynamic shear and pressure loading, weather, debris, and velocity impact; all while remaining lightweight and cost-effective [4].

One substantial aspect of designing a maintainable and operable TPS is to consider the TPS material properties and behavior. Prior to 1999, no experiments had been conducted to determine the shear fatigue or shear creep life of metallic TPS materials. At the same time, high fatigue crack growth rates on the facesheets of metallic TPS are a major concern due to rapid crack propagation resulting in catastrophic failure [30]. Metallic TPS have the potential to provide a lightweight, ductile (hence easily formed and damage resistant), highly maintainable TPS. The void in comprehensive fatigue and fracture analysis of such structures is the foundation to research presented in this thesis. Particularly, aluminum-magnesium foil facesheets with the weight and scope of an aerospace application are examined.

As thickness decreases, fracture toughness increases from plane strain to plane stress. However with further thickness decrease into the foil regime, the toughness can decrease because failure is no longer constrained as the plastic zone becomes equal in magnitude to the thickness. By investigating the micro-structural damage of precracked aluminum sheets of various thicknesses, the consequent material behavior trends of foils are determined.

The objective of the research is to provide a better understanding of the design parameters involved in TPS not only for current, but future flight capability. Although the research involves aluminum-base alloys commonly found in aerospace applications, the results are expected to be comprehensive in nature and will provide insight into the mechanical behavior of thin films manufactured from other metals, used extensively in many engineering applications.

The thesis is outlined as follows:

- Chapter 2 presents a literature review of TPS research, as well as other thin foil fatigue and fracture applications.
- Chapter 3 describes the experimental set up, procedure, material geometry, and details of the fatigue and fracture toughness tests.
- Chapter 4 highlights the results of the tests, and presents SEM micrographs of fracture surfaces.
- Chapter 5 outlines research conclusions and recommendations.

# CHAPTER 2

# BACKGROUND AND LITERATURE REVIEW

## *2.1 TPS Historical Perspective*

With the dawn of space flight, the development of thermal protection systems for aerospace vehicles began. Early thermal protection systems consisted of metal, like the underlying structure itself, but other options were quickly utilized in TPS design. These included ablative coatings and special temperature sensitive paints that were significantly relied on in the Mercury, Apollo, Gemini US space programs during the 1950 and 1960's [4]. More recent TPS made use of ceramic tiles and blankets, and eventually considered complex coatings and superalloys [1]. Accordingly, as material development, processing, and fabrication continues to advance, so does TPS design and performance.

It was not until NASA's Space Shuttle Program beginning in the late 1960's that considerable effort was made to develop a robust, lightweight, and reusable TPS. Although metallic thermal protection systems were considered, ceramic blankets and tiles were chosen as the shuttle's main TPS. The current Shuttle Orbiter utilizes titanium superalloy, refractory metal and pyrolized plastic materials, in addition to ceramic tiles and blankets [4].

Next generation reusable launch vehicles and hypersonic aircraft consider both metallic and ceramic TPS. Metallic TPS concepts initiated during the 1980's when the Saenger hypersonic transportation system program examined metallic-multiwall designs utilizing high temperature alloys [1]. A few of the more highly investigated materials for metallic TPS in recent years include Saffil insulating foam and advanced titanium-based alloys. Second-generation gamma Ti alloys provide good oxidation resistance, while still maintaining higher temperature capability and lower ductility than first-generation titanium aluminides. For this

reason, they are not only considered in future reusable launch vehicle hot structures, but have already been developed as engine cowl components on the Boeing 777 as well as structure surrounding the Tomahawk missile [11]. Perhaps the best example of metallic TPS design is the X-33, Lockheed Martin VentureStar™. This vehicle, a single-stage-to-orbit reusable launch vehicle, proposed a metallic microfiber enclosure surrounded by a honeycomb panel. While the use of a metallic TPS allowed for a more robust and possibly cheaper alternative to traditional TPS, the X-33 sparked the current initiative to examine metallic TPS in next generation space vehicles.

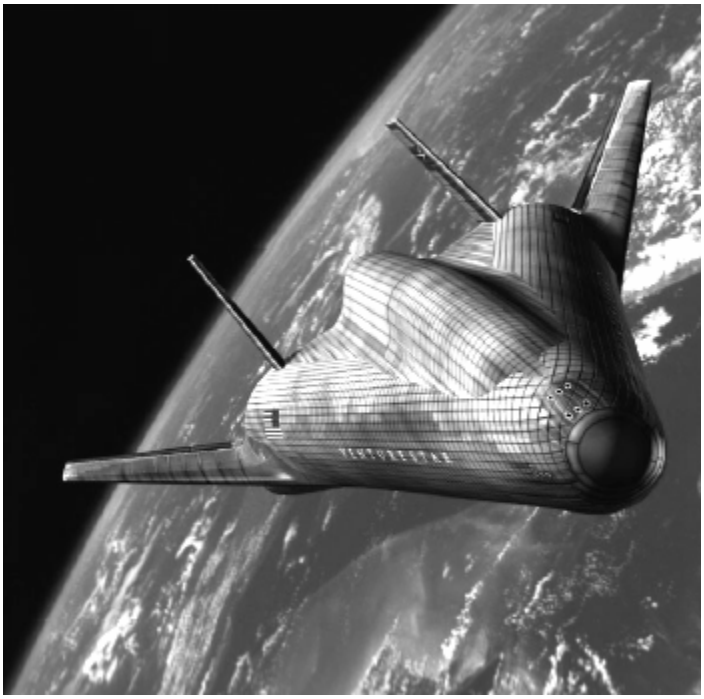

**Figure 2.1: X-33 reusable launch vehicle with metallic TPS[9]**

## *2.2 Types of TPS*

Current reusable TPS designs are categorized as ceramic tiles, ceramic blankets, or metallic concepts, respectively (ablative TPS are not reusable and therefore are not mentioned in this discussion). Ten of the most heavily utilized and/or researched TPS to date are described in the following section. Although no single TPS concept could serve as the vehicle's thermal protection alone, the proper

combination and balance of concepts to most significantly reduce cost and weight while maintaining optimum performance and safety must be determined. Each branch of the lotus diagram in Figure 2.2 outlines a key factor in TPS design; fatigue and fracture considerations span all three categories.

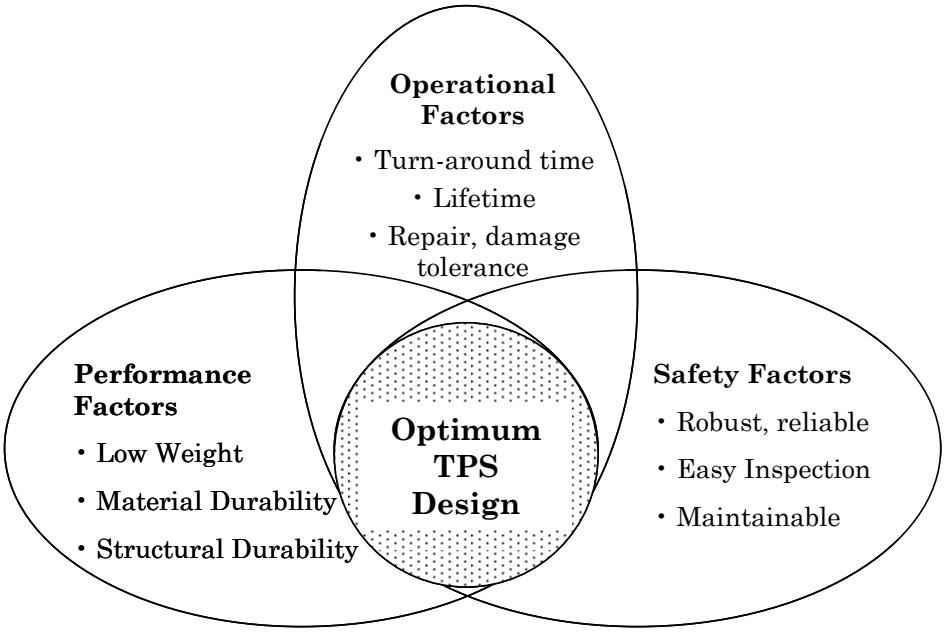


**Figure 2.2: Lotus diagram of optimum TPS design factors**

### Ceramic Blankets

The basic fabrication of blanket TPS consists of flexible fibrous insulation between outer layers of ceramic fabric. These types of TPS are then attached to the structure with room temperature vulcanizing (RTV) adhesive. The immediate advantages of blanket TPS include low initial cost and ease of installation. However, there are also several disadvantages to flexible blankets; the first challenge being that they must be re-waterproofed between each flight, thereby reducing vehicle turn-around time and increasing operational costs. In addition, the coating on blanket TPS make the initially flexible fibers and fabric brittle, and consequently susceptible to damage. Lastly, the quilted nature of blanket TPS can create a rough vehicle exterior that in turn increases turbulence, aerodynamic heating and drag [24].

Advanced Flexible Reusable Surface Insulation (AFRSI)

The AFRSI concept was created in an effort to ease installation and maintenance of prior ceramic blanket TPS. It includes an outer fabric coated with ceramic colloidal silica shown in Figure 2.3, high-purity silica fibers (called C-9 coating), a fiber felt insulation and an inner fabric layer [23].

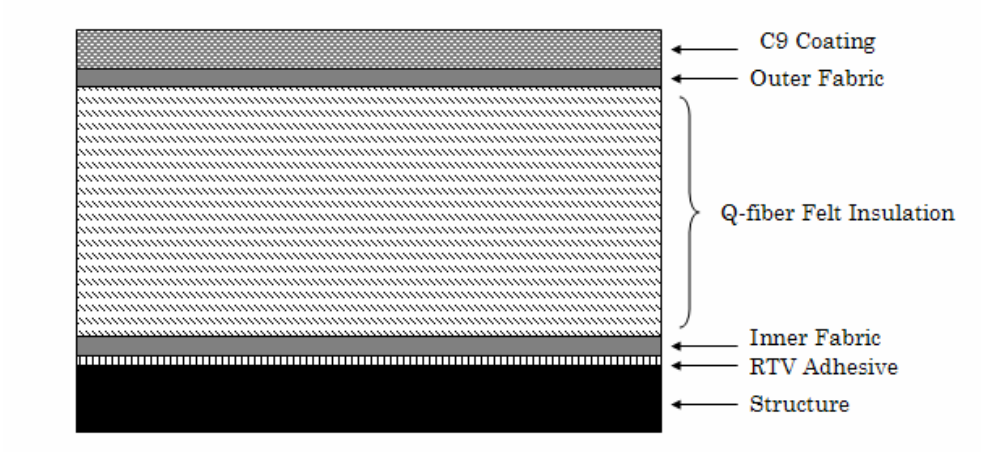


**Figure 2.3: AFRSI Schematic**

Tailorable Advanced Blanket Insulation (TABI)

The TABI thermal protection system was developed as an improvement to the AFRSI concept and is shown in Figure 2.4. It includes woven corrugations in the insulation layer to increase strength and temperature shielding capabilities [24].

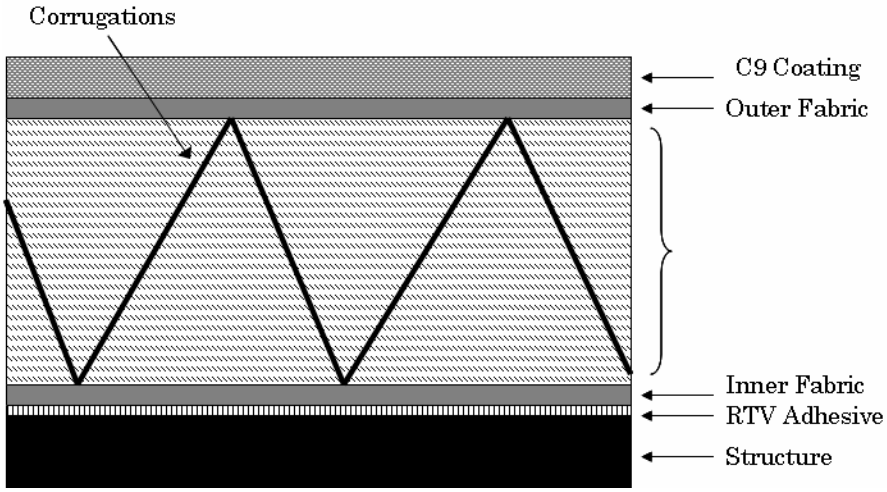


**Figure 2.4: TABI Schematic**

**Ceramic Tiles**

The current Shuttle Orbiter predominantly uses rigid ceramic tiles for thermal insulation. This TPS concept typically consists of tiles placed on top of a felt isolation mounting pad, attached to the structure with RTV adhesive. Rigid ceramic tiles have the highest temperature limits of all the TPS concepts. However, the tiles are limited to 6 x 6 inch squares due to strain isolation and thermal shock design parameters. Additionally, they require heavy damage inspection due to their inherently brittle composition and must be waterproofed after each flight [23].

LI-900 Tiles

The LI-900 tiles consist of rigid, silica fibrous insulation and a protective Reaction-Cured Glass (RCG) coating as shown in Figure 2.5. Like all ceramic tile concepts, they are attached to the underlying vehicle structure with RTV adhesive [24].

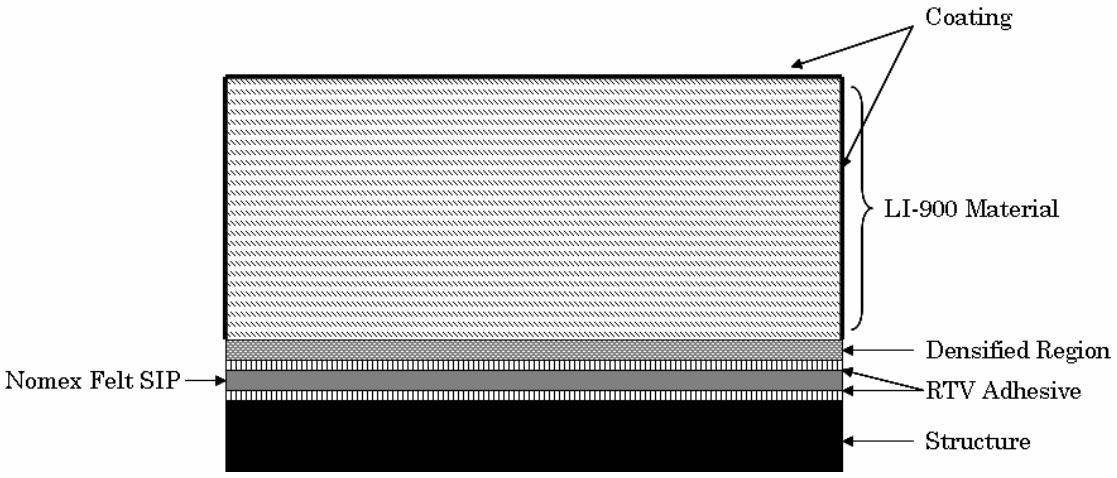


**Figure 2.5: LI-900 Schematic**

Alumina Enhanced Thermal Barrier Tiles (AETB)

One of the most recent research programs on ceramic tiles is the alumina enhanced thermal barriers (AETB) which includes alumina fibers coupled with a coating of toughened uni-piece fibrous insulation (TUFI) [27]. Shown in Figure 2.6,

AETB was created as an improvement to the LI-900 tiles. These tiles exhibit higher strength, durability and operation temperature capabilities [23].

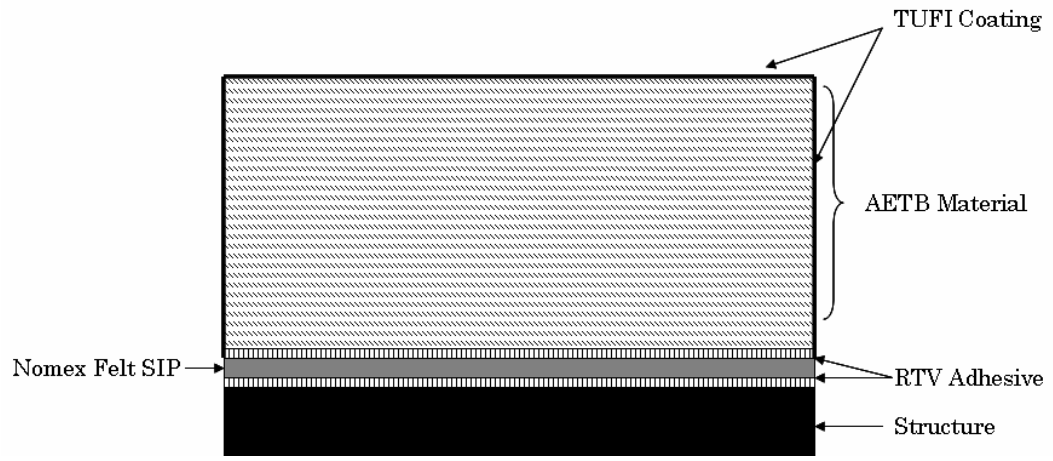


**Figure 2.6: AETB Schematic**

**Metallic Panels**

Metallic TPS are typically comprised of a foil-gage metallic box surrounding a lightweight ceramic fiber insulation, although foam metal and other metallic insulations are also considered. Typical panels utilize superalloys in the hottest regions and titanium alloys in lower temperature regions. Additionally, the outer face of the panel incorporates a honeycomb sandwich to aid load carrying capability and overall durability. Often the weight of the metallic box is negated to some extent by the low density fiber insulations. Consequently, metallic TPS are receiving considerable attention due to their potential weight, maintenance, repair, and cost benefits [24].

Titanium Multiwall (TIMW) Metallic TPS

One of the newest metallic TPS concepts, TIMW shown in Figure 2.7 consists of alternating layers of flat and dimpled metallic insulation enclosed by titanium sidewalls. Nomex felt provides mechanical attachment on the edge of the panels [23].

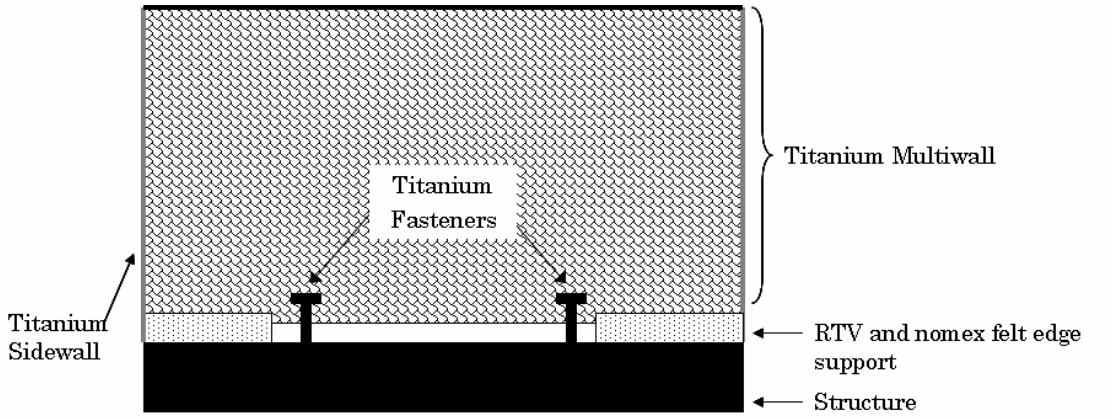


**Figure 2.7: TIMW Schematic**

Superalloy Honeycomb (SA/HC) Metallic TPS

The SA/HC metallic TPS consists of lightweight Cerrachrome and felt insulation sandwiched between two metallic foils, as depicted in Figure 2.8. The outer layer and sidewalls are Inconel 617 with an inner layer of titanium. This particular design has been heavily tested to predict a maximum operational temperature of 2000°F [24].

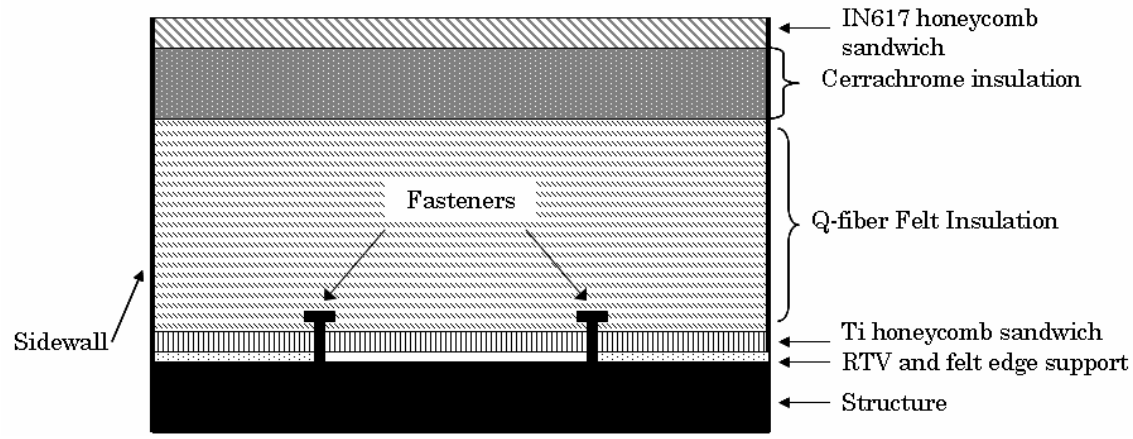


**Figure 2.8: SA/HC Schematic**

Second Generation Superalloy Honeycomb (SA/HC2) Metallic TPS

The SA/HC2 concept, shown in Figure 2.9, was developed as an improvement to the SA/HC TPS. The main modification with SA/HC2 is the incorporation of Saffil alumina fiber insulation, resulting in a lighter weight and higher temperature TPS

system. These panels have been tested to an operational temperature of 2000°F [23] and are considered in the Adaptable Robust Metallic Operable Reusable (ARMOR) program at NASA Langley [25].

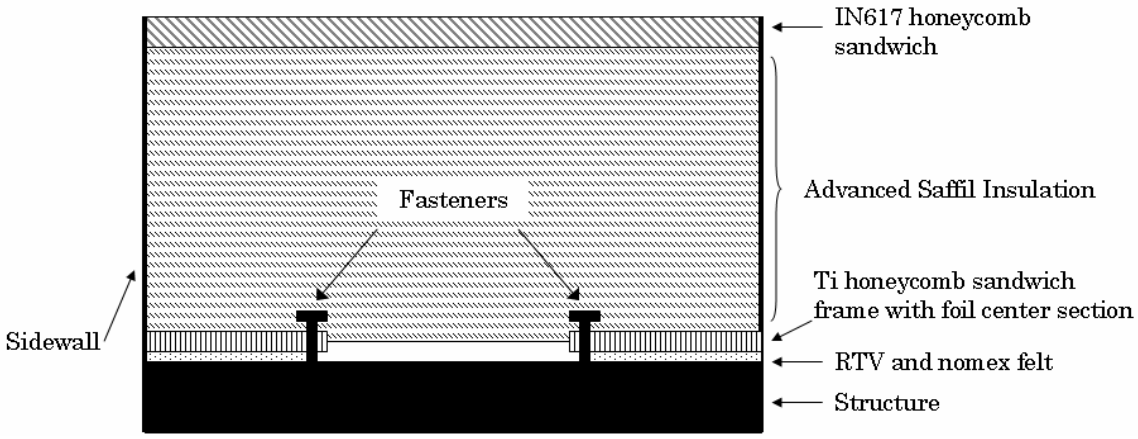


**Figure 2.9: SA/HC2 Schematic**

Titanium Honeycomb (TI/HC) Metallic TPS

The TI/HC concept depicted in Figure 2.10 was developed as a lower temperature and reduced weight metallic TPS. By replacing Inconel components with titanium, the overall operational temperature decreases, but a weight savings of 0.37 lb/ft$^2$ over the SA/HC2 concept is obtained [24].

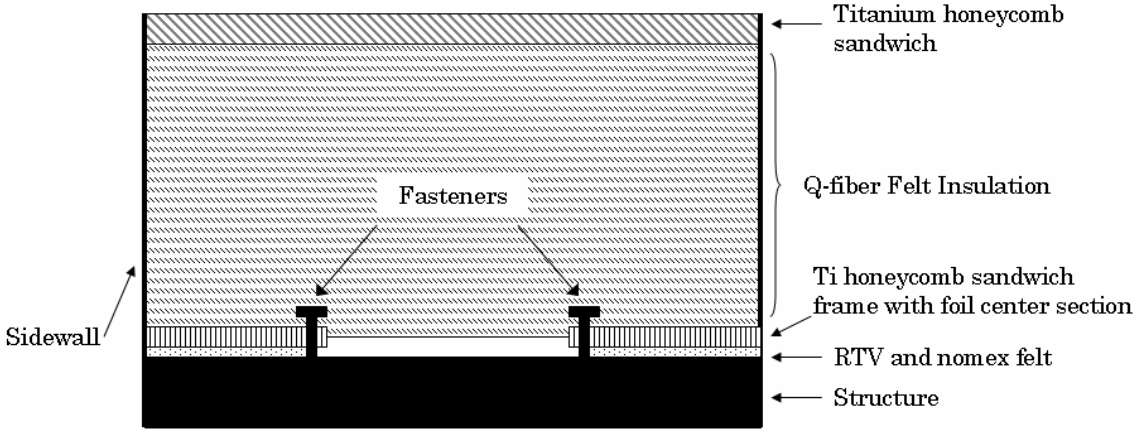


**Figure 2.10: TI/HC Schematic**

Advanced Metallic Honeycomb (AMHC) Metallic TPS

The AMHC concept, shown in Figure 2.11, is currently being developed to improve upon previous superalloy metallic TPS. It consists of a box frame, low conductivity Internal Mulltiscreen Insulation between the outer PM2000, an iron-based alloy, honeycomb sandwich and thin titanium inner facesheet. This design is also the first to consider a quick release fastening system for easier inspection and repair capabilities [23].

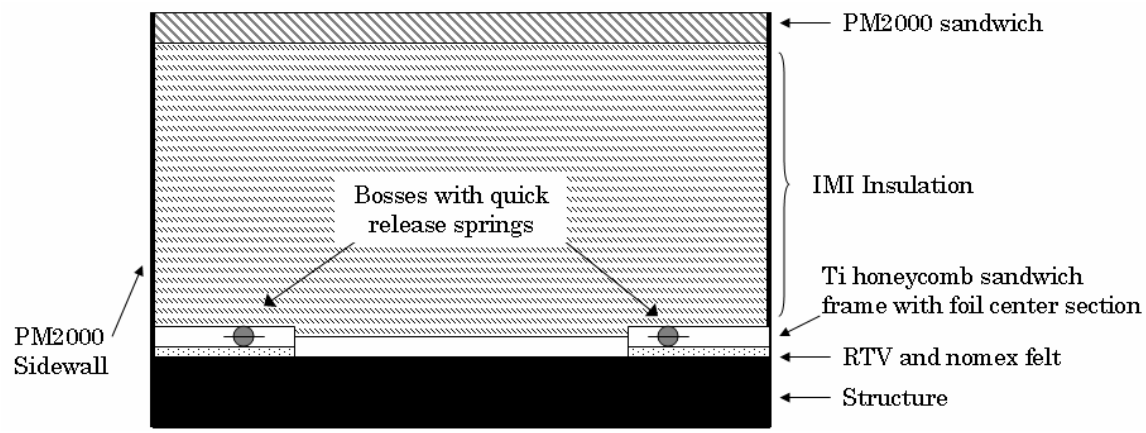


**Figure 2.11: AMCH Schematic**

## *2.3 Ceramic versus Metallic TPS*

With the recent demand to create more reliable and cost effective space travel, significant research effort has been spent studying the potential of metallic and ceramic TPS in hopes of driving the cost of payload to LEO below $1,000/lb. While ceramic TPS are primarily used on the current Shuttle Orbiter, metallic TPS may promise a cheaper, lighter, and more robust TPS system [9]. The general considerations for and against metallic and ceramic TPS are illustrated in Table 2.1 [27].

**Table 2.1: Potential benefits and challenges of metallic versus ceramic TPS**

| TPS | *Pro* | *Con* |
|---|---|---|
| *Metallic* | More robust due to innate ductility | Possible creep, fatigue, and/or oxidation issues |
| | More damage resistant | Expensive manufacturing and material costs |
| | No re-waterproofing (faster turn-around time) | Withstands lower temperatures |
| | Could be part of weight-bearing structure | |
| *Ceramic* | Withstands higher temperatures | Expensive repair and maintenance costs |
| | Easily replaceable | Needs re-waterproofing between flights |
| | | Parasitic weight addition to load-bearing structure |
| | | Less Robust |

Some of the current preliminary studies on metallic TPS examine sizing, creep, flutter, meteoroid/debris risk assessment, and thermal and weight considerations. The two major concerns with any TPS design include cost and weight. A comparison of these practical considerations for various TPS concepts are illustrated in Table 2.2 [27].

**Table 2.2: Weight and cost considerations of metallic versus ceramic TPS**

| Material | TPS Type | Maximum Temperature [°F] | Purchase Cost [$/ft$^2$] | Fabrication Cost [$/ft$^2$] | Area Weight [lb/ft$^2$] |
|---|---|---|---|---|---|
| Carbon fiber CMC[b] | Ceramic | 3000 | 15000 | 479 | 1.70 |
| Advanced C-C[b] | Ceramic | 2900 | 12000 | 428 | 1.70 |
| Shuttle coated C-C[a] | Ceramic | 2700 | 12000 | 724 | 1.70 |
| AEBT[b] | Ceramic | 2600 | 800 | 106 | 1.19 |
| Li-900[a] | Ceramic | 2300 | 1160 | 225 | 1.10 |
| TABI[b] | Ceramic | 2000 | 1030 | 52 | 1.00 |
| AFRSI[a] | Ceramic | 1200 | 330 | 46 | 0.94 |
| Ni superalloy tile | Metallic | 1900 | 4450 | 233 | 2.00 |
| Ni superalloy sheet | Metallic | 1800 | 4450 | 233 | 1.32 |
| TIMW | Metallic | 1100 | 6035 | 201 | 2.16 |

[a] First generation shuttle TPS, [b] Second generation shuttle TPS

### *2.4 Parametric Studies on Metallic TPS*

In order to produce a relatively lightweight, reusable, robust, and economically viable metallic TPS, studies on a number of key parameters are necessary. From a structural standpoint, proper panel sizing, durability and damage tolerance assessments are critical. Specific concerns pertinent to metallic TPS include minimum material gauge, deflection, boundary layer transition, local heating, insulation, oxidation, creep, and fatigue resistance [9].

One recent study on metallic TPS examines the use of metallic foam as the insulating core of the sandwich structure. In 2005 Zhu et al examined two types of metallic TPS, one with a titanium foam core as insulation and the other with Saffil insulation (a fibrous alumina found in the SA/HC2 metallic TPS concept). Zhu et al emphasizes metal foams as potential candidates for the honeycomb core due to their higher thermal conductivity and ability to carry structural loads, unlike ceramic equivalents. This study focuses specifically on thermal and mechanical loads extracted from a windward point on the X-33. The study uses a thermal constraint that the maximum structural temperature should not exceed 450 K, and a mechanical constraint that the stress in both metallic foil facesheets as well as the core must not exceed the material strength. With these parameters in mind, the insulating layers were optimally sized while keeping the facesheets a constant 500 μm thick. Zhu et al determined that the stress constraint was more critical than the thermal, however considering thermal constraint alone, the Saffil insulating core produced a thinner and consequently more lightweight TPS structure [32].

Another recent study in 2003 examines metallic TPS for meteoroid and debris risk assessment. Williamsen et al developed ballistic limit curves to predict when metallic TPS would be damaged from meteoroid and orbital debris. Four penetration cases, each one with deeper impact into the layers of the TPS, are analyzed and overall speed and impact effect are assessed on both titanium and Inconel sandwich coupons. By examining hypervelocity impact threats, Williamsen

et al was able to model curves to predict damage tolerance and assessment of metallic TPS [31].

**ARMOR TPS**

In the past decade, NASA Langley has studied metallic TPS with the Adaptable Robust Metallic Operable Reusable (ARMOR) TPS concept. An ARMOR TPS design, as shown in Figure 2.12, originates from the SA/HC concept and includes a metallic sandwich panel used to re-radiate heat. Panel to panel gaps on the outside of the structure are sealed by overhanging metal foil and used to prevent ingress of hot gases during re-entry. The ARMOR concept is designed with these critical requirements in mind: the TPS panels must withstand aerodynamic pressure, drag, acoustic and dynamic loading experienced during flight, as well as thermal mismatch loading between the TPS and the underlying structure, the TPS must have reasonable risk of failure from debris encountered during launch or orbit, and the TPS must help produce an economically viable RLV TPS. The study defines economic viability by calculating six cost components that equal the total cost of a launch. These cost factors include: 1 – development cost, 2 – vehicle production cost, 3 – flight operations cost (per flight), 4 – recurring cost of recovery, 5 – refurbishment cost, and 6 – cost of launch insurance [5].

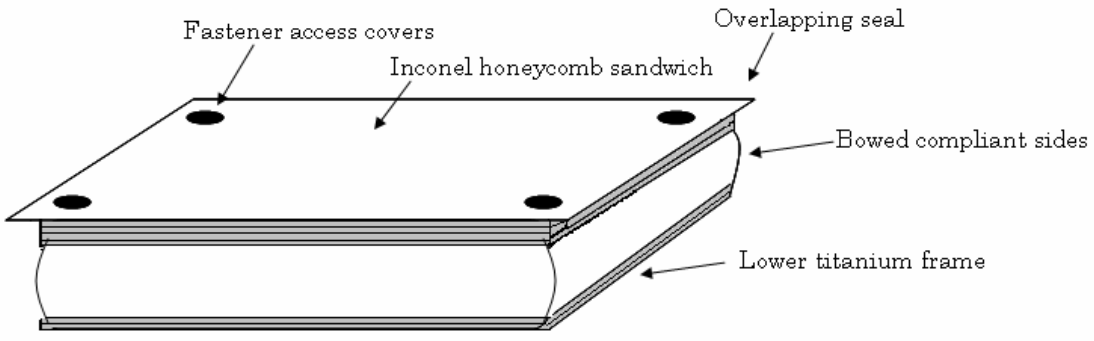


**Figure 2.12: ARMOR TPS panel, outer surface**

Most of the preliminary metallic TPS research on ARMOR involves sizing the TPS structure. One such study on ARMOR sizes the panel configuration by aerothermal heating and cryogenic conditions experienced in three environments: groundhold, ascent, and reentry. Purely analytical in nature, this study considers metallic TPS panels with titanium alloys and Inconel 617 foil sheets ranging from 150 μm to 400 μm in thickness, depending on insulating requirements, with foam-filled honeycomb sandwich construction. Four critical locations on the vehicle were examined and the study specifically focuses on the sizing of the fibrous insulation layer and honeycomb sandwich. After the preliminary sizing process, the overall ARMOR TPS weight was increased by 18% to withstand cryogenic and reentry temperatures [25].

A concurrent ARMOR study examines two critical factors in obtaining economically viable space flight: target gross and empty weights of the vehicle, and establishing and meeting a series of operational goals similar to the FAR (Federal Aviation Regulations) 25 for commercial aircraft. The key mission and operational requirements defined in the study are: minimum 20 year functional life, minimum design life of the airframe of 100 reference missions, post-flight maintenance and preflight operations performed in 7 days or less, vehicle turn-around time in 48 hours, 20 flights before scheduled maintenance, scheduled maintenance not exceeding 14 days, and no more than 3 scheduled maintenance periods per year. Additionally, this particular study introduces the integrated airframe concept, suggesting a thinner, but heavier system may produce the lowest overall weight through a coupled decrease in vehicle weight-bearing capacity and increase in volumetric efficiency. More specifically, the geometrical parameters of the panels were analyzed with the integrated airframe, or 'aeroshell' concept in mind. A lightweight titanium frame was suggested on the lower TPS, leading to a more AMHC type TPS concept. Two immediate benefits of ARMOR TPS include the

design of the pressure seals on the lower, cooler surface of the panel, and the fact that the panels provide added layers of protection above the underlying substructure of the reusable launch vehicle. This study sized the metallic foil facesheets, depending on vehicle location, material and conditions, between 38 μm to 150 μm thick [8].

In 2002, another study on ARMOR determined key factors that would govern the performance of the TPS system for a reusable launch vehicle. Utilizing FEM models, thermal analysis of metallic TPS were performed. Particular attention was paid to the non-load-bearing insulation, where heat shorts exist in the gaps between metallic panel and at mechanical attachments. Sensitivity studies were conducted to determine design drivers on mass and thickness of the improved metallic TPS. Results suggested that one of the crucial thermal performance factors was the radiation in the gaps between panels, where even small spaces among panels could produce large increases in heat reaching the structure. Therefore, the study concluded that reducing the emittance of the gap would not be a practical solution for limiting gap radiation, and suggested eliminating panel to panel gaps from TPS design entirely [3].

A fourth study conducted on ARMOR uses an iterative process to size the TPS panels with thermal and structural load parameters as part of an integrated TPS/cryogenic tank structural wall. This study also includes the addition of a compliant TPS support system (TPSS) as well as performs a creep analysis on the TPS panels. Eight structural load conditions and three thermal load conditions from liftoff, assent and reentry were used on an ARMOR TPS concept that featured subsurface sealing to prevent the panel to panel gap radiation as well as decoupled deformation and thermal expansion between the TPS inner and outer surface. The structural components of the panel were sized to perform successfully under anticipated acoustic, inertial, and aerothermodynamic loading conditions. Unlike

previous ARMOR studies that were purely analytical in nature, this study built four prototype ARMOR panels [5].

## *2.5 Additional Thin Foil Fatigue and Fracture Applications*

Thin foil fatigue and fracture concerns arise in countless engineering applications. Besides its role in thermal protection system design for aerospace applications, it is also a concern in gas turbine engines and miniature drone aircraft. Outside of the aerospace industry, thin foil fatigue and fracture issues appear in fuel cell design in the automotive and power industry, MEMS and solder joints in the electronics industry, fusion reactors in the nuclear industry, as well as many applications in the biomedical field. Figure 2.13 illustrates the typical maximum and minimum gauge thickness of the metals foils utilized in various engineering applications.

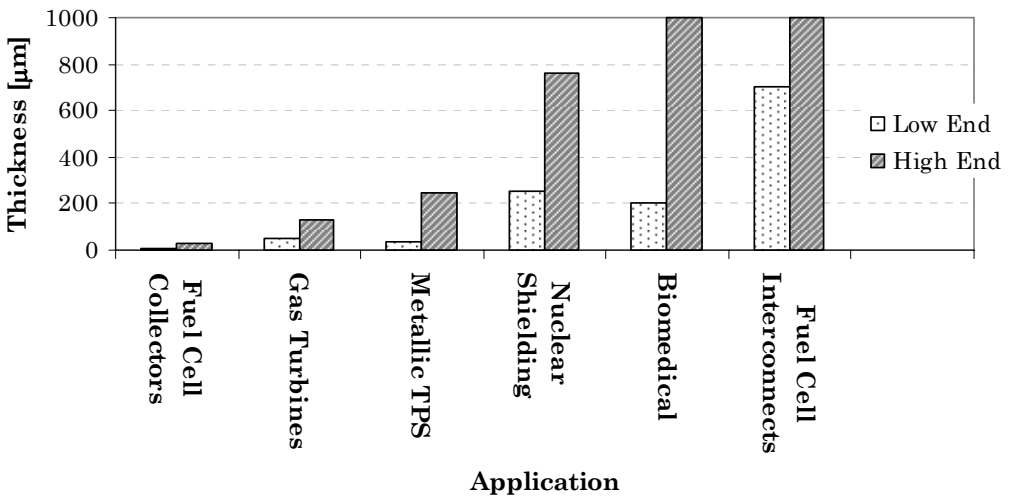


**Figure 2.13: Diagram of upper and lower range foil gauge thickness for various engineering applications**

### Biomedical Applications

Of the many thin component fatigue and fracture applications in the biomedical industry some examples include: artificial heart valves, hip joints, and knee joints, and cosmetic dentistry such as the design of veneers. Much of the

current research aims to further understand and perfect delamination resistant organic coatings on metallic thin films used to allow the body to accept the foreign materials as if it were its own natural material. Liu et al examined surface functional groups in nucleating calcium phosphate deposition on commercially pure titanium foils used in many surgical implants [21] such as a hip joint, whereas Morra and Cassinelli examined thin film deposition onto titanium implants specifically designed for prosthetic dentistry [22].

**Fuel Cell and MEMS Applications**

Thin component fatigue and fracture is becoming a critical concern as electronics and energy providers become smaller and lighter. Hahn et al examined MEMS-based fuel cells for applications like wireless sensor networks, chip cars, or autonomous Microsystems. This research investigates patterning technology for the stainless steel films between 10 μm and 30 μm in thickness, specifically the fabrication of micro flow fields to improve overall fuel cell performance [15].

Additionally Huang et al examined interconnects in solid oxide fuel cells which provide an electric contact between the cathode and anode as well as separates the fuel and air. Typically ceramic interconnects have been used at high operating temperatures; however Huang et al suggests superalloys as promising interconnect candidates. The research focuses on oxidation kinetics to reduce temperatures and improve performance on iron base alloys 1 mm thick [16].

Research on copper foils by Jiang examined electrochemical properties of sintered hydrogen storage to improve weight and power capabilities for fuel cell and battery applications [18], whereas Belhomme et al focuses on the cathode of molten carbonate fuel cells for a more clean and efficient power source than its predecessors. In both cases Belhomme et al and Jiang synthesized several different oxides [2].

Lastly, Son et el particularly focused on tensile and fatigue crack growth of lithographic, galvanformung, abformung, nickel MEMS 10 μm thick. Son et al suggests that because thin films used in the MEMS differ from bulk materials in mechanical properties, their fatigue and fracture properties must be separately determined to improve product design and reliability. Consequently, monotonic tensile tests and fatigue experiments were conducted on the foils. The study concluded that the nickel MEMS exhibited brittle tensile behavior, a Paris relationship between stress intensity factor and crack propagation rate, and an overall reduced fatigue strength due to thickness effects [29].

**Energy Applications**

Metallic foils are used extensively in both nuclear fusion reactor design and gas turbine engines. In particular, James et al examined fatigue crack growth in magnetic fusion reactor (MFR) first-walls. First wall environments in MFR are cyclic in nature, so fatigue resistance is critical in MFR design. As a result, James et al tested stainless steel 254 μm thick at three stress levels: 112 MPa, 147 MPa, 170 MPa. Besides pure fatigue considerations, another major experimental variable in MFR first-walls is the effect of neutron irradiation on crack growth behavior. For this reason some of the specimens were irradiated for post irradiation fatigue testing. Crack lengths were determined by periodically examining specimen with a traveling microscope and the work concluded that relatively large numbers of specimens required for MFR first-wall alloy development program can be produced using a minimum of irradiation space [17].

Puigh et al examined candidate fusion reactor materials, specifically focusing on irradiated and unirradiated titanium alloys (Ti-6Al-4V) 760 μm thick. Center cracked tension and fatigue tests were conducted at ambient conditions with a sine waveform frequency of 5 Hz and a load ratio of 0.1. Fracture toughness values as low as 4.2 MPa√m were observed, and the titanium alloys were shown to exhibit

crack growth rates three times greater than other commonly used metals, such as stainless steel, in fusion reactors [26].

Simms et al examined the honeycomb structures of industrial gas turbines in effort to increase turbine operating efficiency and reduce environmental emissions. Iron and nickel base foils 49 μm to 127 μm thick were examined in natural gas combustion environments undergoing thermal cycles for up to 1500 hours. Specimen surfaces were visually checked and overall oxidation rates and mass gains were plotted in order to determine sensitivities and material reliability [28].

# CHAPTER 3

# METALLIC FOIL FATIGUE & FRACTURE

## *3.1 TPS Relevance*

Metallic thermal protection systems under development for reusable launch vehicles include metallic sandwich panels with honeycomb or foam cores and foil facesheets. In addition to possessing good heat transfer characteristics, these panels must also exhibit structural durability at both elevated temperatures encountered during atmospheric re-entry, as well as extremely cold temperatures encountered in deep space. From a structural standpoint, resistance to shear loading (developed by the friction boundary layer during re-entry), creep and fatigue are crucial. The fact that sandwich panels carry most of the bending, twisting, and in-plane loading in the skins and the core attributes to the bending stiffness and load-bearing capacity is well established, however relatively little information exists regarding the fatigue behavior of such structures [30].

## *3.2 Thin Metallic Foil Research*

In a recent study on the fatigue behavior of Ni-base foils with thicknesses typical of those used for thermal protection systems, crack growth rates were found to be several orders of magnitude higher than that expected for thicker material [20,30]. The high crack growth rates observed in thin foils are of concern for in-plane loading of honeycomb sandwich structures since the core does not significantly contribute to the fatigue crack growth resistance [30]. Consequently, the skins govern the overall fatigue crack growth rate.

In contrast to the results for Ni-base foils where unexpectedly high crack growth rates were observed [20,30], a recent publication by Guo et al [13] on the effect of thickness on the fatigue behavior of 2024-T851 aluminum showed a decrease in fatigue crack growth rate as the specimen thickness was reduced from

12 mm to 2 mm. Guo et al attributed the decrease in crack growth rate to the stress state ahead of the crack tip and the plastic zone size. In addition to stress state and plastic zone variations, the effect of thickness on crack growth rates may be related to changes in microstructure with specimen thickness, particularly in the foil regime (< 250 μm in thickness). Hadrboletz et al and Klein et al examined both copper and aluminum foils between 10 μm and 250 μm and cited immediate crack arrest in fatigue crack growth curves, suggesting plastic zones and variations in material microstructure as instigators [14,19]. Another study by Broek and Schijve [6] determined that for 2024-T3 Alclad sheets, the crack growth rates increased as thickness was increased from 0.6 mm to 4 mm. The seemingly contradictory effect of thickness on the crack growth rate may be related to the ductility and notch sensitivity of the material being tested.

### *3.3 Research Objective*

The goal of the present study was twofold. The initial objective was to determine if the elevated crack growth rates discovered in previous research for Ni-base foils were characteristic of other metallic foils, with the ensuing goal of establishing if foil thickness or loading direction (longitudinal versus transverse) significantly affects crack growth rate. Taking these factors into consideration, the fracture toughness and fatigue crack growth rates of aluminum-magnesium alloy foils with thicknesses between 30 μm and 250 μm were examined. An aluminum base alloy was selected because of its drastically different mechanical behavior compared to high-strength nickel base alloys, as well as its relevance to aerospace applications.

## *3.4 Experimental Procedure*

### Grips and Load Frame

All tests, monotonic tension, fracture toughness and fatigue, were performed using an MTS Model 810 servo-hydraulic load frame. The experimental setup is illustrated in Figure 3.1 and Figure 3.2.

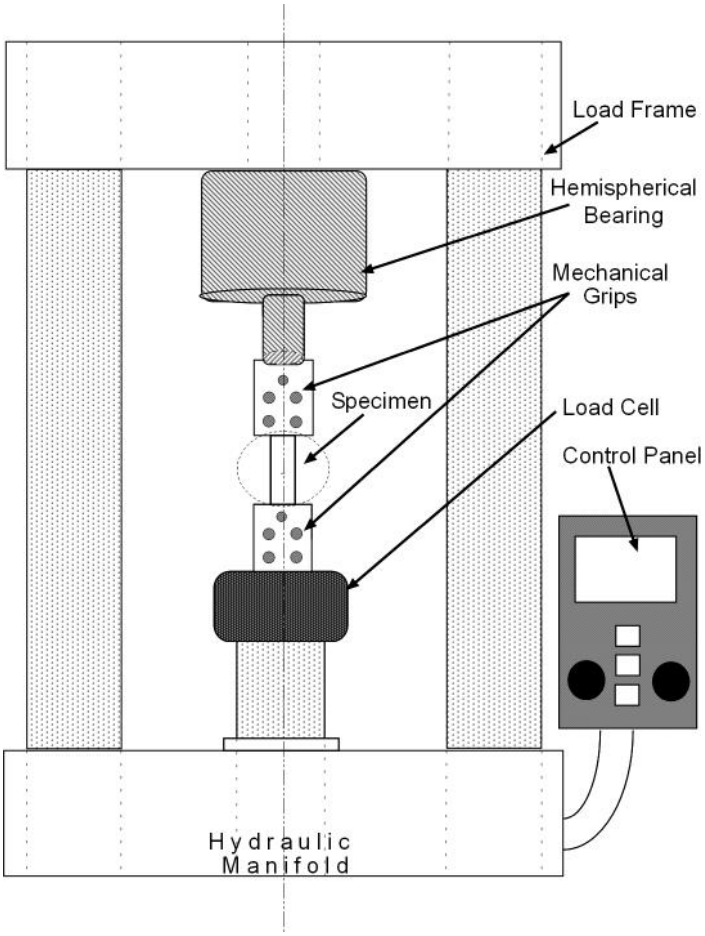


**Figure 3.1: Schematic of experimental setup**

As discussed in greater detail in reference [20], avoiding bending loads and applying the load through the centerline of the test specimen is imperative when testing thin foils. Within the foil regime, even small transverse force components can cause specimen distortion and out-of-plane buckling. To minimize bending strains and ensure pure axial loading, the upper specimen grip was attached to a self-centering hemispherical bearing (Figure 3.2) that was free to swivel and rotate

within its fixture, while the lower grip was rigidly fixed to the load cell. This arrangement allowed the specimen to 'self-align' during initial specimen installation, and coupled with center-notched foils provides uniform crack growth on both sides of the notch [20].

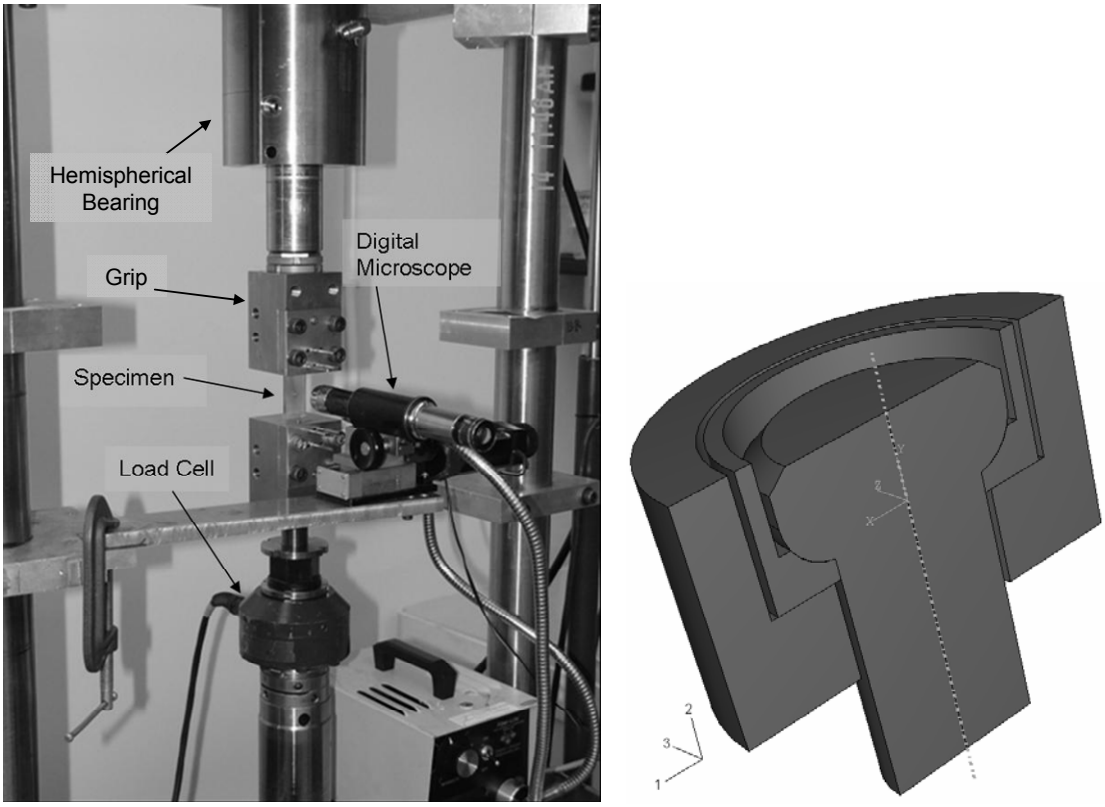


**Figure 3.2: Experimental setup *(left)* and close up schematic of hemispherical bearing *(right)*[20]**

The 30 μm and 100 μm thick foils were face-loaded within the grips, whereas the 250 μm foils utilized both friction and pin loading. With the exception of tensile testing of 250 μm thick foils, all experiments were performed using a 1000 N load cell (a 2000 N load cell was used for tensile testing of 250 μm foils). Strain was measured by use of a linear variable displacement transducer (LVDT) mounted across the upper and lower grip.

**Material and Specimen Geometry**

Rectangular center-notched specimens were used for fracture toughness and fatigue crack growth testing. Specimens were removed from as-rolled 97Al-3Mg foil sheets having a nominal thickness of 30 μm, 100 μm and 250 μm [12].

For the 30 μm thick foil, 150 mm long x 25 mm wide specimens were cut from 150 mm x 150 mm sheets. In order to determine if rolling direction influenced fatigue behavior, the 30 μm specimens were removed with the loading axis either parallel or perpendicular to the rolling direction ($0^o$ or $90^o$). The loading axis was parallel to the rolling direction for all 100 μm and 250 μm thick specimens. Specimens 25 mm wide and either 100 mm or 150 mm long were used for the 100 μm thick foil. For the 250 μm foil, initial tests were performed using specimens 100 mm long x 25 mm wide with a series of 2 mm diameter holes that mated with pins to provide additional loading in the specimen grips. However, this particular specimen geometry was abandoned in favor of longer (150 mm) specimens machined from 150 mm x 150 mm sheets that could be directly face-loaded without pin holes.

For all thicknesses examined, notches 2 mm to 3 mm in length were machined in the center of the specimens by electric discharge machining (EDM) or by use of an end mill. The use of an end mill was found to provide better dimensional quality of the notch. Crack growth was measured on each side of the notch, right and left, as shown in Figure 3.3.

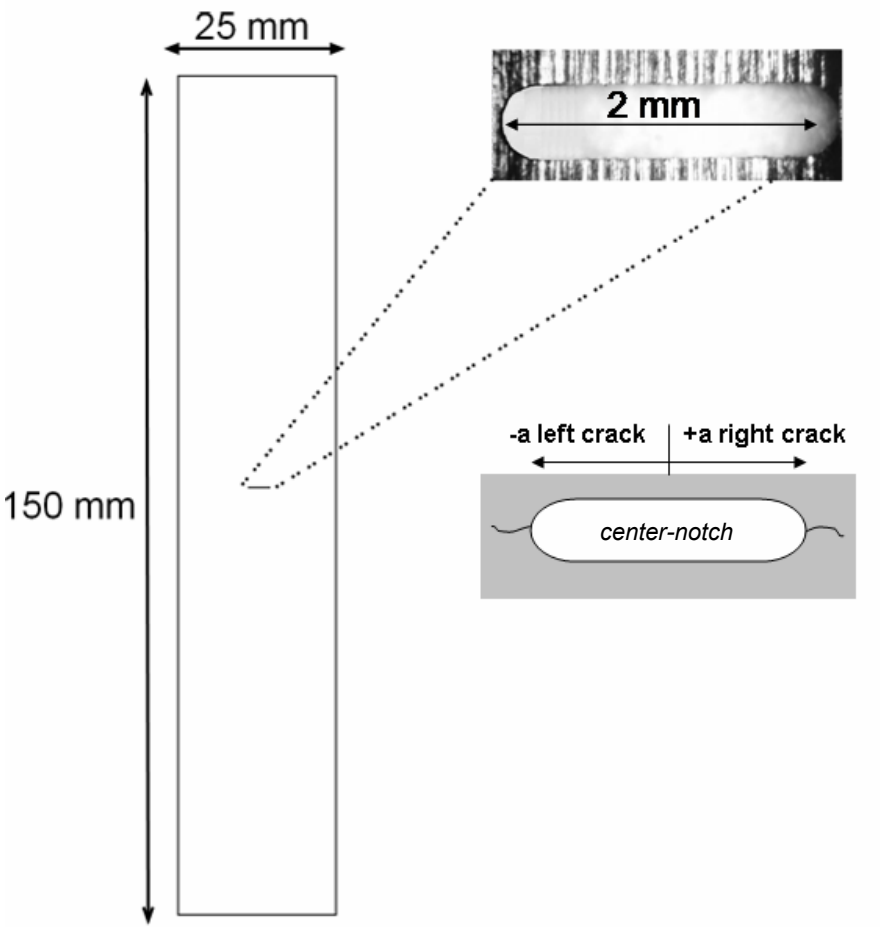


**Figure 3.3: Specimen geometry**

To characterize the foil material prior to fracture toughness and fatigue testing, as well as aid in establishing fatigue loads, the room temperature monotonic tensile behavior was determined using thin specimens from the foil sheets. The 100 μm and 250 μm thick foils were tested with the loading axis parallel to the rolling direction of the foils, whereas the 30 μm foil specimens were loaded with the axis either parallel or perpendicular to the rolling direction.

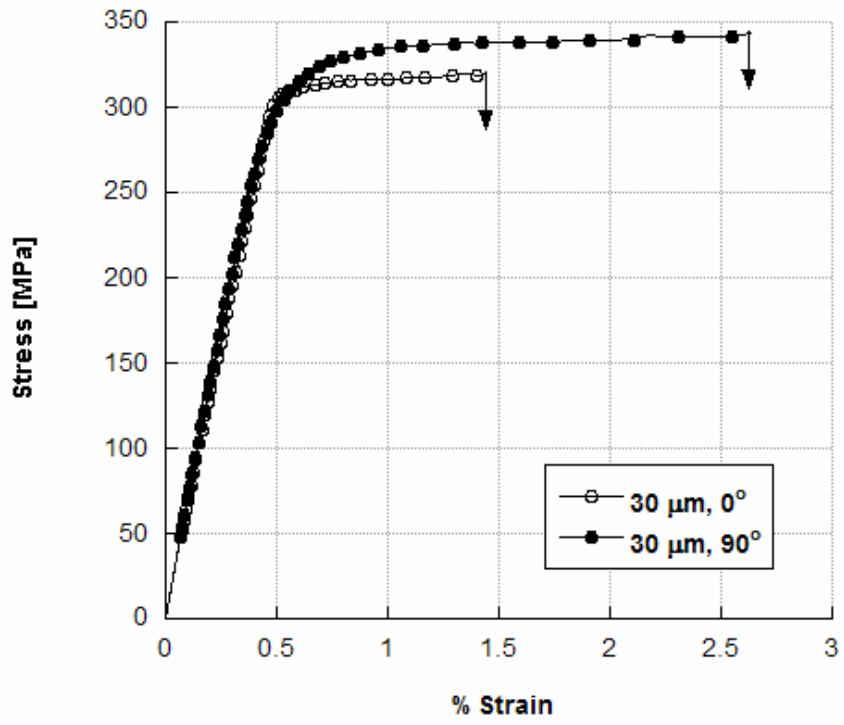


**Figure 3.4: Room temperature monotonic stress strain response of 30 µm Al-Mg foil, transverse and longitudinal orientations**

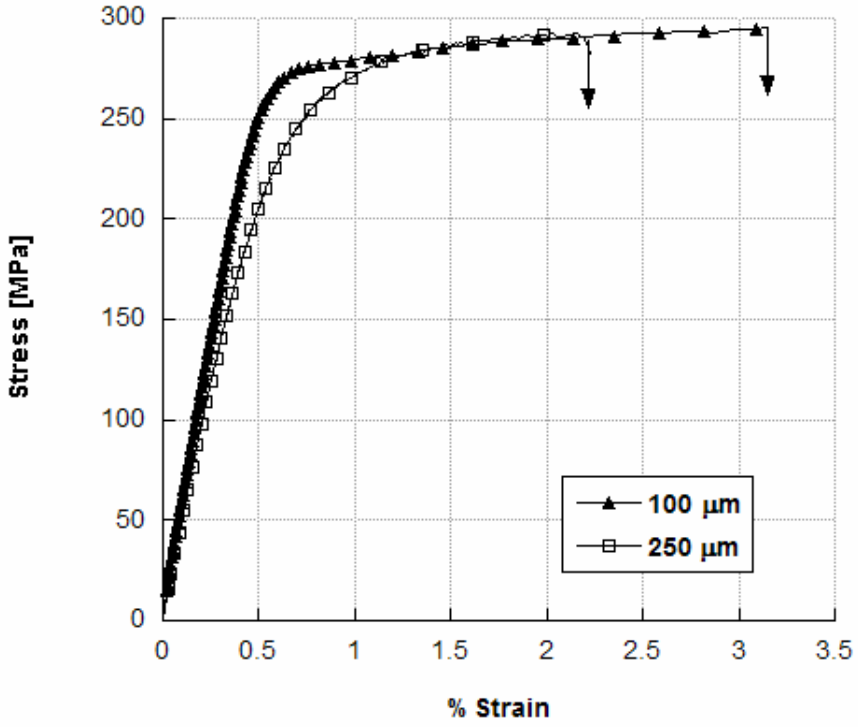


**Figure 3.5: Room temperature monotonic stress strain response of 100 µm and 250 µm thick Al-Mg foil**

Figures 3.4 and 3.5 compare the stress-strain response of longitudinal and transverse specimens removed from the 30 μm thick foil, as well as the longitudinal 100 μm and 250 μm thick foils. Table 3.1 outlines the yield strength, tensile strength, failure strain and elastic modulus of the foils resulting from the monotonic stress-strain with the tensile axis parallel to the rolling direction as compared to similar aluminum alloys from literature. Yield strength was determined by the 0.2% offset slope of the elastic region. It should be noted that the failure strain for all foils was below 4%, considerably lower than what is commonly quoted for typical Al-base alloys [7]. For all tension tests, the loading rate was 0.015 kN/s. Specimen gauge lengths ranged between 40 mm and 80 mm, and all experimental raw data can be found in Appendix A.

**Table 3.1: Room temperature mechanical properties of Al-Mg (97/3) foil**

| Thickness [m] | Loading Direction | 0.2% Offset $\sigma_y$ [MPa] | Ultimate Strength [MPa] | Failure Strain [%] | Elastic Modulus [GPa] |
|---|---|---|---|---|---|
| 30 | 0° | 308 | 320 | 1.4 | 61.7 |
| 30 | 90° | 265 | 340 | 2.6 | 66.7 |
| 100 | 0° | 244 | 295 | 3.2 | 52.4 |
| 250 | 0° | 170 | 290 | 2.2 | 44.4 |
| *Al 5252-O* [7] | | 115 | 240 | 27 | 68.3 |
| *Al 7075-T6* [10] | | 469 | 578 | 11 | 71 |
| *Al 2024-T4* [10] | | 303 | 476 | 20 | 73.1 |

Consistent with the low failure strain, all specimens exhibited a flat fracture surface, indicative of a low ductility material. Notably, the 250 μm foil is the only thickness that exhibited distinct shear failure typical of plane stress. The 30 μm and 100 μm thick foils revealed much different fracture characteristics with limited through-thickness thinning during tensile testing. The 30 μm thick foil flat fracture surface is shown in Figure 3.6.

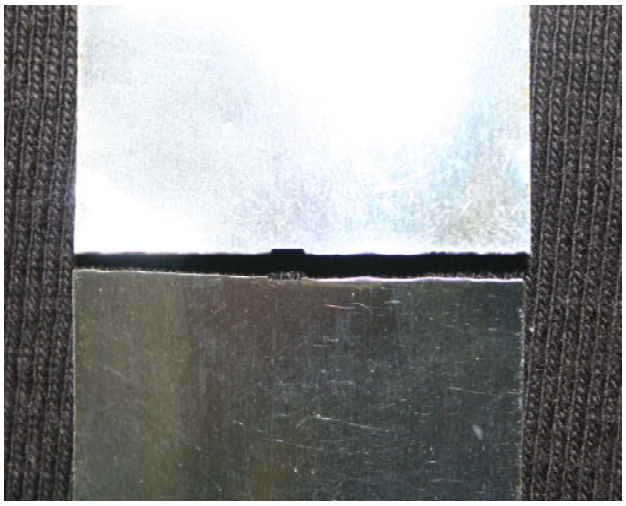

**Figure 3.6: Flat fracture surface of 30 μm thick foil**

### *3.5 Fracture Toughness Tests*

For fracture toughness testing, specimens of each foil thickness were pre-cracked under load control at a stress ratio between 0.2 and 0.3, and a sinusoidal loading frequency between 10 and 20 Hz at ambient conditions. The precracking loads and total fatigue cycles are provided in Table 3.2. Fracture toughness was estimated by loading the precracked specimens until failure at a loading rate of 0.015 kN/s. Ideally, the CTOD should be measured across the crack face in a center-notched specimen. However, in view of the experimental difficulty of making direct measurements on the faces of thin foils, specimen displacement was determined by an LVDT mounted between the grip faces. Using this procedure, the elastic deformation that would occur over the specimen length between the grip faces is included in the force-displacement curves. However, because of the rigidity of the load frame and grips relative to the specimen size, the effect of elastic deformation of the uncracked regions of the foil on the displacement can be estimated by subtracting the compliance of the system from the strain measurements.

**Table 3.2: Summary of the room temperature fracture toughness pre-crack data for Al-Mg foils**

| ID | Thickness [μm] | Loading Direction | R | Frequency [Hz] | Right Pre-crack Length [mm] | Left Pre-crack Length [mm] | Precrack Cycles [x1000] |
|---|---|---|---|---|---|---|---|
| 1 | 30 | 0º | 0.2 | 10 | 1.13 | 0.96 | 40 |
| 2 | 30 | 0º | 0.2 | 10 | 0.99 | 1.09 | 20 |
| 3 | 30 | 90º | 0.2 | 10 | 1.03 | 1.18 | 17 |
| 4 | 30 | 90º | 0.2 | 10 | 0.94 | 1.03 | 13 |
| 5 | 100 | 0º | 0.15 | 10 | 0.4 | 0.4 | 359 |
| 6 | 250 | 0º | 0.2 | 20 | 0.44 | 0.52 | 356 |
| 7 | 250 | 0º | 0.28 | 20 | 0.6 | 0.76 | 303 |
| 8 | 250 | 0º | 0.22 | 20 | 0.8 | 0.8 | 1001 |

## *3.6 Fatigue Tests*

All fatigue tests were performed under load control at a stress ratio of approximately 0.2 and a sinusoidal loading frequency of 10 Hz at ambient conditions. For the 30 μm foils, maximum fatigue stress levels of 120 and 160 MPa were investigated. The 100 μm foils were tested at maximum stress levels of 90, 120 and 160 MPa, and the 250 μm foils were examined at a maximum stress of 70 MPa.

Crack growth was monitored during the fatigue tests by periodically pausing the test and ramping to a stress level approximately 90% of the maximum fatigue stress to aid in opening the crack faces. The use of a center-notched specimen, a necessary condition for symmetric crack growth of thin foils [20], provides two sets of crack growth data for each test specimen. Cracks on the right and left side of the notch were measured using an optical microscope attached to the load frame with a 20 X objective. As discussed in greater length in Chapter 4, in all cases there was excellent agreement between measurements made for cracks on either side of the center-notch. Moreover, due to the inherent nature of foils, measurement of crack lengths was relatively straightforward since cracks were through-thickness and could be illuminated from the backside of the test specimen.

## *3.7 Data Analysis*

The cyclic crack growth behavior outside the threshold regime for crack growth can typically be described by the Paris relation, which equates the cyclic crack growth $da/dN$ and the stress intensity range ΔK by

$$\frac{da}{dN} = C\Delta K^m \qquad (1)$$

The stress intensity range for a center-cracked specimen as a function of the far field stress range is defined in terms of the half-crack length, $a$, by

$$\Delta K = Y\Delta\sigma\sqrt{\pi a} \qquad (2)$$

where $Y$ is the geometry correction factor defined in terms of the ratio (α) of half the length of the crack to half the width of the specimen [6].

$$Y = \frac{1 - 0.5\alpha + 0.326\alpha^2}{\sqrt{1-\alpha}} \qquad (3)$$

The cyclic plastic zone size can be calculated utilizing plane stress conditions for thin foils with

$$r_y = \frac{1}{8\pi}\left(\frac{K}{\sigma_y}\right)^2 \qquad (4)$$

where K is the stress intensity factor defining the local stresses around the crack and $\sigma_y$ is the yield strength of the material.

# CHAPTER 4

# EXPERIMENTAL RESULTS

## *4.1 Fracture Toughness*

Typical load-displacement curves for the foil specimens are given in Figure 4.1 for longitudinally and transversely loaded 30 μm thick foils; and Figure 4.2 for longitudinally loaded 30 μm, 100 μm and 250 μm thick foils. A summary of the fracture toughness values obtained from testing of all three foil thicknesses can be found in Table 4.1 and can be compared to values found in literature for various aluminum alloys, steels and ceramics found in Table 4.2. For all foil specimen tested, the fracture toughness values were substantially lower than the plane stress or plane strain fracture toughness values commonly reported for thicker Al alloys [7]. Fracture toughness was determined by fitting a 95% slope line to the linear elastic region of the experimentally determined force versus displacement data. The point where the 95% slope line and the experimentally determined curve cross is the associated critical load. Utilizing the specimen geometry and crack growth data, the critical stress and corresponding critical stress intensity, otherwise known as fracture toughness, can be calculated using equations (2) and (3) from section 3.7. Consistent with the low toughness values and low ductility from monotonic tensile testing, all specimens exhibited brittle fracture surfaces during toughness testing. Raw data for these tests can be found in Appendix B.

**Table 4.1: Al-Mg fracture toughness values**

| ID | Thickness [μm] | Loading Direction | $K_{Ic}$ [MPa-√m] |
|---|---|---|---|
| 1 | 30 | 0° | 13.4 |
| 2 | 30 | 0° | 13.7 |
| 3 | 30 | 90° | 15.1 |
| 4 | 30 | 90° | 17.4 |
| 5 | 100 | 0° | 13.8 |
| 7 | 250 | 0° | 12.8 |
| 8 | 250 | 0° | 16.9 |
| 9 | 250 | 0° | 13.1 |
| *Average* | | | *14.5* |

**Table 4.2: Various materials fracture toughness values [10]**

| Material | $K_{Ic}$ [MPa-√m] |
|---|---|
| Man-Ten steel | 200 |
| AISI 4340 steel | 130 |
| Al 2024-T3 | 34 |
| Al 7075-T6 | 29 |
| Alumina (+15% $ZrO_2$) | 10 |
| Alumina | 4.0 |
| Silicon carbide | 3.7 |
| Dolomitic limestone | 1.3 |

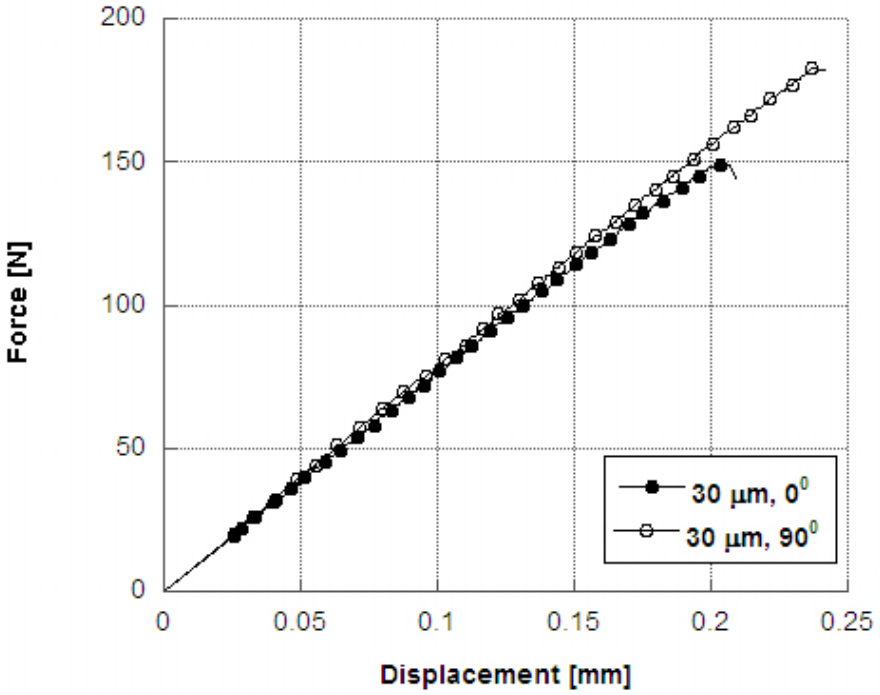


**Figure 4.1: Load-displacement curve illustrating orientation effect on fracture toughness for 30 µm**

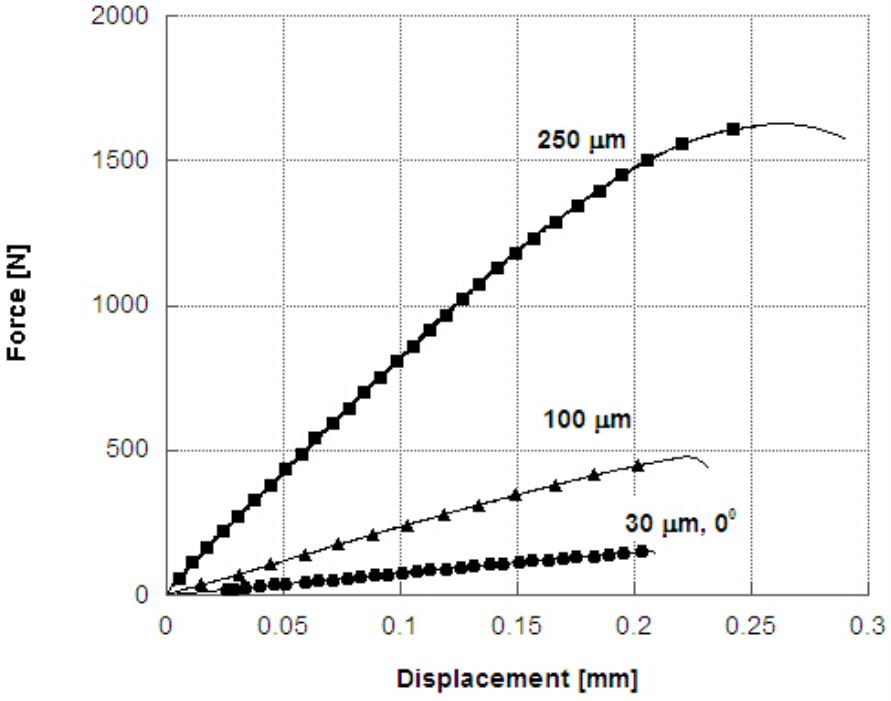


**Figure 4.2: Load-displacement curve illustrating size effect on fracture toughness for 30µm, 100µm, 250 µm thick foils**

The resulting trend of extremely low fracture toughness for foil-thickness metals is consistent with earlier investigations that showed very low fracture toughness for Ni-base foils [30] and 43 μm thick Ti-6Al-4V foils (current work by author). In a study on 43 μm thick Ti-6Al-4V foils, similar to the 97Al-3Mg foils, the fracture toughness was approximately 20% of the plane strain fracture toughness values commonly quoted in the literature [7].

The considerably reduced fracture toughness of metal foils, although influenced by microstructure, is significant. Traditional practice assumes toughness is a minimum for plane-strain conditions, and reaches a maximum value when plane-stress conditions exist. However as illustrated in Figure 4.3, a bell-shaped curve may exist for the thickness dependence of fracture toughness of many metals, with the toughness of foils having values even below plane strain fracture toughness. As a result, basing calculations for critical crack length on an assumed lower bound obtained from plane-strain fracture toughness data, or on a higher bound obtained from the testing of sheet-thickness materials (in the range of 1 mm) is not appropriate for thinner structures. This low toughness trend in the foil regime is of particular concern when designing thermal protection systems utilizing foil-thickness metals, but could also be significant for many other applications including nano-phase foils and wires [1].

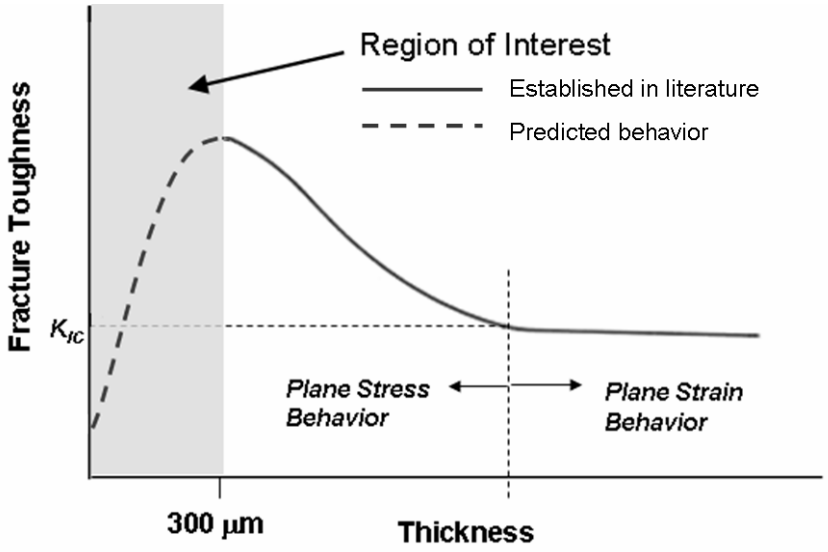


**Figure 4.3: Schematic dependence of fracture toughness on thickness**

## *4.2 Fatigue Crack Growth*

Figures 4.4 through 4.6 show the crack length versus accumulated fatigue cycles for 30 μm, 100 μm and 250 μm thick foils, respectively. Good agreement between the crack length measurements made on the right and left side of the machined notch was obtained, indicating uniform tensile loading of the specimens. Figure 4.7 compares the cyclic dependence of crack length of for 30 μm and 100 μm thick specimens at stress levels of 120 and 160 MPa. Raw data from these tests can be found in Appendix C.

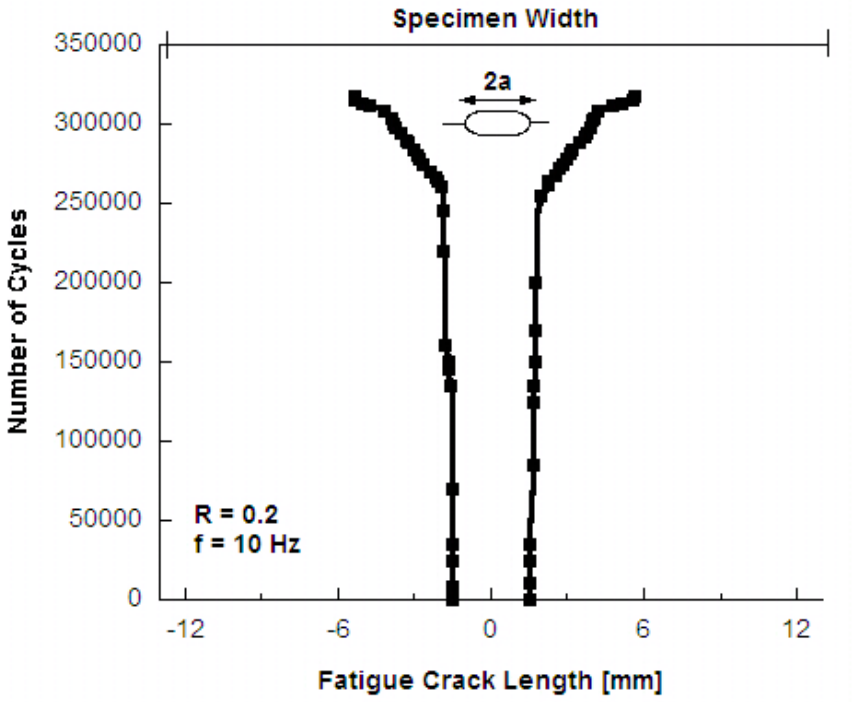


**Figure 4.4: Crack length versus cycles for 250 μm thick foil at a stress level of 70 MPa**

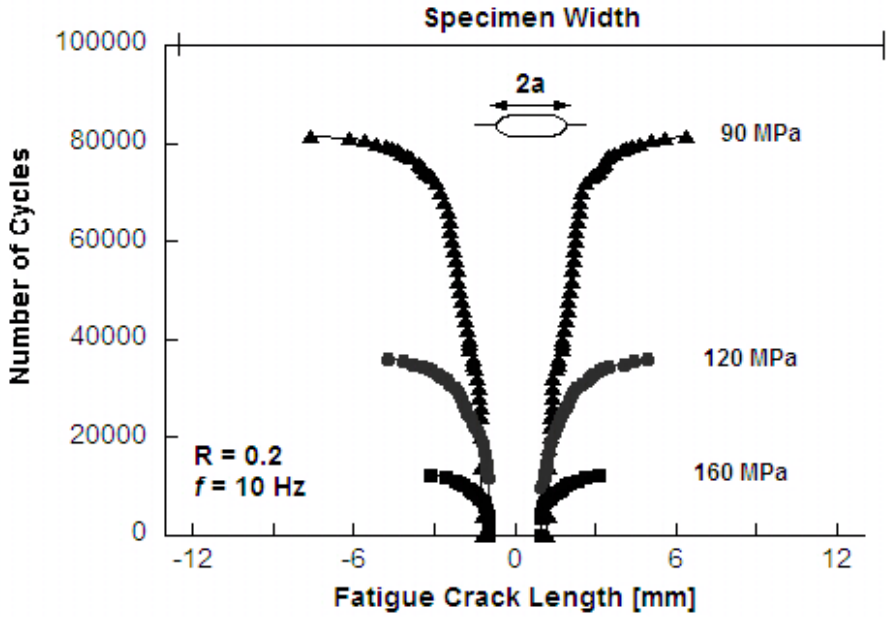


**Figure 4.5: Crack length versus cycles for 100 μm thick foil at three stress levels**

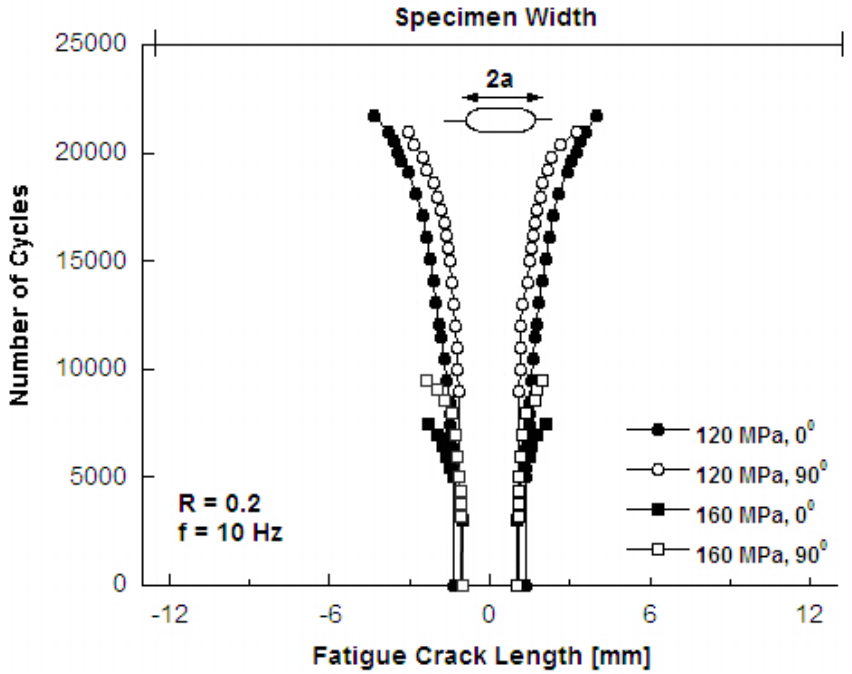


**Figure 4.6: Crack length versus cycles for 30 μm thick foil at two stress levels and both longitudinal and transverse orientation**

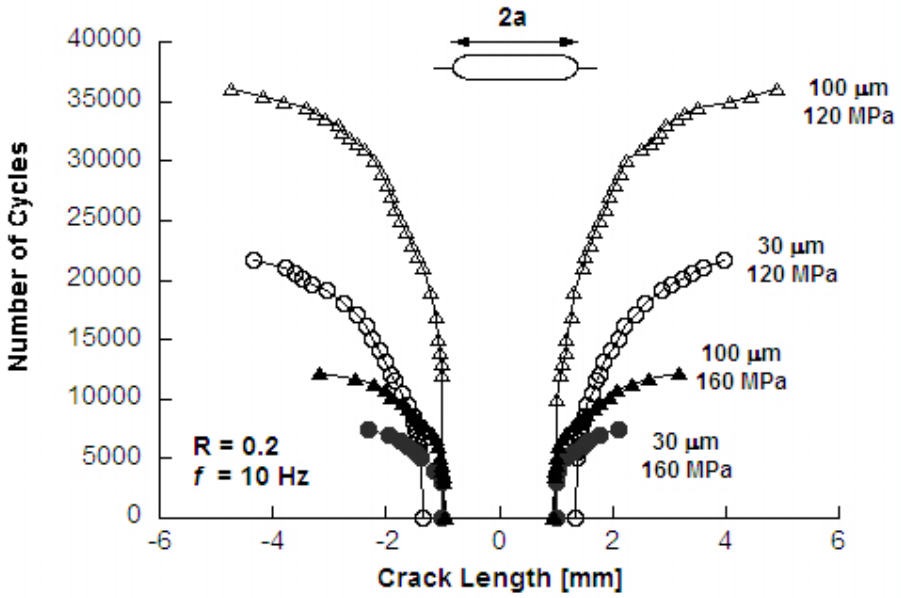


**Figure 4.7: Comparison between crack lengths and cycles for 30 μm and 100 μm thick foils**

For both stress levels examined, the 30 μm foils show a reduction in cycles to failure of approximately 40%. One possible mechanism that may give rise to this reduction in fatigue cycles stems from the larger effect plastic zone roughening would have on crack growth resistance. Consequently, Table 4.3 and 4.4 lists estimated plastic zone size and the ratio of the plastic zone size to thickness for fatigue tested foils. The specimen ID notation in the Tables 4.3 and 4.4 uses 'a' to correspond to the crack growth on the right side of the center-notch and 'b' to correspond to crack growth on the left side of the notch. In general, the ratio of plastic zone to specimen thickness is greater for the 30 μm thick foils than the 100 μm or 250 μm thick foils. The 30 μm thick foils averaged 3.0 plastic zone size to thickness, whereas the 100 μm and 250 μm thick foils only averaged 1.7.

**Table 4.3: Cyclic plastic zone size calculations for 30 μm thick foils**

| ID | Thickness [μm] | Loading Direction | $\sigma_y$ [MPa] | K [MPa√m] | $r_y$ [μm] | $r_y$/thickness |
|---|---|---|---|---|---|---|
| 1a | 30 | 0° | 308 | 14 | 84 | 2.8 |
| 1b | 30 | 0° | 308 | 15 | 94 | 3.1 |
| 2a | 30 | 0° | 308 | 14 | 77 | 2.6 |
| 2b | 30 | 0° | 308 | 13 | 67 | 2.2 |
| 3a | 30 | 0° | 308 | 13 | 72 | 2.4 |
| 3b | 30 | 0° | 308 | 14 | 78 | 2.6 |
| 4a | 30 | 0° | 308 | 14 | 80 | 2.7 |
| 4b | 30 | 0° | 308 | 15 | 89 | 3.0 |
| 5a | 30 | 90° | 265 | 16 | 142 | 4.7 |
| 5b | 30 | 90° | 265 | 15 | 135 | 4.5 |
| 6a | 30 | 90° | 265 | 12 | 88 | 2.9 |
| 6b | 30 | 90° | 265 | 14 | 108 | 3.6 |
| 7a | 30 | 90° | 265 | 10 | 57 | 1.9 |
| 7b | 30 | 90° | 265 | 12 | 77 | 2.6 |
| 8a | 30 | 90° | 265 | 13 | 89 | 3.0 |
| 8b | 30 | 90° | 265 | 12 | 83 | 2.8 |
| *Average* | | | | | | *3.0* |

**Table 4.4: Cyclic plastic zone size calculations for 100 μm and 250 μm thick foils**

| ID | Thickness [μm] | Loading Direction | $\sigma_y$ [MPa] | K [MPa√m] | $r_y$ [μm] | $r_y$/thickness |
|---|---|---|---|---|---|---|
| 1a | 100 | 0° | 244 | 14 | 137 | 1.4 |
| 1b | 100 | 0° | 244 | 17 | 195 | 2.0 |
| 2a | 100 | 0° | 244 | 14 | 133 | 1.3 |
| 2b | 100 | 0° | 244 | 15 | 141 | 1.4 |
| 3a | 100 | 0° | 244 | 16 | 163 | 1.6 |
| 3b | 100 | 0° | 244 | 16 | 169 | 1.7 |
| 4a | 100 | 0° | 244 | 16 | 170 | 1.7 |
| 4b | 100 | 0° | 244 | 16 | 161 | 1.6 |
| 5a | 100 | 0° | 244 | 19 | 229 | 2.3 |
| 5b | 100 | 0° | 244 | 17 | 197 | 2.0 |
| 6a | 100 | 0° | 244 | 16 | 174 | 1.7 |
| 6b | 100 | 0° | 244 | 16 | 174 | 1.7 |
| 7a | 250 | 0° | 170 | 11 | 155 | 1.6 |
| 7b | 250 | 0° | 170 | 10 | 143 | 1.8 |
| *Average 100 μm* | | | | | | *1.7* |

Figures 4.9 through 4.11 illustrate this relationship for the 100 μm foils at 90, 120 and 160 MPa; and Figure 4.8 for 250 μm thick foils at 70 MPa. Figures 4.12 and 4.13 show the crack growth rate ($da/dN$) versus stress intensity range ($\Delta K$) for 30 μm longitudinal and transverse specimens tested at maximum stresses of 120 and 160 MPa. For all specimens, orientations and stress levels examined, the crack growth data fits a Paris relationship (Eq. 1).

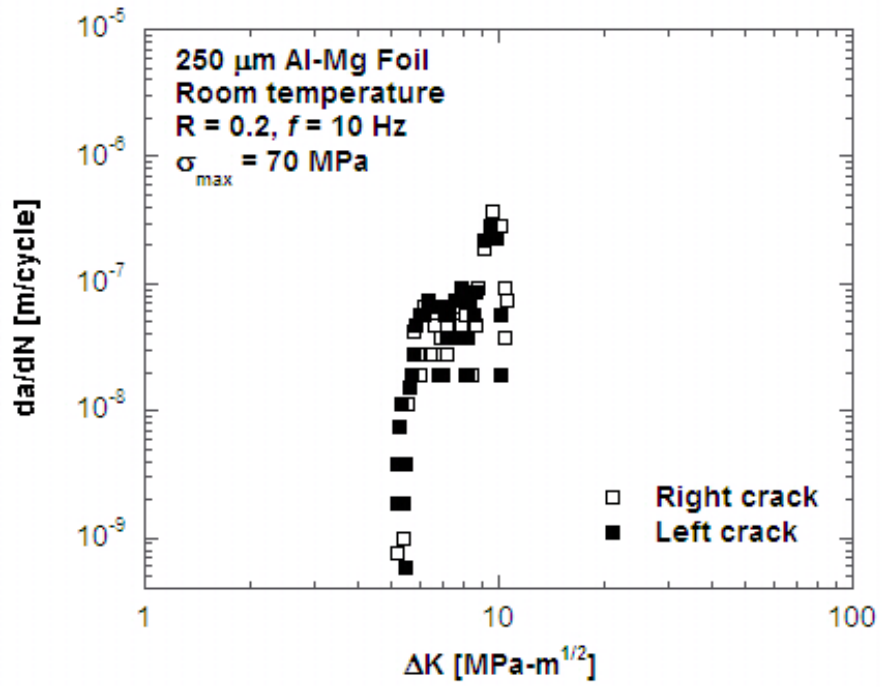


**Figure 4.8: Fatigue crack growth for 250 μm thick foil at 70 MPa**

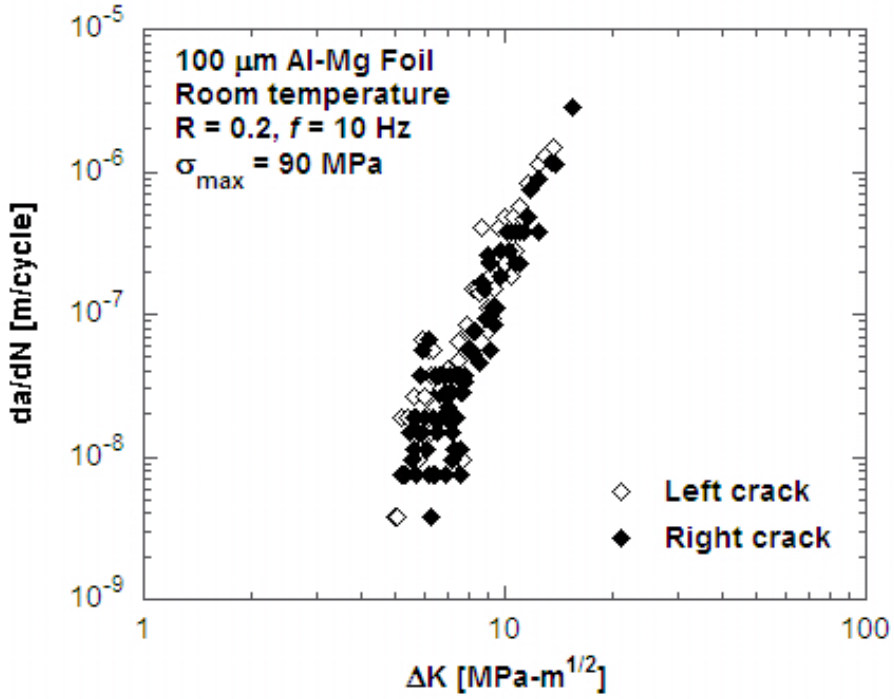


**Figure 4.9: Fatigue crack growth for 100 μm thick foils at 90 MPa**

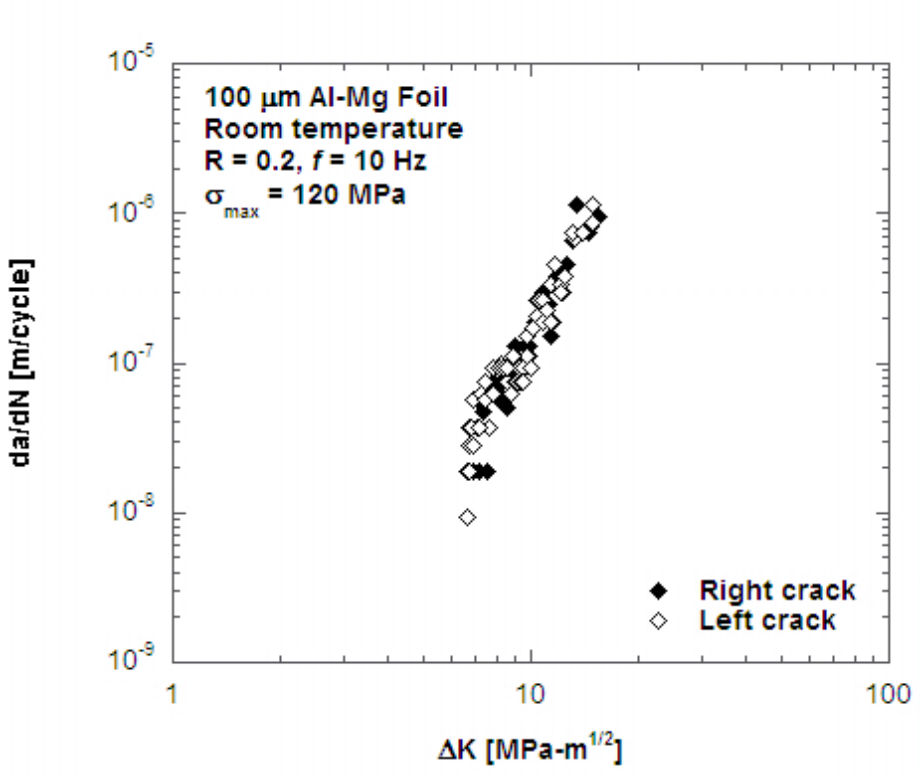


**Figure 4.10: Fatigue crack growth for 100 µm thick foils at 120 MPa**

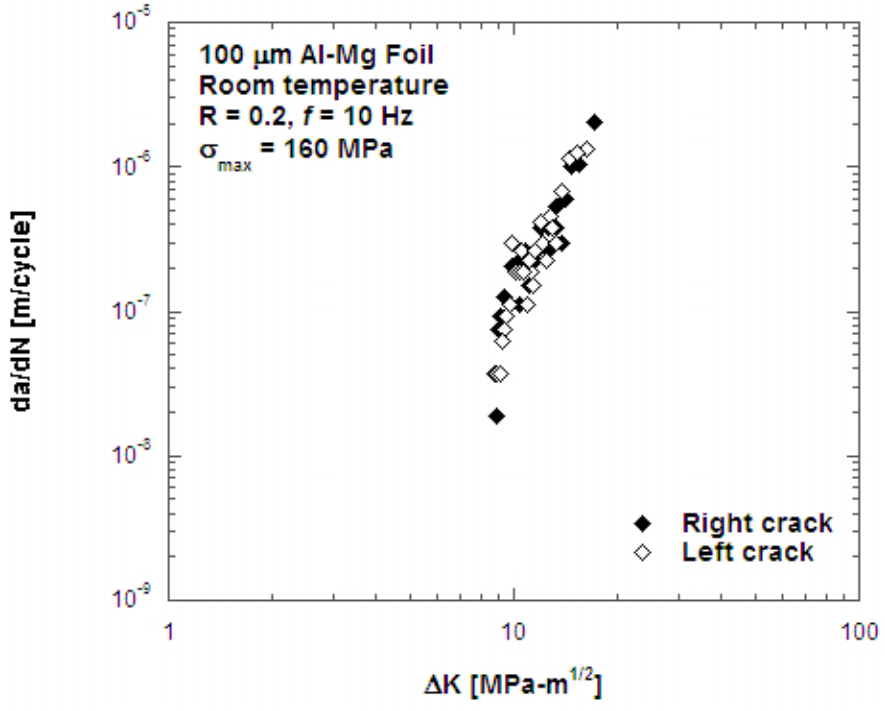


**Figure 4.11: Fatigue crack growth for 100 µm thick foils at 160 MPa**

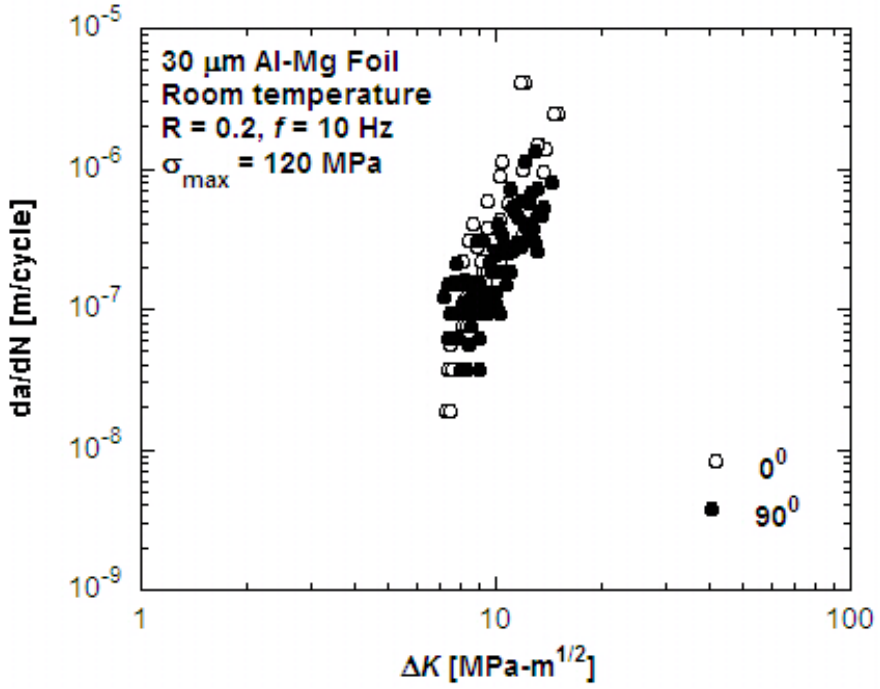


**Figure 4.12: Fatigue crack growth for 30 μm thick foils at 120 MPa**

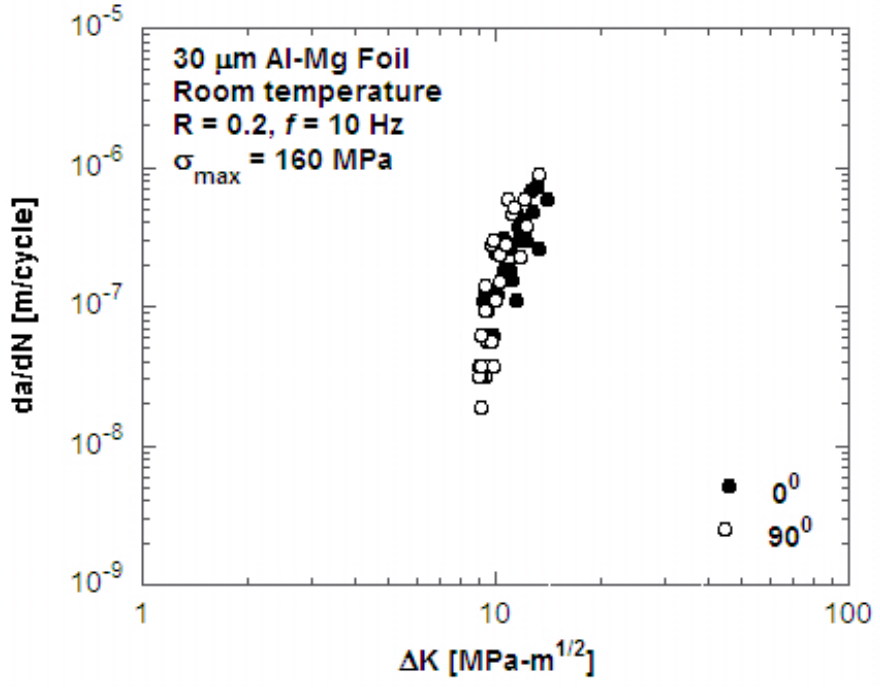


**Figure 4.13: Fatigue crack growth for 30 μm thick foils at 160 MPa**

For the 30 μm specimens (Figures 4.12 and 4.13), loading orientation had no significant influence on crack growth rate. At the two stress levels examined, the crack growth rate exponent, $m$, consistently remained in the range of 4 to 6. Figure 4.14 illustrates crack growth rate data for all specimen examined. The resulting data trends are similar for all thicknesses. A threshold region, $\Delta K_{th}$, becomes apparent around 5 and 7 MPa√m for the 100 μm and 250 μm foils ($da/dN < 10^{-8}$ m/cycle). There is a change in slope at approximately 8 MPa√m for the 30 μm, however, additional tests at lower levels would be required to determine the existence of a threshold region for crack growth.

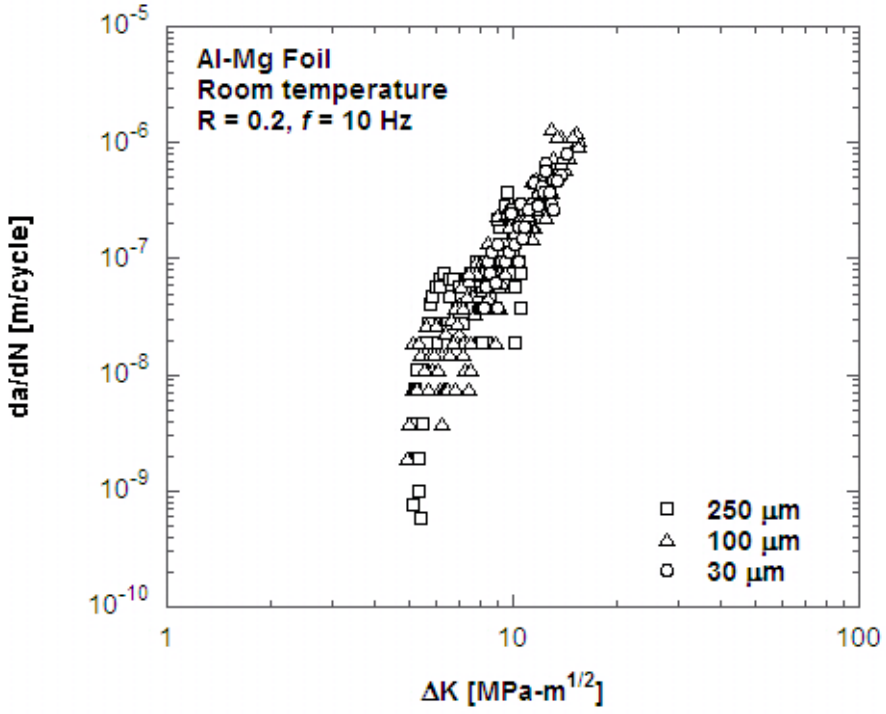


**Figure 4.14: Fatigue crack growth for all foil thicknesses examined**

SEM investigations of the fatigue fracture surface both near and far from the notch are shown in Figures 4.15 through 4.17 for all foil thicknesses. The 250 μm thick foil exhibited a 'stair-step' behavior characteristic of brittle fracture. Additional SEM micrographs can be found in Appendix D.

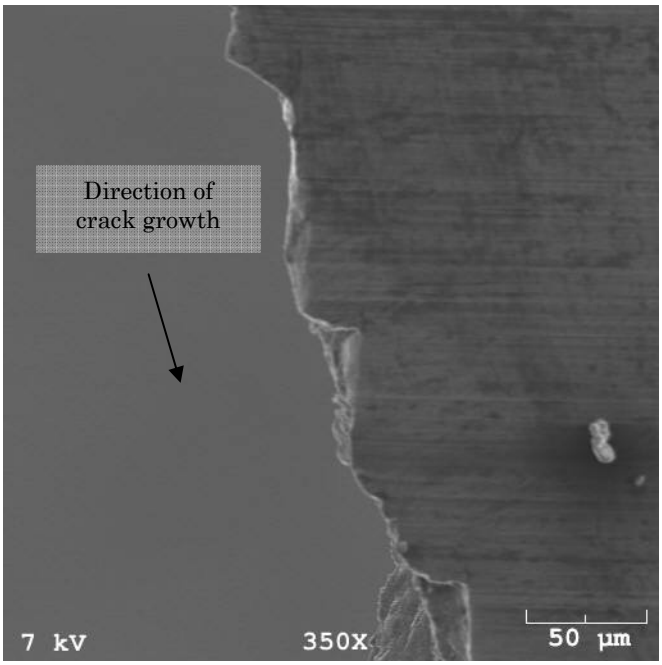


**Figure 4.15: SEM micrograph of 250 µm thick foil fracture surface exhibiting 'stair-step' behavior**

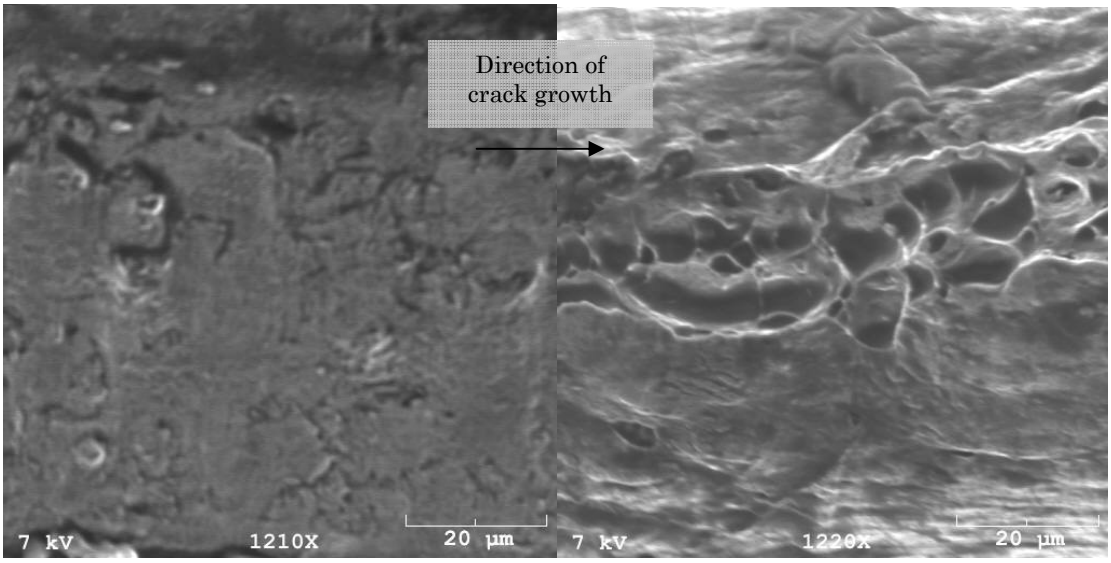


**Figure 4.16: SEM micrographs of 100 µm thick foil fracture surface *(left)* near notched region *(right)* far from notched region**

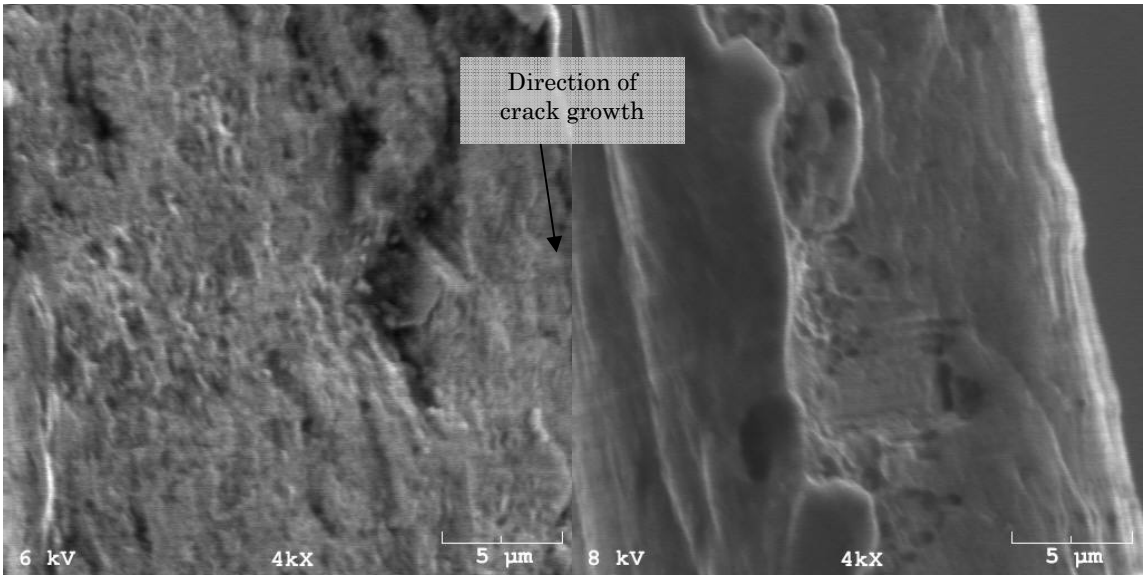


**Figure 4.17: SEM micrographs of 30 □m thick foil (longitudinally loaded) fracture surface *(left)* near notched region *(right)* far from the notched region**

Tables 4.4 and 4.5 compare values for the Paris relation constants ($C$ and $m$) for each thickness tested. The specimen ID notation uses 'a' to represent the crack growth on the right side of the center-notch of a specimen, and 'b' to represent the crack growth on the left side of the notch. Typical Al alloys have C values around $10^{-12}$ and $m$ values between about 3 and 4 [10]. Although the test average C values are in the same order of magnitude as literature values, it appears that crack growth rates are unstable in the foil regime, leading to rapid crack propagation and failure at lower loads. It should be noted that in the 250 µm thick foil case, the cracks arrested. Additionally, the crack on the right side of the notch of specimen 7 resulted in an unusually high $m$ value, however this specimen most likely contained data that fell into Region III or unstable rapid crack propagation just before failure, causing exceptionally high fatigue crack growth values and is thereby left out of the averaged value. Again, the plastic zone size in comparison to the specimen thickness may be the critical crack growth mechanism. The cyclic plastic zone size estimations are found for 30 µm thick in Table 4.3 and for 100 and 250 µm thick in Table 4.4. The plastic zone size ranged from approximately 130 to 470% of the total specimen thickness, generally increasing as specimen thickness decreased.

**Table 4.5: Fatigue test conditions and Paris relation constants for 30 μm thick foil**

| ID | Thickness [μm] | Loading Direction | $\Delta K_{min}$ [MPa-√m] | $\Delta K_{max}$ [MPa-√m] | $\Delta\sigma_{min}$ [MPa] | $\Delta\sigma_{max}$ [MPa] | Paris relation constants C | *m* | $N_T$ [x1000] | $R^2$ [%] |
|---|---|---|---|---|---|---|---|---|---|---|
| 1a | 30 | 0° | 8 | 14 | 24 | 120 | 1E-12 | 5.1 | 22 | 96 |
| 1b | 30 | 0° | 8 | 14 | 24 | 120 | 3E-12 | 4.7 | 22 | 88 |
| 2a | 30 | 0° | 7 | 13 | 23 | 120 | 2E-11 | 4.3 | 24 | 78 |
| 2b | 30 | 0° | 7 | 12 | 23 | 120 | 2E-11 | 4.1 | 24 | 79 |
| 3a | 30 | 0° | 9 | 13 | 32 | 160 | 2E-12 | 5.0 | 8 | 84 |
| 3b | 30 | 0° | 9 | 13 | 32 | 160 | 5E-12 | 4.6 | 8 | 67 |
| 4a | 30 | 0° | 10 | 13 | 33 | 160 | 5E-16 | 8.2 | 9 | 76 |
| 4b | 30 | 0° | 10 | 14 | 33 | 160 | 1E-11 | 4.0 | 9 | 98 |
| 5a | 30 | 90° | 8 | 15 | 24 | 120 | 2E-12 | 5.4 | 6 | 86 |
| 5b | 30 | 90° | 8 | 15 | 24 | 120 | 5E-12 | 5.0 | 6 | 58 |
| 6a | 30 | 90° | 7 | 12 | 24 | 120 | 6E-13 | 5.7 | 21 | 88 |
| 6b | 30 | 90° | 7 | 12 | 24 | 120 | 8E-13 | 5.5 | 21 | 84 |
| 7a | 30 | 90° | 9 | 10 | 33 | 160 | 2E-35 | 29 | 7 | 81 |
| 7b | 30 | 90° | 9 | 11 | 33 | 160 | 2E-16 | 8.9 | 7 | 85 |
| 8a | 30 | 90° | 9 | 12 | 32 | 160 | 7E-17 | 9.1 | 10 | 86 |
| 8b | 30 | 90° | 9 | 13 | 32 | 160 | 2E-17 | 9.6 | 10 | 79 |
| *Average 30 μm* | | 0° | 8.5 | 13.25 | 28 | 140 | 8E-12 | 5.0 | | |
| *Average 30 μm* | | 90° | 8.25 | 12.5 | 28.25 | 140 | 1E-12 | 7.0 | | |

**Table 4.6: Fatigue test conditions and Paris relation constants for 100 μm and 250 μm thick foils**

| ID | Thickness [μm] | Loading Direction | $\Delta K_{min}$ [MPa-√m] | $\Delta K_{max}$ [MPa-√m] | $\Delta\sigma_{min}$ [MPa] | $\Delta\sigma_{max}$ [MPa] | Paris relation constants C | *m* | $N_T$ [x1000] | $R^2$ [%] |
|---|---|---|---|---|---|---|---|---|---|---|
| 1a | 100 | 0° | 5 | 14 | 19 | 90 | 2E-12 | 5.1 | 82 | 87 |
| 1b | 100 | 0° | 5 | 15 | 19 | 90 | 3E-13 | 5.9 | 82 | 81 |
| 2a | 100 | 0° | 5 | 13 | 20 | 90 | 2E-12 | 5.0 | 474 | 95 |
| 2b | 100 | 0° | 5 | 14 | 20 | 90 | 3E-14 | 6.6 | 474 | 93 |
| 3a | 100 | 0° | 7 | 15 | 24 | 120 | 2E-11 | 4.0 | 45 | 91 |
| 3b | 100 | 0° | 7 | 15 | 24 | 120 | 1E-11 | 4.1 | 45 | 93 |
| 4a | 100 | 0° | 7 | 15 | 24 | 120 | 3E-12 | 4.6 | 37 | 89 |
| 4b | 100 | 0° | 7 | 15 | 24 | 120 | 7E-12 | 4.4 | 37 | 92 |
| 5a | 100 | 0° | 9 | 17 | 32 | 160 | 2E-12 | 4.8 | 11 | 89 |
| 5b | 100 | 0° | 9 | 16 | 32 | 160 | 2E-14 | 4.7 | 11 | 87 |
| 6a | 100 | 0° | 9 | 15 | 30 | 160 | 1E-13 | 5.9 | 13 | 85 |
| 6b | 100 | 0° | 9 | 15 | 30 | 160 | 3E-13 | 5.6 | 13 | 80 |
| 7a* | 250 | 0° | 2 | 11 | 16 | 70 | 1E-9 | 5.1 | 320 | 57 |
| 7b* | 250 | 0° | 2 | 10 | 16 | 70 | 2E-9 | 5.0 | 320 | 50 |
| *Average 100 μm* | | | 7 | 14 | 25 | 123 | 4E-12 | 5.0 | | |

** crack arrested*

The mechanisms responsible for these high crack growth rates are not yet fully understood. One possibility could be the formation of a large plastic zone ahead of the crack tip during cycling, resulting in plastic thinning ahead of the crack tip. However, direct examination of the fracture surface in the SEM showed no evidence of plastic thinning. Another possible mechanism is surface roughening ahead of the growing crack. For thick materials, surface roughening would affect only the near-surface regions and although it could promote crack initiation, it would have a smaller influence on overall fatigue life. Conversely for foils, roughening would consume a larger percentage of the cross section; therefore even minor surface roughening on the surface of a foil specimen could have a significant influence on crack growth behavior. It should be noted that at the lowest stress examined for the 250 μm thick foil, 70 MPa, the crack arrested as shown in Figure 4.18.

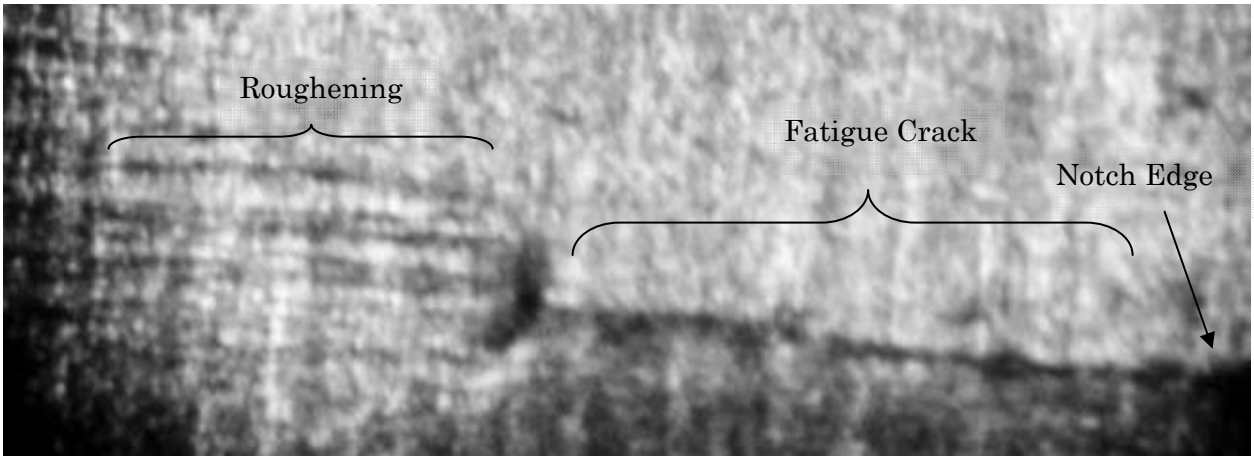


**Figure 4.18: Photomicrography of crack arresting on 250 μm foil fatigued at 70 MPa**

# CHAPTER 5

# CONCLUDING REMARKS

## *5.1 Conclusions*

Based on experimental results obtained from room temperature monotonic tensile, fracture toughness and fatigue crack growth testing of 30 μm, 100 μm and 250 μm thick Al-Mg foils, the following conclusions can be made.

1. Typical tensile strengths for the foils were approximately 300 MPa to 350 MPa. The foils showed limited ductility during monotonic tensile testing, with nominal failure strains below 4% for all thicknesses examined. There was absence of necking at failure for all specimens.

2. In all cases, fracture toughness of the foil specimens was lower than the plane strain fracture toughness of similar aluminum alloys. Additionally, for the range of thicknesses examined fracture toughness was not influenced by specimen thickness. The fracture toughness of the foils studied ranged between 13 and 17 MPa$\sqrt{m}$. The fracture surface was flat, indicative of a low toughness material tested under plane stress conditions.

3. For all foil thicknesses, the fatigue crack growth data could be modeled by a Paris relationship between fatigue crack growth rate and the stress intensity range. For all foil thicknesses, the crack growth rate exponents were higher, consistently averaging between 5 and 7, than what is commonly observed for Mode I crack growth in aluminum alloys with greater thickness.

4. For the 30 μm thick foils, there was no apparent influence of orientation on crack growth rate as can be seen by the similarity in test results of longitudinal and transverse specimen loading.

5. Potential mechanisms influencing the high fatigue crack growth rates in thin metallic foils include: loss of constraint, low fracture toughness, the formation of a large plastic zone ahead of the crack tip, and possible surface roughening within the plastic zone (a through-thickness effect for thin foils).

### *5.2 Recommendations*

From the high fatigue crack growth rates determined in this analysis, coupled with the previously established high fatigue crack growth rates in nickel-base alloys [30], the effect of thickness on the fatigue crack growth of foils is apparent. Further investigation is needed to thoroughly examine the entire foil regime and characterize the thickness effect; however this thesis begins to illuminate a significant and relatively unexplored concern that arises in numerous engineering applications.

The most evident next step for aerospace structures would be to examine these foils as part of a honeycomb sandwich and determine the fatigue and fracture characteristic differences with additional core through-thickness and material. Additionally, factors such as material processing, grain structure and thermal effects need to be considered to fully understand and expand on this phenomenon. If indeed the thickness effect is inherent to the foil geometry and thereby unavoidable, design workarounds must be established.

In the case of foil facesheets used in thermal protection systems, one idea would be to force the core of the honeycomb structure to play a role in deterring crack growth. Two potential ways to do this would be to either impregnate the honeycomb core with an intrinsically ductile material, or create stronger, thicker

ribbon joints for the cracks to encounter. Nonetheless, the potential of thin metallic films and foils in practical engineering applications is immense given the understanding that fatigue and fracture concerns are a function of the material thickness.

# APPENDIX A

# TENSILE TESTS

Specimen ID: Al-Mg-30-14-L
Loading: Longitudinal
Thickness: 30 μm
Width: 12.24 mm
Gauge Length: 66.5 mm
Loading Rate: 0.015 kN/s

| Load [kN] | δ [mm] | Load [kN] | δ [mm] | Load [kN] | δ [mm] | Load [kN] | δ [mm] | Load [kN] | δ [mm] |
|---|---|---|---|---|---|---|---|---|---|
| 0.0177 | 0 | 0.0429 | 0.0695 | 0.0792 | 0.1763 | 0.1123 | 0.2903 | 0.1167 | 0.7717 |
| 0.0178 | 1E-04 | 0.0438 | 0.0727 | 0.0802 | 0.1792 | 0.1126 | 0.2938 | 0.117 | 0.793 |
| 0.0179 | -0.0003 | 0.0448 | 0.0753 | 0.0813 | 0.1826 | 0.1126 | 0.2977 | 0.117 | 0.8154 |
| 0.0177 | -1E-04 | 0.0458 | 0.0778 | 0.0822 | 0.1853 | 0.1128 | 0.303 | 0.1172 | 0.8375 |
| 0.0175 | -1E-04 | 0.0468 | 0.0806 | 0.0831 | 0.1877 | 0.113 | 0.3084 | 0.1174 | 0.8633 |
| 0.0179 | 0.0004 | 0.0478 | 0.0835 | 0.0841 | 0.1911 | 0.1131 | 0.3144 | 0.1171 | 0.8865 |
| 0.0176 | 0.0003 | 0.0485 | 0.0858 | 0.0851 | 0.1941 | 0.1133 | 0.3203 | 0.1174 | 0.9112 |
| 0.0178 | 0.0002 | 0.0494 | 0.0886 | 0.086 | 0.1967 | 0.1135 | 0.3265 | | |
| 0.0182 | 0.0017 | 0.0505 | 0.092 | 0.0869 | 0.1996 | 0.1136 | 0.3335 | | |
| 0.0188 | 0.0017 | 0.0515 | 0.0941 | 0.0877 | 0.202 | 0.1138 | 0.3403 | | |
| 0.0193 | 0.0031 | 0.0524 | 0.097 | 0.0886 | 0.2048 | 0.1141 | 0.3479 | | |
| 0.0199 | 0.005 | 0.0534 | 0.1001 | 0.0896 | 0.2076 | 0.114 | 0.3538 | | |
| 0.0205 | 0.0066 | 0.0544 | 0.1032 | 0.0906 | 0.2101 | 0.1144 | 0.3628 | | |
| 0.0212 | 0.0084 | 0.0555 | 0.106 | 0.0915 | 0.2139 | 0.1145 | 0.3712 | | |
| 0.0219 | 0.0101 | 0.0564 | 0.1089 | 0.0925 | 0.2161 | 0.1146 | 0.3804 | | |
| 0.0227 | 0.0123 | 0.0573 | 0.1115 | 0.0935 | 0.2191 | 0.1148 | 0.3901 | | |
| 0.0235 | 0.014 | 0.0583 | 0.114 | 0.0945 | 0.2223 | 0.115 | 0.4 | | |
| 0.0242 | 0.0165 | 0.0593 | 0.1173 | 0.0955 | 0.226 | 0.1151 | 0.4106 | | |
| 0.0248 | 0.0183 | 0.0603 | 0.1195 | 0.0965 | 0.2285 | 0.1152 | 0.4212 | | |
| 0.0257 | 0.0208 | 0.0612 | 0.1229 | 0.0974 | 0.231 | 0.1153 | 0.4326 | | |
| 0.0264 | 0.0229 | 0.0619 | 0.1249 | 0.0984 | 0.2342 | 0.1153 | 0.4442 | | |
| 0.0273 | 0.025 | 0.0629 | 0.1276 | 0.0993 | 0.2368 | 0.1154 | 0.4569 | | |
| 0.0281 | 0.0273 | 0.0639 | 0.1309 | 0.1 | 0.2389 | 0.1156 | 0.4699 | | |
| 0.0289 | 0.0299 | 0.0649 | 0.1334 | 0.101 | 0.2425 | 0.1156 | 0.4835 | | |
| 0.0299 | 0.0322 | 0.066 | 0.1362 | 0.1019 | 0.2448 | 0.1161 | 0.4969 | | |
| 0.0308 | 0.0349 | 0.067 | 0.1391 | 0.1028 | 0.248 | 0.1159 | 0.5074 | | |
| 0.0317 | 0.037 | 0.0679 | 0.1423 | 0.1038 | 0.2509 | 0.1161 | 0.5215 | | |
| 0.0325 | 0.04 | 0.0689 | 0.1448 | 0.1047 | 0.2543 | 0.116 | 0.536 | | |
| 0.0334 | 0.0425 | 0.0698 | 0.1487 | 0.1056 | 0.2567 | 0.116 | 0.5528 | | |
| 0.0345 | 0.0449 | 0.0708 | 0.1513 | 0.1065 | 0.26 | 0.1162 | 0.5683 | | |
| 0.0355 | 0.048 | 0.0718 | 0.1544 | 0.1074 | 0.2633 | 0.1161 | 0.5857 | | |
| 0.0362 | 0.0498 | 0.0728 | 0.1569 | 0.1082 | 0.2659 | 0.1162 | 0.6023 | | |
| 0.0372 | 0.0533 | 0.0737 | 0.1595 | 0.1091 | 0.2693 | 0.1163 | 0.6197 | | |
| 0.038 | 0.0556 | 0.0747 | 0.1631 | 0.1098 | 0.272 | 0.1163 | 0.6384 | | |
| 0.0391 | 0.0575 | 0.0755 | 0.1646 | 0.1105 | 0.2755 | 0.1163 | 0.6571 | | |
| 0.04 | 0.0609 | 0.0763 | 0.1675 | 0.1111 | 0.2794 | 0.1164 | 0.6759 | | |
| 0.0409 | 0.0632 | 0.0774 | 0.1704 | 0.1115 | 0.2818 | 0.1166 | 0.6949 | | |
| 0.0419 | 0.0669 | 0.0782 | 0.174 | 0.112 | 0.2863 | 0.1165 | 0.7149 | | |

Specimen ID: Al-Mg-30-15-T
Loading: Transverse
Thickness: 30 μm
Width: 12.92 mm
Gauge Length: 66.71 mm
Loading Rate: 0.015 kN/s

| Load [kN] | δ [mm] | Load [kN] | δ [mm] | Load [kN] | δ [mm] | Load [kN] | δ [mm] | Load [kN] | δ [mm] |
|---|---|---|---|---|---|---|---|---|---|
| 0.0191 | 0 | 0.0399 | 0.0515 | 0.0644 | 0.114 | 0.0883 | 0.1791 | 0.1099 | 0.2576 |
| 0.0194 | 0.0003 | 0.0406 | 0.0536 | 0.0651 | 0.1164 | 0.089 | 0.1815 | 0.1104 | 0.26 |
| 0.0197 | 0.0018 | 0.0413 | 0.0547 | 0.0658 | 0.1182 | 0.0894 | 0.183 | 0.111 | 0.2636 |
| 0.02 | 0.0021 | 0.042 | 0.0565 | 0.0664 | 0.1206 | 0.09 | 0.1845 | 0.1114 | 0.2654 |
| 0.0203 | 0.003 | 0.0426 | 0.0586 | 0.067 | 0.1218 | 0.0908 | 0.1857 | 0.1119 | 0.2672 |
| 0.0207 | 0.0042 | 0.0432 | 0.0601 | 0.0678 | 0.1233 | 0.0913 | 0.1878 | 0.1124 | 0.2702 |
| 0.0212 | 0.0042 | 0.0437 | 0.0616 | 0.0682 | 0.1248 | 0.0919 | 0.1908 | 0.1129 | 0.2729 |
| 0.0217 | 0.0054 | 0.0445 | 0.0637 | 0.0689 | 0.1263 | 0.0923 | 0.1908 | 0.1134 | 0.2762 |
| 0.0221 | 0.0065 | 0.0452 | 0.0649 | 0.0696 | 0.1278 | 0.0929 | 0.1926 | 0.1139 | 0.2789 |
| 0.0224 | 0.0068 | 0.0458 | 0.0669 | 0.0702 | 0.1296 | 0.0936 | 0.1945 | 0.1143 | 0.2819 |
| 0.023 | 0.0092 | 0.0465 | 0.0687 | 0.0709 | 0.1311 | 0.0942 | 0.1969 | 0.1149 | 0.2855 |
| 0.0235 | 0.0098 | 0.0472 | 0.0702 | 0.0716 | 0.1329 | 0.0948 | 0.199 | 0.1153 | 0.2883 |
| 0.024 | 0.011 | 0.0477 | 0.0717 | 0.0721 | 0.135 | 0.0954 | 0.2005 | 0.1158 | 0.2916 |
| 0.0245 | 0.0134 | 0.0484 | 0.0735 | 0.0727 | 0.1365 | 0.0959 | 0.2023 | 0.1163 | 0.2955 |
| 0.0252 | 0.014 | 0.049 | 0.0753 | 0.0733 | 0.1389 | 0.0965 | 0.2035 | 0.1167 | 0.2988 |
| 0.0256 | 0.0155 | 0.0497 | 0.0768 | 0.0739 | 0.1401 | 0.0972 | 0.2053 | 0.1172 | 0.3015 |
| 0.0262 | 0.0182 | 0.0502 | 0.0782 | 0.0747 | 0.1419 | 0.0978 | 0.2077 | 0.1177 | 0.3051 |
| 0.0269 | 0.0185 | 0.051 | 0.08 | 0.0751 | 0.1431 | 0.0984 | 0.2098 | 0.118 | 0.3091 |
| 0.0274 | 0.02 | 0.0516 | 0.0809 | 0.0758 | 0.1446 | 0.099 | 0.2119 | 0.1185 | 0.3127 |
| 0.0281 | 0.0215 | 0.0522 | 0.0839 | 0.0764 | 0.1461 | 0.0994 | 0.2138 | 0.1189 | 0.3172 |
| 0.0286 | 0.023 | 0.0529 | 0.0854 | 0.0771 | 0.1482 | 0.1 | 0.2159 | 0.1193 | 0.3199 |
| 0.0292 | 0.0236 | 0.0536 | 0.0866 | 0.0777 | 0.1497 | 0.1007 | 0.2183 | 0.1197 | 0.3242 |
| 0.0298 | 0.0257 | 0.0541 | 0.0881 | 0.0784 | 0.1515 | 0.1012 | 0.2201 | 0.1201 | 0.3284 |
| 0.0305 | 0.0275 | 0.0548 | 0.0899 | 0.0789 | 0.1533 | 0.1017 | 0.2225 | 0.1204 | 0.3323 |
| 0.0311 | 0.0293 | 0.0555 | 0.0919 | 0.0796 | 0.1551 | 0.1022 | 0.2237 | 0.1209 | 0.3372 |
| 0.0317 | 0.0304 | 0.0561 | 0.0934 | 0.0802 | 0.1569 | 0.1028 | 0.2255 | 0.1212 | 0.3411 |
| 0.0322 | 0.0322 | 0.0568 | 0.0946 | 0.0808 | 0.1581 | 0.1034 | 0.2283 | 0.1215 | 0.3454 |
| 0.033 | 0.034 | 0.0574 | 0.0964 | 0.0815 | 0.1602 | 0.104 | 0.2306 | 0.1219 | 0.3502 |
| 0.0336 | 0.0349 | 0.0581 | 0.0979 | 0.0822 | 0.162 | 0.1046 | 0.2327 | 0.1223 | 0.3554 |
| 0.0343 | 0.0364 | 0.0586 | 0.1003 | 0.0826 | 0.1635 | 0.1051 | 0.236 | 0.1226 | 0.3605 |
| 0.0349 | 0.0388 | 0.0593 | 0.1027 | 0.0833 | 0.1647 | 0.1055 | 0.2372 | 0.1231 | 0.3657 |
| 0.0355 | 0.0397 | 0.06 | 0.103 | 0.0839 | 0.168 | 0.1062 | 0.2399 | 0.1233 | 0.3696 |
| 0.0362 | 0.0418 | 0.0606 | 0.1054 | 0.0845 | 0.1683 | 0.1068 | 0.2429 | 0.1236 | 0.3748 |
| 0.0368 | 0.0433 | 0.0611 | 0.1066 | 0.0853 | 0.1707 | 0.1074 | 0.2447 | 0.1239 | 0.3809 |
| 0.0374 | 0.0461 | 0.0618 | 0.1081 | 0.0856 | 0.1719 | 0.1079 | 0.2471 | 0.1242 | 0.3858 |
| 0.0381 | 0.047 | 0.0625 | 0.1093 | 0.0863 | 0.1737 | 0.1084 | 0.2504 | 0.1245 | 0.3918 |
| 0.0387 | 0.0488 | 0.0632 | 0.1113 | 0.0871 | 0.1752 | 0.1089 | 0.2522 | 0.1248 | 0.3979 |
| 0.0393 | 0.05 | 0.0638 | 0.1131 | 0.0877 | 0.1776 | 0.1094 | 0.2549 | 0.125 | 0.4025 |

Specimen ID: Al-Mg-30-15-T
Continued from previous

| Load [kN] | δ [mm] | Load [kN] | δ [mm] |
|---|---|---|---|
| 0.1254 | 0.4089 | 0.1307 | 0.804 |
| 0.1256 | 0.4156 | 0.1309 | 0.821 |
| 0.1258 | 0.422 | 0.1309 | 0.8373 |
| 0.1261 | 0.4292 | 0.131 | 0.855 |
| 0.1264 | 0.4344 | 0.1308 | 0.8721 |
| 0.1264 | 0.4413 | 0.131 | 0.8898 |
| 0.1268 | 0.4495 | 0.1309 | 0.9038 |
| 0.127 | 0.4565 | 0.1309 | 0.9213 |
| 0.1272 | 0.4644 | 0.131 | 0.94 |
| 0.1274 | 0.4723 | 0.1309 | 0.9591 |
| 0.1276 | 0.4781 | 0.131 | 0.9784 |
| 0.1277 | 0.4866 | 0.1311 | 0.9933 |
| 0.1279 | 0.4948 | 0.1311 | 1.0129 |
| 0.1281 | 0.5034 | 0.1312 | 1.0326 |
| 0.1282 | 0.5128 | 0.1311 | 1.0533 |
| 0.1284 | 0.5214 | 0.1312 | 1.073 |
| 0.1285 | 0.5293 | 0.1311 | 1.096 |
| 0.1287 | 0.5388 | 0.1312 | 1.1127 |
| 0.1288 | 0.5483 | 0.1313 | 1.1338 |
| 0.1289 | 0.5581 | 0.1314 | 1.1559 |
| 0.1291 | 0.5692 | 0.1313 | 1.1783 |
| 0.1292 | 0.5787 | 0.1315 | 1.201 |
| 0.1293 | 0.5904 | 0.1315 | 1.2246 |
| 0.1294 | 0.6019 | 0.1315 | 1.242 |
| 0.1296 | 0.6138 | 0.1314 | 1.2658 |
| 0.1297 | 0.626 | 0.1316 | 1.2899 |
| 0.1297 | 0.6395 | 0.1317 | 1.3134 |
| 0.1299 | 0.649 | 0.1316 | 1.3389 |
| 0.13 | 0.6619 | 0.1324 | 1.358 |
| 0.1301 | 0.6742 | 0.1328 | 1.3834 |
| 0.1302 | 0.688 | 0.1324 | 1.4091 |
| 0.1302 | 0.7019 | 0.1323 | 1.4353 |
| 0.1303 | 0.7164 | 0.1322 | 1.4618 |
| 0.1304 | 0.7288 | 0.1325 | 1.4913 |
| 0.1304 | 0.7433 | 0.1324 | 1.5122 |
| 0.1306 | 0.7591 | 0.1323 | 1.5405 |
| 0.1306 | 0.7743 | 0.1323 | 1.5689 |
| 0.1306 | 0.7904 | 0.1325 | 1.5985 |
| | | 0.1326 | 1.6262 |
| | | 0.1331 | 1.6565 |

Specimen ID: Al-Mg-100-13
Loading: Longitudinal
Thickness: 100 μm
Width: 13.5 mm
Gauge Length: 67.85 mm
Loading Rate: 0.015 kN/s

| Load [kN] | δ [mm] | Load [kN] | δ [mm] | Load [kN] | δ [mm] | Load [kN] | δ [mm] | Load [kN] | δ [mm] |
|---|---|---|---|---|---|---|---|---|---|
| 0.0193 | 0 | 0.0537 | 0.0298 | 0.0885 | 0.0601 | 0.1234 | 0.092 | 0.1583 | 0.1241 |
| 0.0199 | 0.0003 | 0.0546 | 0.03 | 0.0894 | 0.0614 | 0.1243 | 0.0932 | 0.1593 | 0.1247 |
| 0.0208 | 0.0011 | 0.0555 | 0.0311 | 0.0902 | 0.0618 | 0.1253 | 0.094 | 0.1602 | 0.1255 |
| 0.0216 | 0.0015 | 0.0566 | 0.032 | 0.0913 | 0.0623 | 0.1263 | 0.0941 | 0.1611 | 0.1271 |
| 0.0226 | 0.0023 | 0.0572 | 0.0328 | 0.0922 | 0.0637 | 0.1272 | 0.0954 | 0.1621 | 0.1271 |
| 0.0232 | 0.0025 | 0.0581 | 0.0333 | 0.0932 | 0.0644 | 0.1281 | 0.096 | 0.1627 | 0.128 |
| 0.024 | 0.0038 | 0.059 | 0.034 | 0.094 | 0.0653 | 0.1292 | 0.0968 | 0.1638 | 0.1294 |
| 0.0249 | 0.0042 | 0.06 | 0.0352 | 0.0951 | 0.0661 | 0.1301 | 0.0981 | 0.1646 | 0.1298 |
| 0.0259 | 0.0052 | 0.0608 | 0.0354 | 0.0959 | 0.0668 | 0.1308 | 0.0988 | 0.1656 | 0.1306 |
| 0.0268 | 0.0059 | 0.0619 | 0.0361 | 0.0969 | 0.0682 | 0.1316 | 0.0992 | 0.1665 | 0.1315 |
| 0.0277 | 0.0065 | 0.0628 | 0.0374 | 0.0978 | 0.0689 | 0.1325 | 0.1002 | 0.1675 | 0.1323 |
| 0.0286 | 0.0071 | 0.0639 | 0.0388 | 0.0988 | 0.0698 | 0.1335 | 0.1006 | 0.1684 | 0.1329 |
| 0.0296 | 0.0078 | 0.0647 | 0.0388 | 0.0995 | 0.0701 | 0.1344 | 0.1019 | 0.1693 | 0.134 |
| 0.0305 | 0.009 | 0.0657 | 0.0397 | 0.1003 | 0.0714 | 0.1354 | 0.1025 | 0.1703 | 0.1351 |
| 0.0315 | 0.0096 | 0.0664 | 0.0404 | 0.1014 | 0.0713 | 0.1362 | 0.1036 | 0.1711 | 0.1357 |
| 0.0325 | 0.0104 | 0.0673 | 0.0419 | 0.1023 | 0.0724 | 0.1372 | 0.1047 | 0.1722 | 0.1358 |
| 0.0332 | 0.0117 | 0.0683 | 0.0424 | 0.1032 | 0.0734 | 0.1382 | 0.1053 | 0.1727 | 0.137 |
| 0.034 | 0.0122 | 0.0692 | 0.0429 | 0.1041 | 0.0743 | 0.1392 | 0.1065 | 0.1737 | 0.1379 |
| 0.035 | 0.0131 | 0.0702 | 0.0438 | 0.1051 | 0.0755 | 0.1401 | 0.1073 | 0.1746 | 0.1387 |
| 0.0359 | 0.0137 | 0.071 | 0.0445 | 0.1059 | 0.0762 | 0.1409 | 0.108 | 0.1756 | 0.14 |
| 0.0368 | 0.0145 | 0.0721 | 0.046 | 0.1069 | 0.077 | 0.1417 | 0.1084 | 0.1765 | 0.1405 |
| 0.0377 | 0.0153 | 0.0729 | 0.0466 | 0.108 | 0.0777 | 0.1426 | 0.1091 | 0.1776 | 0.1417 |
| 0.0387 | 0.0163 | 0.074 | 0.0474 | 0.1089 | 0.0789 | 0.1436 | 0.11 | 0.1785 | 0.1426 |
| 0.0396 | 0.0176 | 0.0748 | 0.0478 | 0.1095 | 0.0795 | 0.1445 | 0.1108 | 0.1793 | 0.1434 |
| 0.0407 | 0.018 | 0.0757 | 0.0491 | 0.1105 | 0.0799 | 0.1455 | 0.1118 | 0.1804 | 0.1447 |
| 0.0414 | 0.0187 | 0.0767 | 0.0497 | 0.1115 | 0.0813 | 0.1463 | 0.1127 | 0.1813 | 0.1449 |
| 0.0425 | 0.019 | 0.0773 | 0.0507 | 0.1124 | 0.0819 | 0.1473 | 0.1137 | 0.1822 | 0.1461 |
| 0.0435 | 0.0201 | 0.0784 | 0.0512 | 0.1134 | 0.0826 | 0.1483 | 0.1147 | 0.1831 | 0.1464 |
| 0.0442 | 0.0206 | 0.0794 | 0.0525 | 0.1144 | 0.0836 | 0.1492 | 0.1156 | 0.1841 | 0.1474 |
| 0.0449 | 0.022 | 0.0802 | 0.0528 | 0.1152 | 0.0847 | 0.1502 | 0.116 | 0.1847 | 0.1487 |
| 0.0461 | 0.0226 | 0.0813 | 0.0535 | 0.1162 | 0.0856 | 0.1511 | 0.1172 | 0.1856 | 0.1494 |
| 0.047 | 0.024 | 0.0822 | 0.0545 | 0.1172 | 0.0861 | 0.1521 | 0.118 | 0.1866 | 0.1498 |
| 0.048 | 0.0242 | 0.083 | 0.0564 | 0.118 | 0.0874 | 0.1527 | 0.1188 | 0.1875 | 0.1508 |
| 0.0488 | 0.0256 | 0.084 | 0.0557 | 0.1191 | 0.0876 | 0.1537 | 0.1193 | 0.1886 | 0.1518 |
| 0.0498 | 0.0259 | 0.0851 | 0.0569 | 0.12 | 0.0889 | 0.1546 | 0.1208 | 0.1894 | 0.1528 |
| 0.0507 | 0.0265 | 0.0858 | 0.0581 | 0.1207 | 0.0895 | 0.1554 | 0.1216 | 0.1903 | 0.1542 |
| 0.0518 | 0.0282 | 0.0868 | 0.0586 | 0.1215 | 0.0908 | 0.1565 | 0.1224 | 0.1914 | 0.1539 |
| 0.0527 | 0.0289 | 0.0878 | 0.0602 | 0.1226 | 0.0911 | 0.1574 | 0.123 | 0.1921 | 0.1551 |

Specimen ID: Al-Mg-100-13
Continued from previous

| Load [kN] | δ [mm] | Load [kN] | δ [mm] | Load [kN] | δ [mm] | Load [kN] | δ [mm] | Load [kN] | δ [mm] |
|---|---|---|---|---|---|---|---|---|---|
| 0.1931 | 0.1559 | 0.2276 | 0.1889 | 0.2622 | 0.2228 | 0.2969 | 0.2595 | 0.3306 | 0.306 |
| 0.194 | 0.1568 | 0.2286 | 0.1893 | 0.2633 | 0.2241 | 0.2977 | 0.2606 | 0.3315 | 0.3072 |
| 0.1948 | 0.1577 | 0.2295 | 0.1899 | 0.2643 | 0.2244 | 0.2987 | 0.2617 | 0.3323 | 0.3089 |
| 0.1957 | 0.1585 | 0.2303 | 0.1914 | 0.2651 | 0.225 | 0.2994 | 0.2622 | 0.3333 | 0.31 |
| 0.1966 | 0.1593 | 0.2313 | 0.192 | 0.266 | 0.2265 | 0.3003 | 0.2637 | 0.3342 | 0.3114 |
| 0.1976 | 0.1601 | 0.2323 | 0.193 | 0.2667 | 0.2273 | 0.3011 | 0.2641 | 0.335 | 0.3136 |
| 0.1984 | 0.1615 | 0.2332 | 0.1942 | 0.2676 | 0.2285 | 0.3021 | 0.2657 | 0.3359 | 0.3151 |
| 0.1995 | 0.1615 | 0.2342 | 0.1947 | 0.2685 | 0.229 | 0.3031 | 0.2667 | 0.3369 | 0.3171 |
| 0.2003 | 0.1619 | 0.235 | 0.196 | 0.2694 | 0.2301 | 0.3039 | 0.2678 | 0.3378 | 0.3181 |
| 0.2012 | 0.1634 | 0.2357 | 0.1959 | 0.2704 | 0.2306 | 0.3049 | 0.2689 | 0.3387 | 0.3197 |
| 0.2021 | 0.164 | 0.2368 | 0.1977 | 0.2713 | 0.2316 | 0.3059 | 0.2702 | 0.3395 | 0.3214 |
| 0.2031 | 0.1649 | 0.2375 | 0.1988 | 0.2722 | 0.2326 | 0.3069 | 0.2719 | 0.3404 | 0.3231 |
| 0.2038 | 0.1661 | 0.2385 | 0.1986 | 0.2733 | 0.2339 | 0.3078 | 0.2731 | 0.3411 | 0.3245 |
| 0.2047 | 0.1669 | 0.2395 | 0.1999 | 0.2741 | 0.2349 | 0.3086 | 0.2742 | 0.3419 | 0.3262 |
| 0.2057 | 0.1675 | 0.2403 | 0.2006 | 0.2751 | 0.2357 | 0.3095 | 0.2748 | 0.3428 | 0.3274 |
| 0.2067 | 0.1682 | 0.2415 | 0.2017 | 0.276 | 0.237 | 0.3103 | 0.2763 | 0.3437 | 0.3297 |
| 0.2075 | 0.169 | 0.2424 | 0.2026 | 0.277 | 0.2377 | 0.3111 | 0.2772 | 0.3444 | 0.3316 |
| 0.2086 | 0.1705 | 0.2433 | 0.2038 | 0.2779 | 0.239 | 0.312 | 0.2783 | 0.3453 | 0.3335 |
| 0.2095 | 0.171 | 0.2441 | 0.2043 | 0.2786 | 0.2392 | 0.313 | 0.2792 | 0.3462 | 0.3354 |
| 0.2104 | 0.1723 | 0.2452 | 0.2052 | 0.2795 | 0.2404 | 0.3139 | 0.281 | 0.3469 | 0.3376 |
| 0.2114 | 0.173 | 0.2461 | 0.2065 | 0.2804 | 0.2411 | 0.3148 | 0.2817 | 0.3479 | 0.339 |
| 0.2123 | 0.1738 | 0.2468 | 0.2068 | 0.2814 | 0.2425 | 0.3156 | 0.2833 | 0.3486 | 0.342 |
| 0.2132 | 0.1746 | 0.2476 | 0.2084 | 0.2822 | 0.2431 | 0.3166 | 0.2845 | 0.3495 | 0.3433 |
| 0.2142 | 0.1755 | 0.2486 | 0.2085 | 0.2832 | 0.2442 | 0.3176 | 0.2854 | 0.3502 | 0.3448 |
| 0.2147 | 0.176 | 0.2495 | 0.2092 | 0.2841 | 0.2451 | 0.3184 | 0.2874 | 0.3509 | 0.3474 |
| 0.2158 | 0.1772 | 0.2505 | 0.2108 | 0.2851 | 0.2462 | 0.3193 | 0.2882 | 0.3517 | 0.3495 |
| 0.2167 | 0.1779 | 0.2513 | 0.2118 | 0.2859 | 0.2475 | 0.32 | 0.289 | 0.3525 | 0.3517 |
| 0.2175 | 0.1788 | 0.2524 | 0.2131 | 0.2869 | 0.2481 | 0.3209 | 0.2907 | 0.3533 | 0.3541 |
| 0.2186 | 0.1792 | 0.2533 | 0.2132 | 0.2878 | 0.2493 | 0.3217 | 0.2922 | 0.3541 | 0.357 |
| 0.2195 | 0.1806 | 0.2542 | 0.2146 | 0.2886 | 0.2502 | 0.3228 | 0.2928 | 0.3548 | 0.3591 |
| 0.2204 | 0.1819 | 0.2551 | 0.2151 | 0.2895 | 0.2515 | 0.3237 | 0.2945 | 0.3556 | 0.3617 |
| 0.2214 | 0.1827 | 0.2561 | 0.2159 | 0.2904 | 0.2521 | 0.3246 | 0.2962 | 0.3563 | 0.3639 |
| 0.2222 | 0.183 | 0.2569 | 0.2171 | 0.2913 | 0.2529 | 0.3254 | 0.2977 | 0.357 | 0.3669 |
| 0.2232 | 0.1844 | 0.2577 | 0.2183 | 0.2922 | 0.2542 | 0.3263 | 0.2991 | 0.3578 | 0.37 |
| 0.2241 | 0.1849 | 0.2585 | 0.2185 | 0.2933 | 0.2551 | 0.3272 | 0.2999 | 0.3584 | 0.372 |
| 0.2249 | 0.1856 | 0.2595 | 0.2195 | 0.294 | 0.2562 | 0.3281 | 0.3011 | 0.3591 | 0.3755 |
| 0.2257 | 0.1868 | 0.2604 | 0.2206 | 0.2949 | 0.2576 | 0.329 | 0.3032 | 0.3598 | 0.3783 |
| 0.2268 | 0.1883 | 0.2613 | 0.2219 | 0.296 | 0.2589 | 0.33 | 0.3049 | 0.3605 | 0.3814 |

Specimen ID: Al-Mg-100-13
Continued from previous

| Load [kN] | δ [mm] | Load [kN] | δ [mm] | Load [kN] | δ [mm] |
|---|---|---|---|---|---|
| 0.3612 | 0.385 | 0.3768 | 0.6642 | 0.3916 | 1.4119 |
| 0.3619 | 0.3884 | 0.3782 | 0.6793 | 0.3927 | 1.4392 |
| 0.3625 | 0.392 | 0.3774 | 0.6926 | 0.3924 | 1.4661 |
| 0.3632 | 0.3954 | 0.3786 | 0.7073 | 0.3936 | 1.4955 |
| 0.3639 | 0.4001 | 0.3782 | 0.7221 | 0.3935 | 1.5245 |
| 0.3646 | 0.4042 | 0.3789 | 0.7335 | 0.3931 | 1.5536 |
| 0.3652 | 0.4085 | 0.3779 | 0.7488 | 0.3945 | 1.5839 |
| 0.3658 | 0.4126 | 0.3791 | 0.765 | 0.3946 | 1.6142 |
| 0.3662 | 0.4162 | 0.3795 | 0.7816 | 0.395 | 1.6441 |
| 0.3668 | 0.4209 | 0.3802 | 0.7994 | 0.3955 | 1.6747 |
| 0.3675 | 0.4263 | 0.3805 | 0.8162 | 0.3954 | 1.7064 |
| 0.3681 | 0.4307 | 0.381 | 0.8347 | 0.3951 | 1.7388 |
| 0.3686 | 0.4366 | 0.3821 | 0.8522 | 0.396 | 1.762 |
| 0.3692 | 0.4418 | 0.3829 | 0.8703 | 0.3957 | 1.7946 |
| 0.3697 | 0.4476 | 0.3832 | 0.8887 | 0.3968 | 1.8278 |
| 0.3702 | 0.4528 | 0.3836 | 0.9076 | 0.3959 | 1.8616 |
| 0.3707 | 0.4595 | 0.3846 | 0.9262 | 0.3955 | 1.897 |
| 0.3712 | 0.4658 | 0.385 | 0.9399 | 0.3964 | 1.9323 |
| 0.3716 | 0.4727 | 0.3852 | 0.9592 | 0.3971 | 1.9673 |
| 0.3719 | 0.4773 | 0.3852 | 0.9797 | 0.3976 | 2.0029 |
| 0.3724 | 0.4842 | 0.3861 | 0.998 | 0.3973 | 2.0399 |
| 0.3726 | 0.4914 | 0.386 | 1.0197 | 0.3992 | 2.0767 |
| 0.3733 | 0.499 | 0.3875 | 1.0401 | 0.3981 | 2.103 |
| 0.3738 | 0.5065 | 0.3878 | 1.061 | | |
| 0.3741 | 0.5148 | 0.3878 | 1.0823 | | |
| 0.3738 | 0.5233 | 0.388 | 1.1024 | | |
| 0.374 | 0.5322 | 0.3882 | 1.1191 | | |
| 0.3743 | 0.541 | 0.3886 | 1.1412 | | |
| 0.3745 | 0.5511 | 0.3898 | 1.164 | | |
| 0.3751 | 0.5609 | 0.3899 | 1.1873 | | |
| 0.3753 | 0.5714 | 0.3895 | 1.2107 | | |
| 0.3753 | 0.5793 | 0.3899 | 1.2349 | | |
| 0.3756 | 0.59 | 0.3903 | 1.2601 | | |
| 0.3755 | 0.6013 | 0.3908 | 1.2847 | | |
| 0.3766 | 0.613 | 0.3909 | 1.3106 | | |
| 0.3757 | 0.6252 | 0.3912 | 1.3364 | | |
| 0.3765 | 0.6377 | 0.3916 | 1.3631 | | |
| 0.3771 | 0.651 | 0.3914 | 1.3844 | | |

Specimen ID: Al-Mg-250-tensile-3
Loading: Longitudinal
Thickness: 250 μm
Width: 3.72 mm
Gauge Length: 42.37 mm
Loading Rate: 0.015 kN/s

| Load [kN] | δ [mm] | Load [kN] | δ [mm] | Load [kN] | δ [mm] | Load [kN] | δ [mm] | Load [kN] | δ [mm] |
|---|---|---|---|---|---|---|---|---|---|
| 0.0155 | 0 | 0.0502 | 0.0319 | 0.0882 | 0.0699 | 0.1261 | 0.1114 | 0.1641 | 0.1582 |
| 0.0157 | 0.0002 | 0.0508 | 0.033 | 0.0892 | 0.071 | 0.1269 | 0.1123 | 0.1649 | 0.1597 |
| 0.0152 | 0.0004 | 0.0519 | 0.0339 | 0.0898 | 0.072 | 0.1284 | 0.1135 | 0.1661 | 0.1611 |
| 0.0155 | 0.0004 | 0.053 | 0.0353 | 0.0907 | 0.0734 | 0.1294 | 0.1151 | 0.1666 | 0.1621 |
| 0.0165 | 0.0008 | 0.0538 | 0.0362 | 0.0918 | 0.0739 | 0.1301 | 0.1156 | 0.1681 | 0.1637 |
| 0.0168 | 0.001 | 0.0548 | 0.037 | 0.0931 | 0.0757 | 0.1316 | 0.1171 | 0.1688 | 0.1652 |
| 0.018 | 0.0025 | 0.0557 | 0.0381 | 0.0945 | 0.0762 | 0.1323 | 0.118 | 0.1702 | 0.1665 |
| 0.0186 | 0.0031 | 0.0571 | 0.0386 | 0.0955 | 0.0773 | 0.1328 | 0.1191 | 0.1705 | 0.1676 |
| 0.02 | 0.0037 | 0.0576 | 0.0403 | 0.0959 | 0.0782 | 0.1338 | 0.1206 | 0.1721 | 0.1689 |
| 0.021 | 0.0053 | 0.0588 | 0.041 | 0.0973 | 0.0795 | 0.1355 | 0.1216 | 0.1731 | 0.1701 |
| 0.0214 | 0.0061 | 0.06 | 0.0423 | 0.0985 | 0.0802 | 0.1359 | 0.1229 | 0.1737 | 0.1719 |
| 0.0225 | 0.0066 | 0.0607 | 0.0427 | 0.0993 | 0.0814 | 0.1375 | 0.1241 | 0.1747 | 0.1735 |
| 0.0238 | 0.0076 | 0.0618 | 0.0438 | 0.1003 | 0.0824 | 0.1382 | 0.1255 | 0.1753 | 0.175 |
| 0.0247 | 0.0087 | 0.0628 | 0.0447 | 0.1009 | 0.0831 | 0.1391 | 0.1267 | 0.1766 | 0.1767 |
| 0.0255 | 0.0095 | 0.0642 | 0.046 | 0.1022 | 0.0848 | 0.1403 | 0.1273 | 0.1774 | 0.1777 |
| 0.0267 | 0.0104 | 0.0649 | 0.0465 | 0.1027 | 0.0852 | 0.1408 | 0.1284 | 0.1785 | 0.1792 |
| 0.0274 | 0.0115 | 0.0658 | 0.0474 | 0.1038 | 0.0868 | 0.1424 | 0.1299 | 0.18 | 0.1812 |
| 0.0286 | 0.012 | 0.0672 | 0.0483 | 0.1051 | 0.0873 | 0.1433 | 0.1311 | 0.1811 | 0.182 |
| 0.0295 | 0.0129 | 0.0681 | 0.0499 | 0.1058 | 0.0886 | 0.144 | 0.1324 | 0.1812 | 0.1843 |
| 0.0308 | 0.0133 | 0.069 | 0.0504 | 0.1068 | 0.0902 | 0.1457 | 0.1341 | 0.1828 | 0.186 |
| 0.032 | 0.0147 | 0.0702 | 0.0517 | 0.1082 | 0.0906 | 0.1462 | 0.1353 | 0.1841 | 0.1874 |
| 0.0322 | 0.0157 | 0.0713 | 0.0528 | 0.1091 | 0.0921 | 0.1476 | 0.136 | 0.1843 | 0.1887 |
| 0.0338 | 0.0163 | 0.0721 | 0.0537 | 0.1102 | 0.0933 | 0.148 | 0.1379 | 0.1857 | 0.1904 |
| 0.0342 | 0.0175 | 0.0731 | 0.0543 | 0.1113 | 0.0943 | 0.1494 | 0.1381 | 0.1861 | 0.1916 |
| 0.0358 | 0.0182 | 0.0736 | 0.0558 | 0.1124 | 0.0955 | 0.1501 | 0.1396 | 0.1878 | 0.1937 |
| 0.0364 | 0.0188 | 0.0745 | 0.0569 | 0.1129 | 0.0963 | 0.1506 | 0.1408 | 0.1885 | 0.1952 |
| 0.0379 | 0.02 | 0.0761 | 0.0579 | 0.1139 | 0.0976 | 0.1516 | 0.1423 | 0.1898 | 0.1966 |
| 0.0382 | 0.0213 | 0.0771 | 0.059 | 0.1155 | 0.0985 | 0.1533 | 0.1436 | 0.1904 | 0.1983 |
| 0.0399 | 0.0222 | 0.0783 | 0.0601 | 0.1159 | 0.0992 | 0.1542 | 0.1455 | 0.1915 | 0.1998 |
| 0.0403 | 0.0234 | 0.0793 | 0.0606 | 0.1173 | 0.1009 | 0.1549 | 0.1461 | 0.1927 | 0.2018 |
| 0.0421 | 0.025 | 0.0797 | 0.0617 | 0.1184 | 0.102 | 0.1557 | 0.1476 | 0.1939 | 0.2031 |
| 0.0428 | 0.0249 | 0.0813 | 0.0628 | 0.1194 | 0.1028 | 0.1573 | 0.1483 | 0.1941 | 0.2048 |
| 0.044 | 0.0258 | 0.0824 | 0.0635 | 0.1199 | 0.1042 | 0.1583 | 0.15 | 0.1952 | 0.2071 |
| 0.0443 | 0.0273 | 0.083 | 0.0652 | 0.1207 | 0.1062 | 0.1593 | 0.1512 | 0.1965 | 0.2082 |
| 0.0459 | 0.0281 | 0.0837 | 0.0657 | 0.1219 | 0.1058 | 0.1603 | 0.153 | 0.197 | 0.2096 |
| 0.047 | 0.0291 | 0.0847 | 0.0676 | 0.1233 | 0.1078 | 0.1611 | 0.1542 | 0.1986 | 0.2115 |
| 0.0478 | 0.0299 | 0.0864 | 0.0684 | 0.1237 | 0.1094 | 0.1619 | 0.1551 | 0.1988 | 0.2135 |
| 0.0484 | 0.0313 | 0.0871 | 0.0685 | 0.1249 | 0.1099 | 0.1627 | 0.1565 | 0.2005 | 0.2153 |

Specimen ID: Al-Mg-250-tensile-3
Continued from previous

| Load [kN] | δ [mm] | Load [kN] | δ [mm] | Load [kN] | δ [mm] |
|---|---|---|---|---|---|
| 0.2009 | 0.2169 | 0.2351 | 0.311 | 0.2622 | 0.5257 |
| 0.2017 | 0.2184 | 0.2363 | 0.3145 | 0.2626 | 0.5349 |
| 0.2031 | 0.221 | 0.2375 | 0.3183 | 0.2631 | 0.544 |
| 0.2043 | 0.2229 | 0.2379 | 0.3206 | 0.2642 | 0.5547 |
| 0.2045 | 0.2244 | 0.2386 | 0.3248 | 0.2638 | 0.5639 |
| 0.2063 | 0.2264 | 0.2392 | 0.3281 | 0.265 | 0.5748 |
| 0.2066 | 0.2282 | 0.2408 | 0.3321 | 0.265 | 0.5849 |
| 0.2074 | 0.23 | 0.2412 | 0.3366 | 0.2651 | 0.5958 |
| 0.2082 | 0.232 | 0.2424 | 0.3404 | 0.266 | 0.6069 |
| 0.2099 | 0.2345 | 0.2431 | 0.3451 | 0.2662 | 0.619 |
| 0.2099 | 0.2365 | 0.2439 | 0.3489 | 0.2672 | 0.6306 |
| 0.2116 | 0.2382 | 0.2441 | 0.3536 | 0.2676 | 0.6425 |
| 0.2125 | 0.2405 | 0.2453 | 0.3575 | 0.2669 | 0.6549 |
| 0.2131 | 0.2424 | 0.2463 | 0.3627 | 0.2675 | 0.6678 |
| 0.2137 | 0.245 | 0.2468 | 0.367 | 0.2683 | 0.6817 |
| 0.2151 | 0.2468 | 0.2478 | 0.3718 | 0.2688 | 0.6957 |
| 0.2161 | 0.2491 | 0.2483 | 0.3775 | 0.269 | 0.7096 |
| 0.2167 | 0.2515 | 0.2493 | 0.3822 | 0.2693 | 0.7241 |
| 0.218 | 0.2541 | 0.25 | 0.3871 | 0.2694 | 0.7388 |
| 0.2183 | 0.2562 | 0.25 | 0.3928 | 0.2699 | 0.755 |
| 0.2198 | 0.2587 | 0.2506 | 0.3975 | 0.2698 | 0.7713 |
| 0.2208 | 0.261 | 0.2514 | 0.4032 | 0.271 | 0.7876 |
| 0.2211 | 0.2634 | 0.2526 | 0.4091 | 0.2708 | 0.8054 |
| 0.2225 | 0.2665 | 0.2529 | 0.4153 | 0.2709 | 0.8231 |
| 0.2229 | 0.2689 | 0.2543 | 0.4219 | 0.2714 | 0.8407 |
| 0.2244 | 0.2709 | 0.2544 | 0.4277 | 0.2708 | 0.8588 |
| 0.2246 | 0.2747 | 0.2549 | 0.4339 | 0.2713 | 0.8777 |
| 0.2262 | 0.277 | 0.256 | 0.441 | 0.2721 | 0.8968 |
| 0.2271 | 0.2793 | 0.2567 | 0.4465 | 0.27 | 0.9167 |
| 0.2277 | 0.2823 | 0.2571 | 0.4532 | | |
| 0.2281 | 0.2851 | 0.2576 | 0.461 | | |
| 0.2299 | 0.2887 | 0.2587 | 0.4685 | | |
| 0.2299 | 0.2912 | 0.2584 | 0.4756 | | |
| 0.2314 | 0.2946 | 0.259 | 0.4839 | | |
| 0.2317 | 0.2974 | 0.2599 | 0.4918 | | |
| 0.2326 | 0.3008 | 0.2604 | 0.4997 | | |
| 0.2334 | 0.304 | 0.2616 | 0.5082 | | |
| 0.235 | 0.3072 | 0.262 | 0.5166 | | |

# APPENDIX B

# FRACTURE TOUGHNESS TESTS

Specimen ID: 8
Loading: Longitudinal
Thickness: 250 μm
Loading Rate: 0.015 kN/s

| Load [N] | δ [mm] | Load [N] | δ [mm] | Load [N] | δ [mm] | Load [N] | δ [mm] | Load [N] | δ [mm] |
|---|---|---|---|---|---|---|---|---|---|
| 21.4 | 0.003 | 255.8 | 0.0379 | 490.2 | 0.074 | 720.7 | 0.1122 | 953 | 0.1557 |
| 28.3 | 0.0036 | 262.3 | 0.0388 | 496.3 | 0.0751 | 727.4 | 0.1134 | 959.2 | 0.1571 |
| 35.3 | 0.0052 | 269.4 | 0.0402 | 503.3 | 0.0765 | 734 | 0.115 | 965.6 | 0.1587 |
| 42.5 | 0.0066 | 276 | 0.0411 | 510.4 | 0.0783 | 740.7 | 0.1157 | 972.2 | 0.1599 |
| 49.7 | 0.0071 | 282.6 | 0.0418 | 516.8 | 0.0786 | 747.4 | 0.1173 | 979 | 0.1611 |
| 56.1 | 0.0089 | 289.2 | 0.0434 | 523.3 | 0.0792 | 754.7 | 0.1189 | 985.3 | 0.1636 |
| 62.3 | 0.0095 | 296.1 | 0.044 | 530.2 | 0.0811 | 761.1 | 0.1198 | 991.8 | 0.1634 |
| 69.2 | 0.0105 | 302.5 | 0.0454 | 536.6 | 0.082 | 767.4 | 0.1216 | 998.8 | 0.1654 |
| 76.1 | 0.0114 | 309.3 | 0.0459 | 543.1 | 0.0829 | 774 | 0.1219 | 1005.5 | 0.1673 |
| 82.2 | 0.0125 | 317.3 | 0.0468 | 549.4 | 0.084 | 780.7 | 0.1228 | 1012.3 | 0.1682 |
| 89.1 | 0.0129 | 324 | 0.0484 | 556.5 | 0.0856 | 787.8 | 0.1249 | 1018.5 | 0.1694 |
| 95.9 | 0.0143 | 330.7 | 0.05 | 562.5 | 0.0863 | 794 | 0.1258 | 1025.2 | 0.1708 |
| 103 | 0.0154 | 337.1 | 0.0505 | 569.8 | 0.087 | 800.4 | 0.1274 | 1032 | 0.1719 |
| 109.2 | 0.0159 | 343.9 | 0.0514 | 576.3 | 0.0882 | 807 | 0.1283 | 1039 | 0.174 |
| 115.9 | 0.0172 | 350.4 | 0.0528 | 582.4 | 0.0888 | 814 | 0.1299 | 1045 | 0.1747 |
| 122.9 | 0.0182 | 357.5 | 0.0535 | 589 | 0.0909 | 820.4 | 0.1306 | 1051.6 | 0.1759 |
| 129.3 | 0.0193 | 364.4 | 0.055 | 595.4 | 0.0911 | 826.7 | 0.1315 | 1058.6 | 0.1775 |
| 136 | 0.0202 | 370.8 | 0.0557 | 602.5 | 0.0925 | 833.5 | 0.1334 | 1065 | 0.1791 |
| 142.8 | 0.0211 | 377.5 | 0.0566 | 609.1 | 0.0939 | 840.4 | 0.1345 | 1071.8 | 0.1803 |
| 149.3 | 0.0222 | 384.2 | 0.0576 | 615.1 | 0.095 | 846.8 | 0.1352 | 1078.7 | 0.1821 |
| 155.8 | 0.0236 | 390.9 | 0.0587 | 622.2 | 0.0964 | 853.4 | 0.1361 | 1085.7 | 0.1833 |
| 162.4 | 0.0243 | 397.5 | 0.0594 | 628.5 | 0.0969 | 860 | 0.138 | 1091.8 | 0.1851 |
| 168.6 | 0.0256 | 404.2 | 0.0605 | 635.2 | 0.0975 | 866.5 | 0.1391 | 1098.4 | 0.1863 |
| 175.6 | 0.0261 | 410.7 | 0.0626 | 641.5 | 0.0987 | 873.4 | 0.1403 | 1105 | 0.1877 |
| 182.1 | 0.0272 | 417.8 | 0.0626 | 648.1 | 0.1003 | 879.5 | 0.1414 | 1111.4 | 0.1893 |
| 188.4 | 0.0286 | 424.3 | 0.0642 | 654.3 | 0.1014 | 886.6 | 0.1424 | 1117.8 | 0.1912 |
| 195.2 | 0.0286 | 430.8 | 0.0651 | 661.5 | 0.1026 | 893.1 | 0.144 | 1124.9 | 0.1918 |
| 202.4 | 0.0302 | 436.8 | 0.0655 | 668.5 | 0.1037 | 899.7 | 0.1456 | 1131.5 | 0.1932 |
| 208.8 | 0.0309 | 444 | 0.0664 | 674.7 | 0.104 | 906.2 | 0.1463 | 1137.8 | 0.196 |
| 215.5 | 0.032 | 450.9 | 0.0678 | 680.9 | 0.1056 | 912.8 | 0.1477 | 1144.5 | 0.1979 |
| 222.3 | 0.0334 | 456.7 | 0.069 | 687.8 | 0.1069 | 919.3 | 0.1495 | 1151.6 | 0.1983 |
| 228.9 | 0.0343 | 463.3 | 0.0694 | 694.8 | 0.1076 | 925.7 | 0.1504 | 1158.3 | 0.1996 |
| 236.2 | 0.0345 | 470.4 | 0.0703 | 701.5 | 0.109 | 932.3 | 0.1518 | 1164.5 | 0.2007 |
| 242 | 0.0361 | 477.2 | 0.0722 | 708.3 | 0.1102 | 939 | 0.1532 | 1171.7 | 0.203 |
| 248.8 | 0.0368 | 483.7 | 0.0733 | 714.1 | 0.1108 | 946.1 | 0.1544 | 1178.2 | 0.2051 |

Specimen ID: 8
Continued from previous

| Load [N] | δ [mm] |
|---|---|
| 1184.6 | 0.2069 |
| 1191.3 | 0.2083 |
| 1197.9 | 0.2108 |
| 1204.8 | 0.2122 |
| 1211 | 0.2136 |
| 1217.7 | 0.2154 |
| 1223.9 | 0.2175 |
| 1230.9 | 0.2198 |
| 1237.5 | 0.2212 |
| 1244.5 | 0.2233 |
| 1250.7 | 0.2246 |
| 1257.7 | 0.2276 |
| 1264.2 | 0.2292 |
| 1270.9 | 0.2311 |
| 1278.2 | 0.2336 |
| 1284.6 | 0.2359 |
| 1291.4 | 0.2378 |
| 1297.9 | 0.2401 |
| 1304.7 | 0.2424 |
| 1311.2 | 0.2461 |
| 1317.5 | 0.2484 |
| 1324.4 | 0.2516 |
| 1331.1 | 0.2546 |
| 1337.5 | 0.2576 |
| 1343.9 | 0.2625 |
| 1350.8 | 0.2666 |
| 1356.1 | 0.2729 |

Specimen ID: 7
Loading: Longitudinal
Thickness: 250 μm
Loading Rate: 0.015 kN/s

| Load [N] | δ [mm] | Load [N] | δ [mm] | Load [N] | δ [mm] | Load [N] | δ [mm] | Load [N] | δ [mm] |
|---|---|---|---|---|---|---|---|---|---|
| 33.2 | 0.0022 | 266.6 | 0.0298 | 499.1 | 0.059 | 731.2 | 0.0887 | 962.3 | 0.1176 |
| 40.1 | 0.0036 | 273.3 | 0.031 | 505.9 | 0.0597 | 738.1 | 0.0892 | 969.2 | 0.1195 |
| 46.2 | 0.0038 | 279.9 | 0.0317 | 512.3 | 0.061 | 744.2 | 0.0906 | 975.6 | 0.12 |
| 53 | 0.0057 | 286.4 | 0.0326 | 519.2 | 0.0619 | 750.7 | 0.0908 | 982.4 | 0.1204 |
| 60.1 | 0.0062 | 293.1 | 0.0333 | 525.4 | 0.0626 | 757.7 | 0.0917 | 989 | 0.1218 |
| 67.6 | 0.0072 | 300.1 | 0.0349 | 531.9 | 0.0627 | 764.5 | 0.0931 | 995.4 | 0.1237 |
| 73.9 | 0.0074 | 306.2 | 0.0352 | 538.8 | 0.0638 | 771.2 | 0.0936 | 1001.9 | 0.1236 |
| 80.8 | 0.0081 | 313.3 | 0.0358 | 545.5 | 0.0649 | 777.4 | 0.0938 | 1009.2 | 0.1241 |
| 87.2 | 0.0086 | 319.9 | 0.0363 | 551.9 | 0.0663 | 783.8 | 0.0952 | 1015.4 | 0.1255 |
| 93.8 | 0.0096 | 326.7 | 0.0377 | 558.5 | 0.0663 | 790.6 | 0.096 | 1022.4 | 0.1264 |
| 100.5 | 0.0105 | 333 | 0.0386 | 565.3 | 0.0675 | 797.1 | 0.098 | 1028.9 | 0.1274 |
| 107.3 | 0.0105 | 339.9 | 0.0395 | 571.6 | 0.0684 | 803.5 | 0.098 | 1035.1 | 0.1279 |
| 113.8 | 0.0117 | 346.8 | 0.0405 | 578.1 | 0.0696 | 810.4 | 0.0987 | 1041.7 | 0.1288 |
| 121.2 | 0.0123 | 353.7 | 0.0418 | 585.3 | 0.0696 | 816.7 | 0.1001 | 1048.7 | 0.1292 |
| 127.7 | 0.0131 | 360.2 | 0.0416 | 591.4 | 0.0702 | 823.3 | 0.1006 | 1054.5 | 0.1306 |
| 134.4 | 0.0137 | 366.6 | 0.0425 | 598.1 | 0.0714 | 829.9 | 0.1009 | 1061.5 | 0.1311 |
| 140.7 | 0.0156 | 373 | 0.0439 | 605.2 | 0.0728 | 836.9 | 0.1018 | 1068.2 | 0.1323 |
| 147.2 | 0.0156 | 380.1 | 0.0442 | 612.1 | 0.073 | 843.2 | 0.1029 | 1074.7 | 0.1334 |
| 154.1 | 0.0156 | 386.5 | 0.0453 | 618.1 | 0.0735 | 849.9 | 0.1041 | 1081.1 | 0.1341 |
| 160.6 | 0.0166 | 392.4 | 0.0463 | 624.5 | 0.0749 | 856.4 | 0.1046 | 1087.8 | 0.1353 |
| 167.8 | 0.0173 | 399.6 | 0.0463 | 631.5 | 0.0749 | 863.3 | 0.105 | 1094.7 | 0.136 |
| 174.1 | 0.0186 | 406 | 0.0479 | 638.2 | 0.0769 | 869.8 | 0.1058 | 1101.4 | 0.1369 |
| 181 | 0.0193 | 412.8 | 0.0488 | 644.9 | 0.0772 | 876.6 | 0.1069 | 1107.8 | 0.1374 |
| 187.4 | 0.0201 | 419.3 | 0.0497 | 651.1 | 0.0781 | 882.9 | 0.1086 | 1114.8 | 0.1392 |
| 193.7 | 0.0212 | 426 | 0.0504 | 658.1 | 0.0789 | 889.9 | 0.109 | 1121.1 | 0.1401 |
| 200.7 | 0.0221 | 433 | 0.0507 | 665.3 | 0.0796 | 896.6 | 0.1099 | 1127.9 | 0.1415 |
| 207.3 | 0.0228 | 439.4 | 0.0514 | 671.8 | 0.0805 | 903 | 0.1104 | 1134.2 | 0.1418 |
| 213.7 | 0.0235 | 445.8 | 0.0527 | 678.1 | 0.0812 | 909.6 | 0.1111 | 1141.1 | 0.1429 |
| 220.5 | 0.0238 | 452.7 | 0.053 | 684.7 | 0.0823 | 916.3 | 0.1121 | 1147.3 | 0.1443 |
| 227.5 | 0.0256 | 459.5 | 0.0543 | 691 | 0.0826 | 923.2 | 0.1132 | 1154.1 | 0.145 |
| 234 | 0.0259 | 465.4 | 0.0553 | 698 | 0.084 | 929.6 | 0.1139 | 1160.8 | 0.1461 |
| 240.3 | 0.0266 | 472.2 | 0.0558 | 704.5 | 0.0847 | 936.1 | 0.1144 | 1167.6 | 0.1466 |
| 247.1 | 0.0275 | 479 | 0.0567 | 710.8 | 0.0856 | 942.8 | 0.1151 | 1173.9 | 0.1478 |
| 254 | 0.0286 | 485.3 | 0.0576 | 717.5 | 0.0868 | 949.2 | 0.1164 | 1180.6 | 0.1487 |
| 260.4 | 0.0291 | 492.3 | 0.0583 | 724.3 | 0.0875 | 956.4 | 0.1172 | 1187.4 | 0.1503 |

Specimen ID: 7
Continued from previous

| Load [N] | δ [mm] | Load [N] | δ [mm] | Load [N] | δ [mm] |
|---|---|---|---|---|---|
| 1193.7 | 0.151 | 1373.2 | 0.1811 | 1551.8 | 0.2198 |
| 1200.7 | 0.1522 | 1380.5 | 0.1819 | 1558.4 | 0.2215 |
| 1206.6 | 0.1524 | 1386.9 | 0.1826 | 1565 | 0.2224 |
| 1213.2 | 0.1535 | 1393.6 | 0.1843 | 1571.6 | 0.2249 |
| 1220.3 | 0.1545 | 1399.4 | 0.1861 | 1578.2 | 0.2278 |
| 1226.5 | 0.1558 | 1406 | 0.1865 | 1584.6 | 0.2299 |
| 1232.9 | 0.1567 | 1412.6 | 0.1872 | 1590.9 | 0.2332 |
| 1240.1 | 0.1586 | 1419.7 | 0.1893 | 1597.9 | 0.2358 |
| 1246.5 | 0.1593 | 1426.4 | 0.1904 | 1603.5 | 0.2391 |
| 1253.2 | 0.1597 | 1432.7 | 0.1916 | 1609.9 | 0.2443 |
| 1259.7 | 0.1611 | 1438.9 | 0.1925 | 1617 | 0.2496 |
| 1266.2 | 0.1616 | 1445.9 | 0.1936 | 1623.6 | 0.255 |
| 1272.6 | 0.1628 | 1452.5 | 0.195 | 1627.3 | 0.2628 |
| 1281.3 | 0.164 | 1459.1 | 0.1964 | | |
| 1288.3 | 0.1657 | 1466.1 | 0.198 | | |
| 1294.5 | 0.1673 | 1472.7 | 0.1996 | | |
| 1301.3 | 0.168 | 1478.9 | 0.2007 | | |
| 1307.8 | 0.1689 | 1485.3 | 0.2025 | | |
| 1314.1 | 0.17 | 1492.3 | 0.2041 | | |
| 1321 | 0.1707 | 1499.5 | 0.2053 | | |
| 1327.4 | 0.1718 | 1505.6 | 0.2073 | | |
| 1334 | 0.1733 | 1512.1 | 0.208 | | |
| 1341 | 0.1748 | 1518.8 | 0.2099 | | |
| 1347.1 | 0.176 | 1525.3 | 0.2114 | | |
| 1354.2 | 0.1769 | 1532 | 0.2132 | | |
| 1360.6 | 0.1776 | 1538.4 | 0.2148 | | |
| 1367.2 | 0.1797 | 1545.3 | 0.2167 | | |

Specimen ID: 6
Loading: Longitudinal
Thickness: 250 μm
Loading Rate: 0.015 kN/s

| Load [N] | δ [mm] | Load [N] | δ [mm] | Load [N] | δ [mm] | Load [N] | δ [mm] | Load [N] | δ [mm] |
|---|---|---|---|---|---|---|---|---|---|
| 14.9 | 0.0031 | 236.1 | 0.0334 | 455 | 0.0617 | 672.3 | 0.0918 | 889.2 | 0.1233 |
| 22.8 | 0.0048 | 242.6 | 0.0342 | 460.8 | 0.0635 | 678.4 | 0.093 | 895.3 | 0.1243 |
| 29 | 0.0051 | 248.6 | 0.0346 | 467.4 | 0.0642 | 684.7 | 0.0939 | 901.8 | 0.1255 |
| 35 | 0.0074 | 254.8 | 0.0356 | 473.7 | 0.0643 | 690.6 | 0.0946 | 908.2 | 0.1261 |
| 41.5 | 0.0072 | 261.1 | 0.0365 | 479.8 | 0.0657 | 697.5 | 0.0949 | 914.4 | 0.1269 |
| 47.9 | 0.0089 | 267.3 | 0.0379 | 486 | 0.0661 | 703.1 | 0.0963 | 920.4 | 0.128 |
| 53.8 | 0.0096 | 273.7 | 0.0379 | 492.2 | 0.0675 | 709.3 | 0.0974 | 926.9 | 0.1294 |
| 60.2 | 0.0099 | 280.3 | 0.0389 | 498.3 | 0.068 | 715.5 | 0.0983 | 933.2 | 0.1303 |
| 66.1 | 0.0122 | 286.3 | 0.0403 | 504.6 | 0.069 | 722 | 0.0991 | 939.5 | 0.131 |
| 73 | 0.0125 | 292.3 | 0.041 | 510.8 | 0.0701 | 727.7 | 0.1004 | 945.5 | 0.1315 |
| 79.3 | 0.0137 | 298.8 | 0.0417 | 516.6 | 0.0711 | 734.4 | 0.1009 | 951.9 | 0.1329 |
| 85.3 | 0.0142 | 304.8 | 0.0424 | 523.2 | 0.0718 | 740.4 | 0.1016 | 957.7 | 0.134 |
| 91.6 | 0.0147 | 311.2 | 0.0429 | 529.2 | 0.072 | 746.5 | 0.1023 | 964.2 | 0.1345 |
| 98.1 | 0.0158 | 317.6 | 0.0439 | 535.3 | 0.0732 | 753.4 | 0.1035 | 969.8 | 0.1362 |
| 104.3 | 0.0171 | 323.9 | 0.0449 | 541.7 | 0.0735 | 759.1 | 0.1047 | 976.7 | 0.1364 |
| 110.4 | 0.0171 | 329.9 | 0.046 | 548 | 0.0751 | 765.6 | 0.1058 | 982.2 | 0.1371 |
| 116.2 | 0.0189 | 336.3 | 0.0467 | 554.5 | 0.0758 | 771.8 | 0.1072 | 988.4 | 0.1391 |
| 122.9 | 0.0192 | 342.7 | 0.0479 | 560.4 | 0.0772 | 778.1 | 0.1072 | 994.4 | 0.1394 |
| 129.5 | 0.0204 | 349.1 | 0.0479 | 566.5 | 0.0781 | 784.1 | 0.1077 | 1000.7 | 0.1403 |
| 135.5 | 0.0215 | 355.1 | 0.0493 | 572.8 | 0.0781 | 790.5 | 0.1096 | 1006.8 | 0.1415 |
| 142.5 | 0.0222 | 361.6 | 0.0505 | 578.7 | 0.0794 | 796.6 | 0.1101 | 1013.1 | 0.142 |
| 148.7 | 0.0232 | 367.7 | 0.0505 | 585.3 | 0.0807 | 802.7 | 0.1107 | 1019.1 | 0.1431 |
| 155.3 | 0.0235 | 374.1 | 0.051 | 591.6 | 0.0801 | 808.5 | 0.1119 | 1025.6 | 0.144 |
| 161.4 | 0.0242 | 380 | 0.0517 | 597.3 | 0.0815 | 814.7 | 0.1126 | 1031.6 | 0.1447 |
| 167.4 | 0.0256 | 386.2 | 0.0531 | 603.6 | 0.0828 | 821.4 | 0.1135 | 1037.6 | 0.1461 |
| 174 | 0.026 | 392.6 | 0.0534 | 609.7 | 0.0836 | 827.1 | 0.1145 | 1043.8 | 0.1468 |
| 179.8 | 0.0267 | 398.7 | 0.0553 | 615.8 | 0.0845 | 833.6 | 0.1156 | 1051.1 | 0.1488 |
| 186.1 | 0.0267 | 405.3 | 0.0555 | 622.5 | 0.0855 | 839.9 | 0.1163 | 1057.5 | 0.1499 |
| 192.4 | 0.028 | 411.2 | 0.0557 | 628.7 | 0.0862 | 845.8 | 0.1171 | 1063.8 | 0.1508 |
| 198.5 | 0.0287 | 417.4 | 0.0572 | 634.8 | 0.0871 | 851.7 | 0.1182 | 1070.1 | 0.1513 |
| 204.5 | 0.0299 | 423.3 | 0.0574 | 641.2 | 0.0875 | 858.4 | 0.1192 | 1076.3 | 0.1525 |
| 210.3 | 0.0313 | 429.8 | 0.059 | 647 | 0.0885 | 864.8 | 0.1194 | 1082.6 | 0.1532 |
| 216.8 | 0.031 | 436.1 | 0.0595 | 653.5 | 0.0895 | 870.5 | 0.1208 | 1088.3 | 0.1545 |
| 223.6 | 0.032 | 442.2 | 0.06 | 659.6 | 0.0902 | 877.1 | 0.1217 | 1094.8 | 0.1559 |
| 230.1 | 0.0325 | 448.4 | 0.0616 | 665.7 | 0.0915 | 883.4 | 0.1222 | 1101.1 | 0.1564 |

Specimen ID: 6
Continued from previous

| Load [N] | δ [mm] | Load [N] | δ [mm] | Load [N] | δ [mm] |
|---|---|---|---|---|---|
| 1107.2 | 0.1575 | 1273.9 | 0.1885 | 1441.8 | 0.2321 |
| 1113.4 | 0.1584 | 1280.2 | 0.1904 | 1447.6 | 0.2343 |
| 1119.8 | 0.1603 | 1286.5 | 0.1916 | 1454 | 0.2365 |
| 1126 | 0.161 | 1292.7 | 0.1932 | 1459.7 | 0.2389 |
| 1131.9 | 0.1622 | 1299 | 0.1944 | 1466.2 | 0.2409 |
| 1138.5 | 0.1628 | 1304.9 | 0.1956 | 1472.6 | 0.2445 |
| 1144.3 | 0.1644 | 1311.3 | 0.1972 | 1478.9 | 0.2465 |
| 1150.3 | 0.1652 | 1317.3 | 0.1986 | 1485.3 | 0.2493 |
| 1156.4 | 0.1665 | 1323.3 | 0.1998 | 1491 | 0.253 |
| 1162.9 | 0.1674 | 1329.5 | 0.2018 | 1497.6 | 0.2571 |
| 1169 | 0.1689 | 1336.1 | 0.2028 | 1503.6 | 0.2606 |
| 1175.3 | 0.1689 | 1342.1 | 0.2047 | 1508.5 | 0.2655 |
| 1181.5 | 0.1705 | 1348.2 | 0.2061 | 1513.2 | 0.2779 |
| 1187.5 | 0.1716 | 1354.3 | 0.2073 | 1322 | 0.3511 |
| 1193.6 | 0.1728 | 1360.6 | 0.2089 | | |
| 1199.8 | 0.1744 | 1366.9 | 0.2107 | | |
| 1206.1 | 0.1751 | 1373.3 | 0.2122 | | |
| 1212.2 | 0.1765 | 1379.4 | 0.2136 | | |
| 1218.1 | 0.1774 | 1385.8 | 0.2152 | | |
| 1224.6 | 0.1792 | 1392.1 | 0.2177 | | |
| 1230.7 | 0.1801 | 1398.5 | 0.2191 | | |
| 1236.8 | 0.1827 | 1404.5 | 0.2208 | | |
| 1242.9 | 0.1829 | 1410.9 | 0.2222 | | |
| 1249 | 0.1843 | 1416.5 | 0.2242 | | |
| 1255 | 0.1854 | 1423.1 | 0.2268 | | |
| 1261.1 | 0.1864 | 1429.2 | 0.2278 | | |
| 1267.7 | 0.1871 | 1435.3 | 0.2305 | | |

Specimen ID: 5
Loading: Longitudinal
Thickness: 100 μm
Loading Rate: 0.015 kN/s

| Load [N] | δ [mm] | Load [N] | δ [mm] | Load [N] | δ [mm] | Load [N] | δ [mm] |
|---|---|---|---|---|---|---|---|
| 25 | 0.0102 | 146 | 0.0615 | 266 | 0.1127 | 386 | 0.1688 |
| 28 | 0.0114 | 150 | 0.0634 | 269 | 0.1146 | 389 | 0.1704 |
| 32 | 0.0132 | 153 | 0.0643 | 273 | 0.1155 | 392 | 0.1718 |
| 35 | 0.0145 | 156 | 0.0659 | 276 | 0.1171 | 396 | 0.1738 |
| 38 | 0.0166 | 160 | 0.0668 | 279 | 0.1194 | 399 | 0.175 |
| 42 | 0.0179 | 163 | 0.0686 | 283 | 0.1196 | 403 | 0.177 |
| 46 | 0.0195 | 167 | 0.0699 | 286 | 0.1219 | 406 | 0.1786 |
| 49 | 0.0208 | 170 | 0.072 | 290 | 0.1237 | 410 | 0.1804 |
| 52 | 0.0226 | 174 | 0.0738 | 293 | 0.1251 | 413 | 0.1827 |
| 56 | 0.024 | 177 | 0.0749 | 296 | 0.1265 | 417 | 0.1843 |
| 59 | 0.0258 | 180 | 0.0756 | 300 | 0.1283 | 420 | 0.1861 |
| 63 | 0.0278 | 184 | 0.0774 | 303 | 0.1297 | 424 | 0.1877 |
| 66 | 0.0287 | 187 | 0.079 | 307 | 0.1315 | 427 | 0.1895 |
| 70 | 0.0299 | 191 | 0.0802 | 310 | 0.1333 | 431 | 0.1918 |
| 74 | 0.0317 | 194 | 0.0811 | 314 | 0.1338 | 434 | 0.1941 |
| 77 | 0.0333 | 198 | 0.0833 | 317 | 0.1365 | 437 | 0.1959 |
| 80 | 0.0344 | 201 | 0.0847 | 321 | 0.1372 | 441 | 0.1977 |
| 84 | 0.0357 | 205 | 0.0861 | 324 | 0.1391 | 444 | 0.1998 |
| 87 | 0.0375 | 208 | 0.0877 | 327 | 0.1405 | 448 | 0.2012 |
| 91 | 0.0382 | 212 | 0.0893 | 331 | 0.1423 | 451 | 0.2039 |
| 94 | 0.0398 | 215 | 0.0904 | 334 | 0.1441 | 454 | 0.2055 |
| 97 | 0.0416 | 218 | 0.0913 | 337 | 0.1457 | 458 | 0.2078 |
| 101 | 0.0434 | 221 | 0.0931 | 341 | 0.147 | 461 | 0.2101 |
| 104 | 0.0443 | 225 | 0.0945 | 345 | 0.1489 | 465 | 0.2123 |
| 108 | 0.047 | 228 | 0.0961 | 348 | 0.1502 | 468 | 0.2153 |
| 111 | 0.0475 | 232 | 0.0979 | 351 | 0.1523 | 472 | 0.2174 |
| 115 | 0.0482 | 235 | 0.0995 | 355 | 0.1534 | 475 | 0.2194 |
| 119 | 0.0498 | 239 | 0.1004 | 358 | 0.1552 | 478 | 0.2224 |
| 122 | 0.0518 | 242 | 0.1025 | 362 | 0.157 | | |
| 125 | 0.0527 | 245 | 0.1036 | 365 | 0.1584 | | |
| 129 | 0.0541 | 249 | 0.1054 | 369 | 0.1604 | | |
| 132 | 0.0559 | 252 | 0.1063 | 372 | 0.1618 | | |
| 136 | 0.0568 | 256 | 0.1079 | 375 | 0.1636 | | |
| 139 | 0.0586 | 259 | 0.1098 | 379 | 0.1647 | | |
| 143 | 0.0602 | 262 | 0.1114 | 382 | 0.1663 | | |

Specimen ID: 4
Loading: Transverse
Thickness: 30 μm
Loading Rate: 0.015 kN/s

| Load [N] | δ [mm] | Load [N] | δ [mm] | Load [N] | δ [mm] | Load [N] | δ [mm] | Load [N] | δ [mm] |
|---|---|---|---|---|---|---|---|---|---|
| 0 | 0 | 45 | 0.0565 | 73 | 0.0917 | 98 | 0.124 | 122 | 0.1552 |
| 19 | 0.0249 | 46 | 0.0576 | 74 | 0.0928 | 98 | 0.1245 | 122 | 0.1563 |
| 20 | 0.0251 | 47 | 0.0585 | 74 | 0.0938 | 99 | 0.1259 | 123 | 0.1573 |
| 20 | 0.0254 | 48 | 0.0596 | 75 | 0.0959 | 99 | 0.1264 | 124 | 0.1576 |
| 21 | 0.0262 | 48 | 0.0604 | 76 | 0.0967 | 100 | 0.1272 | 124 | 0.1593 |
| 22 | 0.0271 | 49 | 0.0615 | 77 | 0.0983 | 101 | 0.1283 | 125 | 0.1598 |
| 22 | 0.0279 | 50 | 0.0625 | 78 | 0.0986 | 102 | 0.1292 | 126 | 0.1604 |
| 23 | 0.029 | 51 | 0.0635 | 78 | 0.0994 | 102 | 0.13 | 126 | 0.1615 |
| 24 | 0.0298 | 51 | 0.0646 | 79 | 0.1002 | 103 | 0.1313 | 127 | 0.1628 |
| 25 | 0.0308 | 52 | 0.0656 | 80 | 0.1013 | 104 | 0.1322 | 128 | 0.1631 |
| 25 | 0.0318 | 53 | 0.0666 | 80 | 0.1019 | 104 | 0.133 | 129 | 0.1653 |
| 26 | 0.0329 | 54 | 0.0676 | 81 | 0.103 | 105 | 0.1335 | 129 | 0.1653 |
| 27 | 0.0338 | 55 | 0.0685 | 82 | 0.104 | 106 | 0.1346 | 130 | 0.1659 |
| 28 | 0.0347 | 55 | 0.0696 | 82 | 0.1043 | 107 | 0.1357 | 131 | 0.1669 |
| 28 | 0.0356 | 56 | 0.0706 | 83 | 0.1057 | 107 | 0.1368 | 131 | 0.1678 |
| 29 | 0.0365 | 57 | 0.0717 | 84 | 0.1065 | 108 | 0.1371 | 132 | 0.1689 |
| 30 | 0.0376 | 58 | 0.0726 | 84 | 0.1068 | 108 | 0.1382 | 133 | 0.1694 |
| 31 | 0.0384 | 59 | 0.0737 | 85 | 0.1081 | 109 | 0.1393 | 133 | 0.1702 |
| 31 | 0.0395 | 59 | 0.0746 | 86 | 0.1087 | 110 | 0.1395 | 134 | 0.1713 |
| 32 | 0.0407 | 60 | 0.0757 | 86 | 0.1103 | 110 | 0.1415 | 135 | 0.1724 |
| 33 | 0.0415 | 61 | 0.0766 | 87 | 0.1106 | 111 | 0.142 | 136 | 0.1733 |
| 34 | 0.0424 | 62 | 0.0777 | 88 | 0.1114 | 112 | 0.1426 | 136 | 0.1741 |
| 35 | 0.0435 | 63 | 0.0786 | 89 | 0.1125 | 113 | 0.1437 | 137 | 0.1752 |
| 35 | 0.0446 | 64 | 0.0798 | 89 | 0.1136 | 113 | 0.1447 | 138 | 0.176 |
| 36 | 0.0455 | 64 | 0.0806 | 90 | 0.1144 | 114 | 0.1453 | 138 | 0.1768 |
| 37 | 0.0465 | 65 | 0.0816 | 91 | 0.115 | 115 | 0.1467 | 139 | 0.1779 |
| 38 | 0.0476 | 66 | 0.0827 | 91 | 0.1163 | 115 | 0.1469 | 140 | 0.179 |
| 39 | 0.0484 | 67 | 0.0838 | 92 | 0.1169 | 116 | 0.148 | 140 | 0.1801 |
| 40 | 0.0495 | 68 | 0.0848 | 93 | 0.1182 | 117 | 0.1486 | 141 | 0.1807 |
| 40 | 0.0505 | 68 | 0.0856 | 93 | 0.1185 | 117 | 0.1497 | 142 | 0.1812 |
| 41 | 0.0515 | 69 | 0.0868 | 94 | 0.1199 | 118 | 0.1508 | 142 | 0.1818 |
| 42 | 0.0525 | 70 | 0.0877 | 95 | 0.1204 | 119 | 0.1516 | 143 | 0.1832 |
| 43 | 0.0535 | 71 | 0.0888 | 95 | 0.1212 | 120 | 0.153 | 144 | 0.184 |
| 43 | 0.0545 | 71 | 0.0896 | 96 | 0.1229 | 120 | 0.1535 | 144 | 0.1845 |
| 44 | 0.0554 | 72 | 0.0906 | 97 | 0.1223 | 121 | 0.1541 | 145 | 0.1859 |

Specimen ID: 4
Continued from previous

| Load [N] | δ [mm] | Load [N] | δ [mm] |
|---|---|---|---|
| 146 | 0.187 | 165 | 0.2121 |
| 147 | 0.1878 | 166 | 0.2123 |
| 147 | 0.1889 | 166 | 0.2134 |
| 148 | 0.1898 | 167 | 0.2146 |
| 148 | 0.1903 | 168 | 0.2154 |
| 149 | 0.1917 | 169 | 0.2162 |
| 150 | 0.1922 | 169 | 0.2168 |
| 151 | 0.1936 | 170 | 0.2184 |
| 151 | 0.1944 | 171 | 0.2195 |
| 152 | 0.1947 | 171 | 0.2198 |
| 153 | 0.1961 | 172 | 0.2212 |
| 154 | 0.1969 | 173 | 0.2217 |
| 154 | 0.1975 | 173 | 0.2223 |
| 155 | 0.1986 | 174 | 0.2237 |
| 156 | 0.1991 | 175 | 0.2248 |
| 156 | 0.2005 | 175 | 0.2259 |
| 157 | 0.2016 | 176 | 0.227 |
| 158 | 0.2027 | 177 | 0.2278 |
| 158 | 0.203 | 177 | 0.2289 |
| 159 | 0.2038 | 178 | 0.2297 |
| 160 | 0.2049 | 179 | 0.2303 |
| 160 | 0.2057 | 179 | 0.2317 |
| 161 | 0.2068 | 180 | 0.2325 |
| 162 | 0.2082 | 180 | 0.2336 |
| 162 | 0.2088 | 181 | 0.2342 |
| 163 | 0.2099 | 182 | 0.2355 |
| 164 | 0.2107 | 183 | 0.2361 |

Specimen ID: 3
Loading: Transverse
Thickness: 30 μm
Loading Rate: 0.015 kN/s

| Load [N] | δ [mm] | Load [N] | δ [mm] | Load [N] | δ [mm] | Load [N] | δ [mm] | Load [N] | δ [mm] |
|---|---|---|---|---|---|---|---|---|---|
| 0 | 0 | 42 | 0.0542 | 66 | 0.0865 | 91 | 0.1186 | 115 | 0.1505 |
| 19 | 0.0244 | 43 | 0.0554 | 67 | 0.0868 | 92 | 0.1195 | 116 | 0.1513 |
| 20 | 0.0259 | 43 | 0.056 | 68 | 0.0885 | 92 | 0.1204 | 116 | 0.1528 |
| 20 | 0.0262 | 44 | 0.058 | 68 | 0.0897 | 93 | 0.1215 | 117 | 0.1534 |
| 21 | 0.0268 | 45 | 0.058 | 69 | 0.0905 | 94 | 0.1218 | 118 | 0.1548 |
| 22 | 0.0279 | 45 | 0.0592 | 70 | 0.0911 | 94 | 0.123 | 118 | 0.1554 |
| 22 | 0.0282 | 46 | 0.0598 | 70 | 0.092 | 95 | 0.1238 | 119 | 0.1574 |
| 23 | 0.0294 | 47 | 0.0609 | 71 | 0.0929 | 96 | 0.1253 | 120 | 0.1577 |
| 24 | 0.0302 | 47 | 0.0615 | 72 | 0.0937 | 97 | 0.1253 | 120 | 0.1583 |
| 24 | 0.0314 | 48 | 0.0627 | 72 | 0.0949 | 97 | 0.1273 | 121 | 0.1595 |
| 25 | 0.032 | 49 | 0.0635 | 73 | 0.0964 | 98 | 0.1276 | 122 | 0.16 |
| 26 | 0.0328 | 50 | 0.0647 | 74 | 0.0969 | 98 | 0.1282 | 122 | 0.1609 |
| 26 | 0.0328 | 50 | 0.0656 | 75 | 0.0978 | 99 | 0.1293 | 123 | 0.1618 |
| 27 | 0.0343 | 51 | 0.0664 | 75 | 0.0984 | 100 | 0.1305 | 124 | 0.1632 |
| 27 | 0.0357 | 52 | 0.067 | 76 | 0.0996 | 101 | 0.1311 | 125 | 0.1638 |
| 28 | 0.036 | 52 | 0.0679 | 76 | 0.1001 | 101 | 0.1322 | 125 | 0.1653 |
| 29 | 0.0369 | 53 | 0.0687 | 77 | 0.1013 | 102 | 0.1334 | 126 | 0.1658 |
| 30 | 0.0375 | 54 | 0.0699 | 78 | 0.1019 | 103 | 0.1342 | 127 | 0.1667 |
| 30 | 0.0383 | 54 | 0.0708 | 79 | 0.103 | 103 | 0.1357 | 127 | 0.1682 |
| 31 | 0.0398 | 55 | 0.0722 | 79 | 0.1039 | 104 | 0.1363 | 128 | 0.1687 |
| 31 | 0.0403 | 56 | 0.0725 | 80 | 0.1048 | 105 | 0.1371 | 129 | 0.1693 |
| 32 | 0.0415 | 56 | 0.0737 | 81 | 0.106 | 106 | 0.138 | 129 | 0.1699 |
| 33 | 0.0421 | 57 | 0.0745 | 81 | 0.1065 | 106 | 0.1397 | 130 | 0.1711 |
| 34 | 0.0435 | 58 | 0.0754 | 82 | 0.108 | 107 | 0.1397 | 131 | 0.1725 |
| 34 | 0.0441 | 59 | 0.0763 | 83 | 0.1083 | 107 | 0.1409 | 131 | 0.1734 |
| 35 | 0.0453 | 59 | 0.0772 | 83 | 0.1092 | 108 | 0.1409 | 132 | 0.1748 |
| 36 | 0.0467 | 60 | 0.0792 | 84 | 0.1103 | 109 | 0.1423 | 133 | 0.1751 |
| 36 | 0.0473 | 61 | 0.0792 | 85 | 0.1112 | 109 | 0.1435 | 134 | 0.176 |
| 37 | 0.0484 | 61 | 0.0801 | 86 | 0.1118 | 110 | 0.1441 | 134 | 0.1766 |
| 38 | 0.049 | 62 | 0.0809 | 86 | 0.113 | 111 | 0.1452 | 135 | 0.178 |
| 38 | 0.0496 | 63 | 0.0818 | 87 | 0.1138 | 112 | 0.1461 | 135 | 0.1786 |
| 39 | 0.0508 | 64 | 0.0827 | 88 | 0.115 | 112 | 0.1476 | 136 | 0.1795 |
| 40 | 0.0516 | 64 | 0.0833 | 88 | 0.1156 | 113 | 0.1481 | 137 | 0.1801 |
| 41 | 0.0531 | 65 | 0.0847 | 89 | 0.117 | 113 | 0.1493 | 138 | 0.1809 |
| 41 | 0.0534 | 66 | 0.0862 | 90 | 0.118 | 114 | 0.1496 | 138 | 0.1818 |

Specimen ID: 3
Continued from previous

| Load [N] | δ [mm] | Load [N] | δ [mm] |
|---|---|---|---|
| 139 | 0.1827 | 157 | 0.2092 |
| 140 | 0.1844 | 158 | 0.2101 |
| 140 | 0.1853 | 154 | 0.2107 |
| 141 | 0.1865 | 155 | 0.2124 |
| 142 | 0.1873 | | |
| 142 | 0.1888 | | |
| 143 | 0.1894 | | |
| 144 | 0.19 | | |
| 144 | 0.1905 | | |
| 145 | 0.1917 | | |
| 146 | 0.1926 | | |
| 147 | 0.194 | | |
| 147 | 0.1949 | | |
| 148 | 0.1967 | | |
| 149 | 0.1972 | | |
| 149 | 0.1981 | | |
| 150 | 0.1987 | | |
| 151 | 0.1996 | | |
| 151 | 0.201 | | |
| 152 | 0.201 | | |
| 152 | 0.2034 | | |
| 153 | 0.2034 | | |
| 154 | 0.2039 | | |
| 155 | 0.2054 | | |
| 155 | 0.2072 | | |
| 156 | 0.2074 | | |
| 157 | 0.2083 | | |

Specimen ID: 2
Loading: Longitudinal
Thickness: 30 μm
Loading Rate: 0.015 kN/s

| Load [N] | δ [mm] | Load [N] | δ [mm] | Load [N] | δ [mm] | Load [N] | δ [mm] | Load [N] | δ [mm] |
|---|---|---|---|---|---|---|---|---|---|
| 0 | 0 | 39 | 0.0513 | 63 | 0.0831 | 87 | 0.1147 | 111 | 0.1472 |
| 19 | 0.0254 | 40 | 0.0511 | 64 | 0.0839 | 88 | 0.1163 | 112 | 0.1483 |
| 19 | 0.0251 | 40 | 0.053 | 65 | 0.0847 | 89 | 0.1166 | 113 | 0.1494 |
| 19 | 0.0254 | 41 | 0.0532 | 65 | 0.0861 | 89 | 0.1177 | 113 | 0.15 |
| 19 | 0.0246 | 42 | 0.0552 | 66 | 0.0864 | 90 | 0.1188 | 114 | 0.1508 |
| 20 | 0.0254 | 43 | 0.0552 | 67 | 0.0878 | 91 | 0.1194 | 115 | 0.1525 |
| 20 | 0.026 | 43 | 0.0565 | 67 | 0.0886 | 91 | 0.1194 | 115 | 0.153 |
| 20 | 0.0268 | 44 | 0.0576 | 68 | 0.0894 | 92 | 0.121 | 116 | 0.1536 |
| 21 | 0.0273 | 45 | 0.059 | 69 | 0.09 | 93 | 0.1216 | 117 | 0.1547 |
| 22 | 0.0281 | 45 | 0.0593 | 69 | 0.0908 | 94 | 0.1221 | 117 | 0.1558 |
| 22 | 0.0287 | 46 | 0.0601 | 70 | 0.0924 | 94 | 0.1238 | 118 | 0.1561 |
| 23 | 0.0292 | 47 | 0.0606 | 71 | 0.0927 | 95 | 0.1246 | 119 | 0.1575 |
| 23 | 0.03 | 47 | 0.0617 | 72 | 0.0938 | 96 | 0.1257 | 120 | 0.1588 |
| 24 | 0.0306 | 48 | 0.0628 | 72 | 0.0949 | 96 | 0.1268 | 120 | 0.1597 |
| 25 | 0.0314 | 49 | 0.0636 | 73 | 0.096 | 97 | 0.1271 | 121 | 0.1611 |
| 25 | 0.033 | 49 | 0.0645 | 74 | 0.0965 | 98 | 0.1285 | 121 | 0.1611 |
| 26 | 0.0333 | 50 | 0.0658 | 74 | 0.0974 | 98 | 0.1296 | 122 | 0.1624 |
| 27 | 0.0347 | 51 | 0.0669 | 75 | 0.0982 | 99 | 0.1298 | 123 | 0.1633 |
| 27 | 0.0358 | 52 | 0.0677 | 76 | 0.0996 | 100 | 0.1315 | 124 | 0.1641 |
| 28 | 0.0363 | 52 | 0.0686 | 76 | 0.1001 | 100 | 0.1318 | 124 | 0.1652 |
| 29 | 0.0374 | 53 | 0.0697 | 77 | 0.1009 | 101 | 0.1334 | 125 | 0.1663 |
| 29 | 0.0396 | 54 | 0.0708 | 78 | 0.102 | 102 | 0.1337 | 126 | 0.1666 |
| 30 | 0.039 | 54 | 0.0708 | 78 | 0.1029 | 102 | 0.1348 | 126 | 0.1677 |
| 31 | 0.0401 | 55 | 0.0724 | 79 | 0.104 | 103 | 0.1356 | 127 | 0.1691 |
| 32 | 0.0404 | 56 | 0.0732 | 80 | 0.1042 | 104 | 0.1365 | 128 | 0.1699 |
| 32 | 0.042 | 56 | 0.0735 | 81 | 0.1056 | 105 | 0.1381 | 128 | 0.1707 |
| 33 | 0.0434 | 57 | 0.0749 | 81 | 0.1067 | 105 | 0.1387 | 129 | 0.1719 |
| 33 | 0.0437 | 58 | 0.076 | 82 | 0.107 | 106 | 0.1398 | 130 | 0.1721 |
| 34 | 0.0448 | 58 | 0.0771 | 83 | 0.1081 | 106 | 0.1406 | 130 | 0.1732 |
| 35 | 0.0456 | 59 | 0.0779 | 83 | 0.1092 | 107 | 0.1414 | 131 | 0.1738 |
| 36 | 0.0464 | 60 | 0.0782 | 84 | 0.1111 | 108 | 0.1423 | 132 | 0.1752 |
| 36 | 0.0472 | 61 | 0.0793 | 85 | 0.1117 | 108 | 0.1436 | 133 | 0.1766 |
| 37 | 0.0483 | 61 | 0.0809 | 85 | 0.1114 | 109 | 0.1439 | 133 | 0.1779 |
| 38 | 0.0489 | 62 | 0.0809 | 86 | 0.1125 | 110 | 0.145 | 134 | 0.1788 |
| 38 | 0.0497 | 63 | 0.082 | 87 | 0.1141 | 111 | 0.1461 | 135 | 0.1793 |

Specimen ID: 2
Continued from previous

| Load [N] | δ [mm] |
|---|---|
| 135 | 0.1802 |
| 136 | 0.1804 |
| 136 | 0.1827 |
| 137 | 0.1824 |
| 138 | 0.184 |
| 139 | 0.1849 |
| 139 | 0.1863 |
| 140 | 0.1879 |
| 141 | 0.1882 |
| 141 | 0.1893 |
| 142 | 0.1904 |
| 143 | 0.1915 |
| 143 | 0.1923 |
| 144 | 0.1934 |
| 144 | 0.1945 |
| 145 | 0.1956 |
| 146 | 0.1976 |
| 146 | 0.1976 |
| 147 | 0.1987 |
| 148 | 0.1995 |
| 148 | 0.2009 |
| 149 | 0.2022 |
| 149 | 0.2033 |
| 148 | 0.2047 |
| 149 | 0.2069 |

Specimen ID: 1
Loading: Longitudinal
Thickness: 100 μm
Loading Rate: 0.015 kN/s

| Load [N] | δ [mm] | Load [N] | δ [mm] | Load [N] | δ [mm] | Load [N] | δ [mm] | Load [N] | δ [mm] |
|---|---|---|---|---|---|---|---|---|---|
| 0 | 0 | 39 | 0.0483 | 63 | 0.0804 | 88 | 0.1133 | 112 | 0.146 |
| 19 | 0.023 | 40 | 0.049 | 64 | 0.0811 | 88 | 0.1141 | 112 | 0.1468 |
| 19 | 0.0234 | 41 | 0.0497 | 65 | 0.0818 | 89 | 0.1155 | 113 | 0.1478 |
| 19 | 0.0234 | 41 | 0.0508 | 66 | 0.0829 | 90 | 0.1158 | 114 | 0.1493 |
| 19 | 0.0234 | 42 | 0.0515 | 66 | 0.0839 | 90 | 0.1173 | 115 | 0.1503 |
| 19 | 0.023 | 43 | 0.0525 | 67 | 0.0846 | 91 | 0.1183 | 115 | 0.1514 |
| 20 | 0.0237 | 43 | 0.0536 | 68 | 0.0864 | 92 | 0.119 | 116 | 0.1521 |
| 20 | 0.0244 | 44 | 0.0543 | 69 | 0.0871 | 93 | 0.1197 | 117 | 0.1532 |
| 21 | 0.0255 | 45 | 0.0557 | 69 | 0.0878 | 93 | 0.1212 | 117 | 0.1539 |
| 22 | 0.0259 | 46 | 0.0564 | 70 | 0.0889 | 94 | 0.1219 | 118 | 0.1553 |
| 22 | 0.0266 | 46 | 0.0568 | 71 | 0.0892 | 95 | 0.1222 | 119 | 0.156 |
| 23 | 0.0269 | 47 | 0.0582 | 71 | 0.0903 | 95 | 0.1233 | 119 | 0.1574 |
| 24 | 0.028 | 48 | 0.0589 | 72 | 0.0914 | 96 | 0.1244 | 120 | 0.1578 |
| 24 | 0.0287 | 48 | 0.0604 | 72 | 0.0924 | 97 | 0.1261 | 121 | 0.1589 |
| 25 | 0.0298 | 49 | 0.0611 | 73 | 0.0935 | 97 | 0.1261 | 121 | 0.1599 |
| 25 | 0.0308 | 50 | 0.0618 | 74 | 0.0942 | 98 | 0.1268 | 122 | 0.161 |
| 26 | 0.0316 | 50 | 0.0629 | 75 | 0.096 | 99 | 0.1286 | 123 | 0.1617 |
| 27 | 0.0316 | 51 | 0.0636 | 75 | 0.0967 | 100 | 0.1297 | 124 | 0.1628 |
| 27 | 0.0333 | 52 | 0.0654 | 76 | 0.0974 | 100 | 0.1304 | 124 | 0.1642 |
| 28 | 0.0344 | 52 | 0.0661 | 77 | 0.0977 | 101 | 0.1311 | 125 | 0.1653 |
| 29 | 0.0351 | 53 | 0.0664 | 77 | 0.0992 | 102 | 0.1325 | 126 | 0.166 |
| 30 | 0.0358 | 54 | 0.0671 | 78 | 0.0999 | 102 | 0.1325 | 126 | 0.1671 |
| 30 | 0.0365 | 55 | 0.0686 | 79 | 0.1009 | 103 | 0.1347 | 127 | 0.1678 |
| 31 | 0.0372 | 55 | 0.0689 | 79 | 0.102 | 103 | 0.1354 | 128 | 0.1689 |
| 32 | 0.039 | 56 | 0.0703 | 80 | 0.1031 | 104 | 0.1361 | 128 | 0.1706 |
| 32 | 0.039 | 57 | 0.0711 | 81 | 0.1034 | 105 | 0.1372 | 129 | 0.171 |
| 33 | 0.0404 | 57 | 0.0718 | 82 | 0.1048 | 106 | 0.1379 | 130 | 0.1721 |
| 34 | 0.0415 | 58 | 0.0728 | 82 | 0.1055 | 106 | 0.1382 | 130 | 0.1731 |
| 34 | 0.0422 | 59 | 0.0732 | 83 | 0.107 | 107 | 0.1393 | 131 | 0.1735 |
| 35 | 0.0426 | 59 | 0.075 | 84 | 0.1077 | 108 | 0.1404 | 132 | 0.1753 |
| 36 | 0.044 | 60 | 0.0758 | 84 | 0.1087 | 108 | 0.1418 | 132 | 0.176 |
| 37 | 0.0447 | 61 | 0.0761 | 85 | 0.1094 | 109 | 0.1432 | 133 | 0.1771 |
| 37 | 0.0458 | 62 | 0.0772 | 86 | 0.1102 | 110 | 0.1436 | 134 | 0.1774 |
| 38 | 0.0461 | 62 | 0.0783 | 86 | 0.1112 | 110 | 0.1443 | 134 | 0.1788 |
| 39 | 0.0468 | 63 | 0.0797 | 87 | 0.1123 | 111 | 0.1457 | 135 | 0.1792 |

Specimen ID: 1
Continued from previous

| Load [N] | δ [mm] |
|---|---|
| 136 | 0.1803 |
| 136 | 0.1813 |
| 137 | 0.1831 |
| 138 | 0.1838 |
| 139 | 0.1842 |
| 139 | 0.1856 |
| 140 | 0.1874 |
| 141 | 0.1878 |
| 141 | 0.1888 |
| 142 | 0.1903 |
| 143 | 0.191 |
| 143 | 0.1921 |
| 144 | 0.1928 |
| 145 | 0.1938 |
| 145 | 0.1949 |
| 146 | 0.1963 |
| 147 | 0.1971 |
| 147 | 0.1981 |
| 148 | 0.1992 |
| 148 | 0.2013 |
| 149 | 0.2017 |
| 149 | 0.2024 |
| 148 | 0.2042 |
| 149 | 0.2071 |
| 150 | 0.2085 |

# APPENDIX C

# FATIGUE TESTS

Specimen ID: 1
Loading: Longitudinal
Thickness: 30 μm
Notch Length: 2.70 mm

| Right Side a | | Left Side b | |
|---|---|---|---|
| Cycles | Crack Growth [mm] | Cycles | Crack Growth [mm] |
| 0 | 0 | 0 | 0 |
| 5000 | 0.01875 | 5000 | 0.0375 |
| 5500 | 0.0375 | 5500 | 0.05625 |
| 6000 | 0.05625 | 6000 | 0.075 |
| 6500 | 0.075 | 6500 | 0.09375 |
| 7000 | 0.09375 | 7000 | 0.1125 |
| 7500 | 0.1125 | 7500 | 0.13125 |
| 8000 | 0.13125 | 8000 | 0.15 |
| 8500 | 0.15 | 8500 | 0.16875 |
| 9500 | 0.20625 | 9500 | 0.2625 |
| 10500 | 0.28125 | 10500 | 0.375 |
| 11500 | 0.375 | 11500 | 0.50625 |
| 12100 | 0.4125 | 12100 | 0.5625 |
| 13100 | 0.50625 | 13100 | 0.65625 |
| 14100 | 0.6375 | 14100 | 0.76875 |
| 15100 | 0.75 | 15100 | 0.9 |
| 16100 | 0.8625 | 16100 | 0.99375 |
| 17100 | 1.05 | 17100 | 1.14375 |
| 18100 | 1.2375 | 18100 | 1.40625 |
| 19100 | 1.5375 | 19100 | 1.6875 |
| 19600 | 1.6875 | 19600 | 1.96875 |
| 20100 | 1.875 | 20100 | 2.11875 |
| 20600 | 2.0625 | 20600 | 2.25 |
| 21000 | 2.25 | 21000 | 2.4375 |
| 21700 | 2.625 | 21700 | 3 |

Specimen ID: 2
Loading: Longitudinal
Thickness: 30 μm
Notch Length: 2.06 mm

| Right Side a | | Left Side b | |
|---|---|---|---|
| Cycles | Crack Growth [mm] | Cycles | Crack Growth [mm] |
| 0 | 0 | 0 | 0 |
| 13000 | 0.05625 | 13000 | 0.01875 |
| 14000 | 0.13125 | 14000 | 0.0375 |
| 15000 | 0.28125 | 15000 | 0.1125 |
| 15600 | 0.375 | 15600 | 0.1875 |
| 16200 | 0.4125 | 16200 | 0.225 |
| 16800 | 0.46875 | 16800 | 0.28125 |
| 17500 | 0.58125 | 17500 | 0.43125 |
| 18000 | 0.65625 | 18000 | 0.4875 |
| 18600 | 0.84375 | 18600 | 0.58125 |
| 19200 | 0.91875 | 19200 | 0.65625 |
| 19800 | 0.975 | 19800 | 0.75 |
| 20400 | 1.05 | 20400 | 0.84375 |
| 21000 | 1.1625 | 21000 | 1.03125 |
| 21600 | 1.40625 | 21600 | 1.1625 |
| 22200 | 1.55625 | 22200 | 1.3125 |
| 22800 | 1.875 | 22800 | 1.51875 |
| 23300 | 2.175 | 23300 | 1.875 |
| 23800 | 2.85 | 23800 | 2.4375 |

Specimen ID: 3
Loading: Longitudinal
Thickness: 30 μm
Notch Length: 2.00 mm

| Right Side a | | Left Side b | |
|---|---|---|---|
| Cycles | Crack Growth [mm] | Cycles | Crack Growth [mm] |
| 0 | 0 | 0 | 0 |
| 3000 | 0.01875 | 3000 | 0.01875 |
| 4000 | 0.05625 | 4000 | 0.13125 |
| 5000 | 0.1875 | 5000 | 0.375 |
| 5500 | 0.31875 | 5500 | 0.46875 |
| 6000 | 0.46875 | 6000 | 0.6 |
| 6500 | 0.5625 | 6500 | 0.75 |
| 7000 | 0.7875 | 7000 | 0.95625 |
| 7500 | 1.125 | 7500 | 1.3125 |

Specimen ID: 4
Loading: Longitudinal
Thickness: 30 μm
Notch Length: 2.06 mm

| Right Side a | | Left Side b | |
|---|---|---|---|
| Cycles | Crack Growth [mm] | Cycles | Crack Growth [mm] |
| 0 | 0 | 0 | 0 |
| 4000 | 0.01875 | 4000 | 0.0375 |
| 4500 | 0.05625 | 4500 | 0.09375 |
| 5000 | 0.075 | 5000 | 0.15 |
| 5600 | 0.1125 | 5600 | 0.3375 |
| 6200 | 0.1875 | 6200 | 0.43125 |
| 6700 | 0.28125 | 6700 | 0.4875 |
| 7200 | 0.4125 | 7200 | 0.675 |
| 7700 | 0.6 | 7700 | 0.91875 |
| 8200 | 0.75 | 8200 | 1.05 |
| 8700 | 1.125 | 8700 | 1.35 |

Specimen ID: 5
Loading: Transverse
Thickness: 30 μm
Notch Length: 2.53 mm

| Right Side a | | Left Side b | |
|---|---|---|---|
| Cycles | Crack Growth [mm] | Cycles | Crack Growth [mm] |
| 0 | 0 | 0 | 0 |
| 600 | 0.05625 | 600 | 0.0375 |
| 1200 | 0.09375 | 1200 | 0.09375 |
| 1800 | 0.15 | 1800 | 0.15 |
| 2400 | 0.28125 | 2400 | 0.20625 |
| 3000 | 0.525 | 3000 | 0.39375 |
| 3600 | 0.65625 | 3600 | 0.5625 |
| 4100 | 0.84375 | 4100 | 0.8625 |
| 4600 | 1.40625 | 4600 | 1.3125 |
| 4800 | 2.23125 | 4800 | 2.1375 |
| 5000 | 2.53125 | 5000 | 2.4375 |
| 5200 | 2.8125 | 5200 | 2.625 |
| 5500 | 3.5625 | 5500 | 3.375 |

Specimen ID: 6
Loading: Transverse
Thickness: 30 μm
Notch Length: 2.14 mm

| Right Side a | | Left Side b | |
|---|---|---|---|
| Cycles | Crack Growth [mm] | Cycles | Crack Growth [mm] |
| 0 | 0 | 0 | 0 |
| 9000 | 0.0375 | 9000 | 0.075 |
| 10000 | 0.05625 | 10000 | 0.13125 |
| 11000 | 0.075 | 11000 | 0.15 |
| 12000 | 0.1125 | 12000 | 0.1875 |
| 13000 | 0.16875 | 13000 | 0.28125 |
| 14000 | 0.31875 | 14000 | 0.375 |
| 15000 | 0.39375 | 15000 | 0.45 |
| 15600 | 0.46875 | 15600 | 0.50625 |
| 16200 | 0.54375 | 16200 | 0.58125 |
| 16800 | 0.61875 | 16800 | 0.6375 |
| 17400 | 0.69375 | 17400 | 0.76875 |
| 18000 | 0.80625 | 18000 | 0.8625 |
| 18600 | 0.91875 | 18600 | 1.05 |
| 19200 | 1.0875 | 19200 | 1.3125 |
| 19800 | 1.21875 | 19800 | 1.4625 |
| 20400 | 1.55625 | 20400 | 1.7625 |
| 21000 | 2.15625 | 21000 | 1.96875 |

Specimen ID: 7
Loading: Transverse
Thickness: 30 μm
Notch Length: 2.06 mm

| Right Side a | | Left Side b | |
|---|---|---|---|
| Cycles | Crack Growth [mm] | Cycles | Crack Growth [mm] |
| 0 | 0 | 0 | 0 |
| 3600 | 0.01875 | 3600 | 0.0375 |
| 4200 | 0.0375 | 4200 | 0.075 |
| 5200 | 0.05625 | 5200 | 0.16875 |
| 5700 | 0.075 | 5700 | 0.31875 |
| 6100 | 0.13125 | 6100 | 0.4125 |
| 6500 | 0.16875 | 6500 | 0.525 |
| 6900 | 0.28125 | 6900 | 0.73125 |

Specimen ID: 8
Loading: Transverse
Thickness: 30 μm
Notch Length: 2.08 mm

| Right Side a | | Left Side b | |
|---|---|---|---|
| Cycles | Crack Growth [mm] | Cycles | Crack Growth [mm] |
| 0 | 0 | 0 | 0 |
| 3200 | 0.01875 | 3200 | 0.01875 |
| 3800 | 0.0375 | 3800 | 0.0375 |
| 4400 | 0.05625 | 4400 | 0.075 |
| 5000 | 0.075 | 5000 | 0.13125 |
| 6000 | 0.13125 | 6000 | 0.1875 |
| 7000 | 0.16875 | 7000 | 0.225 |
| 8000 | 0.28125 | 8000 | 0.375 |
| 8600 | 0.6375 | 8600 | 0.65625 |
| 9100 | 0.75 | 9100 | 0.95625 |
| 9500 | 0.9 | 9500 | 1.3125 |

Specimen ID: 1
Loading: Longitudinal
Thickness: 100 μm
Notch Length: 2.4 mm

| Right Side a | | | | Left Side b | | | |
|---|---|---|---|---|---|---|---|
| Cycles | Crack Growth [mm] | Cycles | Crack Growth [mm] | Cycles | Crack Growth [mm] | Cycles | Crack Growth [mm] |
| 0 | 0 | 70000 | 1.3125 | 0 | 0 | 73500 | 1.93125 |
| 4000 | 0.0375 | 72000 | 1.4625 | 4000 | 0.01875 | 74000 | 2.0625 |
| 8000 | 0.05625 | 73000 | 1.6125 | 14000 | 0.0375 | 74500 | 2.175 |
| 14000 | 0.075 | 73500 | 1.6875 | 20000 | 0.05625 | 75000 | 2.23125 |
| 18000 | 0.09375 | 74000 | 1.89375 | 24000 | 0.075 | 75500 | 2.2875 |
| 20000 | 0.1125 | 74500 | 1.96875 | 26000 | 0.09375 | 76000 | 2.34375 |
| 22000 | 0.13125 | 75000 | 2.00625 | 28000 | 0.1125 | 77000 | 2.625 |
| 24000 | 0.15 | 75500 | 2.0625 | 30000 | 0.15 | 77500 | 2.8125 |
| 26000 | 0.16875 | 76000 | 2.15625 | 32000 | 0.1875 | 78000 | 3 |
| 28000 | 0.1875 | 77000 | 2.25 | 34000 | 0.2625 | 78500 | 3.1875 |
| 30000 | 0.20625 | 77500 | 2.325 | 35000 | 0.31875 | 79000 | 3.375 |
| 32000 | 0.225 | 78000 | 2.53125 | 36000 | 0.3375 | 79500 | 3.5625 |
| 34000 | 0.35625 | 78500 | 2.775 | 38000 | 0.46875 | 80000 | 3.9375 |
| 35000 | 0.4125 | 79000 | 2.90625 | 39000 | 0.4875 | 80500 | 4.3875 |
| 36000 | 0.45 | 79500 | 3.15 | 40000 | 0.50625 | 81000 | 4.96875 |
| 38000 | 0.5625 | 80000 | 3.43125 | 42000 | 0.58125 | 81500 | 6.375 |
| 39000 | 0.58125 | 80500 | 3.84375 | 44000 | 0.65625 | | |
| 40000 | 0.6 | 81000 | 4.40625 | 46000 | 0.73125 | | |
| 42000 | 0.65625 | 81500 | 5.15625 | 48000 | 0.7875 | | |
| 44000 | 0.7125 | | | 50000 | 0.825 | | |
| 46000 | 0.76875 | | | 52000 | 0.9 | | |
| 48000 | 0.80625 | | | 54000 | 0.91875 | | |
| 50000 | 0.84375 | | | 56000 | 0.975 | | |
| 52000 | 0.9 | | | 58000 | 1.05 | | |
| 54000 | 0.9375 | | | 60000 | 1.125 | | |
| 56000 | 0.975 | | | 62000 | 1.18125 | | |
| 58000 | 1.0125 | | | 64000 | 1.2375 | | |
| 60000 | 1.05 | | | 66000 | 1.3125 | | |
| 62000 | 1.06875 | | | 68000 | 1.425 | | |
| 64000 | 1.1625 | | | 70000 | 1.5375 | | |
| 66000 | 1.21875 | | | 72000 | 1.6875 | | |
| 68000 | 1.2375 | | | 73000 | 1.85625 | | |

Specimen ID: 2
Loading: Longitudinal
Thickness: 100 μm
Notch Length: 1.98 mm

| Right Side a | | Left Side b | |
|---|---|---|---|
| Cycles | Crack Growth [mm] | Cycles | Crack Growth [mm] |
| 0 | 0 | 0 | 0 |
| 380000 | 0.01875 | 315000 | 0.01875 |
| 390000 | 0.0375 | 320000 | 0.0375 |
| 395000 | 0.046875 | 325000 | 0.05625 |
| 400000 | 0.05625 | 330000 | 0.1125 |
| 405000 | 0.075 | 335000 | 0.15 |
| 410000 | 0.09375 | 340000 | 0.1875 |
| 415000 | 0.1875 | 345000 | 0.225 |
| 420000 | 0.28125 | 350000 | 0.3 |
| 425000 | 0.4125 | 355000 | 0.35625 |
| 430000 | 0.46875 | 360000 | 0.39375 |
| 435000 | 0.6 | 365000 | 0.46875 |
| 440000 | 0.675 | 370000 | 0.54375 |
| 445000 | 0.7875 | 375000 | 0.6 |
| 450000 | 0.9375 | 380000 | 0.6375 |
| 455000 | 1.14375 | 385000 | 0.65625 |
| 460000 | 1.4625 | 390000 | 0.69375 |
| 462000 | 1.63125 | 395000 | 0.73125 |
| 464000 | 1.78125 | 400000 | 0.76875 |
| 466000 | 2.0625 | 405000 | 0.84375 |
| 468000 | 2.53125 | 410000 | 0.9375 |
| 469000 | 2.775 | 415000 | 0.975 |
| 470000 | 3 | 420000 | 1.0875 |
| 471000 | 3.1875 | 425000 | 1.1625 |
| 472000 | 3.46875 | 430000 | 1.21875 |
| 473000 | 3.9375 | 435000 | 1.3125 |
| 474000 | 5.25 | 440000 | 1.35 |

Specimen ID: 3
Loading: Longitudinal
Thickness: 100 μm
Notch Length: 1.9 mm

| Right Side a | | Left Side b | |
|---|---|---|---|
| Cycles | Crack Growth [mm] | Cycles | Crack Growth [mm] |
| 0 | 0 | 0 | 0 |
| 18000 | 0.01875 | 16000 | 0.01875 |
| 20000 | 0.0375 | 18000 | 0.0375 |
| 22000 | 0.075 | 20000 | 0.05625 |
| 23000 | 0.1125 | 22000 | 0.1125 |
| 24000 | 0.16875 | 23000 | 0.16875 |
| 25500 | 0.225 | 24000 | 0.20625 |
| 26500 | 0.28125 | 25500 | 0.3 |
| 28000 | 0.375 | 26500 | 0.35625 |
| 29500 | 0.46875 | 28000 | 0.4125 |
| 31000 | 0.5625 | 29500 | 0.50625 |
| 32500 | 0.675 | 31000 | 0.65625 |
| 34000 | 0.75 | 32500 | 0.76875 |
| 35000 | 0.84375 | 34000 | 0.8625 |
| 36000 | 0.975 | 35000 | 0.9375 |
| 37000 | 1.05 | 36000 | 1.03125 |
| 38000 | 1.18125 | 37000 | 1.125 |
| 39000 | 1.3125 | 38000 | 1.2375 |
| 40000 | 1.5 | 39000 | 1.33125 |
| 41000 | 1.70625 | 40000 | 1.5375 |
| 42000 | 1.95 | 41000 | 1.725 |
| 43000 | 2.34375 | 42000 | 2.0625 |
| 44000 | 3 | 43000 | 2.4 |
| 45000 | 3.825 | 44000 | 3.075 |

Specimen ID: 4
Loading: Longitudinal
Thickness: 100 μm
Notch Length: 1.96 mm

| Right Side a | | Left Side b | |
|---|---|---|---|
| Cycles | Crack Growth [mm] | Cycles | Crack Growth [mm] |
| 0 | 0 | 0 | 0 |
| 10000 | 0.01875 | 12000 | 0.01875 |
| 12000 | 0.1125 | 13000 | 0.0375 |
| 13000 | 0.13125 | 14000 | 0.05625 |
| 14000 | 0.1875 | 15000 | 0.09375 |
| 15000 | 0.20625 | 17000 | 0.15 |
| 17000 | 0.3 | 19000 | 0.225 |
| 19000 | 0.3375 | 21000 | 0.375 |
| 21000 | 0.4875 | 22000 | 0.46875 |
| 22000 | 0.54375 | 23000 | 0.5625 |
| 23000 | 0.6375 | 24000 | 0.65625 |
| 24000 | 0.7125 | 25000 | 0.75 |
| 25000 | 0.7875 | 26000 | 0.8625 |
| 26000 | 0.9 | 27000 | 0.9375 |
| 27000 | 0.975 | 28000 | 1.0125 |
| 28000 | 1.06875 | 29000 | 1.0875 |
| 29000 | 1.1625 | 30000 | 1.2375 |
| 30000 | 1.275 | 31000 | 1.40625 |
| 31000 | 1.5375 | 31500 | 1.5375 |
| 31500 | 1.6875 | 32000 | 1.66875 |
| 32000 | 1.8 | 32500 | 1.78125 |
| 32500 | 1.875 | 33000 | 1.875 |
| 33000 | 1.96875 | 33500 | 2.1 |
| 33500 | 2.15625 | 34000 | 2.25 |
| 34000 | 2.30625 | 34500 | 2.4375 |
| 34500 | 2.53125 | 35000 | 2.8125 |
| 35000 | 3.09375 | 35500 | 3.1875 |
| 35500 | 3.46875 | 36000 | 3.75 |
| 36000 | 3.9375 | | |

Specimen ID: 5
Loading: Longitudinal
Thickness: 100 μm
Notch Length: 1.96 mm

| Right Side a | | Left Side b | |
|---|---|---|---|
| Cycles | Crack Growth [mm] | Cycles | Crack Growth [mm] |
| 0 | 0 | 0 | 0 |
| 2000 | 0.01875 | 2000 | 0.01875 |
| 3000 | 0.05625 | 3000 | 0.0375 |
| 3500 | 0.09375 | 3500 | 0.09375 |
| 4000 | 0.13125 | 4000 | 0.13125 |
| 4500 | 0.16875 | 4500 | 0.16875 |
| 5500 | 0.375 | 5500 | 0.28125 |
| 6000 | 0.43125 | 6000 | 0.375 |
| 6500 | 0.5625 | 6500 | 0.50625 |
| 7000 | 0.6375 | 7000 | 0.5625 |
| 7500 | 0.75 | 7500 | 0.65625 |
| 8000 | 0.9375 | 8000 | 0.7875 |
| 8500 | 1.125 | 8500 | 0.9375 |
| 9000 | 1.3125 | 9000 | 1.1625 |
| 9500 | 1.4625 | 9500 | 1.3125 |
| 10000 | 1.96875 | 10000 | 1.875 |
| 10500 | 3 | 10500 | 2.53125 |

Specimen ID: 6
Loading: Longitudinal
Thickness: 100 μm
Notch Length: 1.90 mm

| Right Side a | | Left Side b | |
|---|---|---|---|
| Cycles | Crack Growth [mm] | Cycles | Crack Growth [mm] |
| 0 | 0 | 0 | 0 |
| 3500 | 0.01875 | 3000 | 0.01875 |
| 4000 | 0.0375 | 3500 | 0.0375 |
| 4500 | 0.05625 | 4000 | 0.05625 |
| 5000 | 0.075 | 4500 | 0.075 |
| 6000 | 0.09375 | 5000 | 0.09375 |
| 6600 | 0.15 | 6000 | 0.13125 |
| 7200 | 0.225 | 6600 | 0.16875 |
| 7700 | 0.375 | 7200 | 0.225 |
| 8200 | 0.4875 | 7700 | 0.375 |
| 8700 | 0.6 | 8200 | 0.46875 |
| 9200 | 0.7125 | 8700 | 0.5625 |
| 9700 | 0.84375 | 9200 | 0.675 |
| 10200 | 0.99375 | 9700 | 0.75 |
| 10700 | 1.125 | 10200 | 0.95625 |
| 11200 | 1.3875 | 10700 | 1.06875 |
| 11700 | 1.6875 | 11200 | 1.25625 |
| 12200 | 2.2125 | 11700 | 1.59375 |
| | | 12200 | 2.2125 |

Specimen ID: 7
Loading: Longitudinal
Thickness: 250 μm
Notch Length: 3.0 mm

| Right Side a | | | | Left Side b | | | |
|---|---|---|---|---|---|---|---|
| Cycles | Crack Growth [mm] | Cycles | Crack Growth [mm] | Cycles | Crack Growth [mm] | Cycles | Crack Growth [mm] |
| 50000 | 0 | 302000 | 2.4 | 50000 | 0 | 304000 | 2.2875 |
| 85000 | 0.0375 | 304000 | 2.4375 | 135000 | 0.01875 | 306000 | 2.4375 |
| 100000 | 0.05625 | 306000 | 2.53125 | 140000 | 0.05625 | 308000 | 2.55 |
| 125000 | 0.075 | 308000 | 2.625 | 145000 | 0.075 | 310000 | 2.71875 |
| 135000 | 0.09375 | 310000 | 2.8125 | 150000 | 0.09375 | 312000 | 3.15 |
| 140000 | 0.1125 | 312000 | 3.1875 | 155000 | 0.13125 | 313000 | 3.43125 |
| 150000 | 0.13125 | 313000 | 3.5625 | 160000 | 0.1875 | 314000 | 3.65625 |
| 160000 | 0.15 | 314000 | 3.84375 | 180000 | 0.225 | 315000 | 3.7125 |
| 170000 | 0.16875 | 315000 | 3.9375 | 245000 | 0.2625 | 316000 | 3.73125 |
| 245000 | 0.24375 | 316000 | 3.975 | 255000 | 0.3 | 317000 | 3.75 |
| 255000 | 0.35625 | 317000 | 4.05 | 260000 | 0.375 | *Crack arrested* | |
| 260000 | 0.5625 | *Crack arrested* | | 262000 | 0.4125 | | |
| 262000 | 0.61875 | | | 264000 | 0.46875 | | |
| 264000 | 0.65625 | | | 266000 | 0.5625 | | |
| 266000 | 0.7875 | | | 268000 | 0.675 | | |
| 268000 | 0.9375 | | | 270000 | 0.7875 | | |
| 270000 | 0.99375 | | | 272000 | 0.9375 | | |
| 272000 | 1.0875 | | | 274000 | 1.06875 | | |
| 274000 | 1.21875 | | | 276000 | 1.2 | | |
| 276000 | 1.29375 | | | 278000 | 1.2375 | | |
| 278000 | 1.35 | | | 280000 | 1.275 | | |
| 280000 | 1.4625 | | | 282000 | 1.3125 | | |
| 282000 | 1.51875 | | | 284000 | 1.425 | | |
| 284000 | 1.59375 | | | 286000 | 1.5 | | |
| 286000 | 1.725 | | | 288000 | 1.6125 | | |
| 288000 | 1.875 | | | 290000 | 1.6875 | | |
| 290000 | 1.96875 | | | 292000 | 1.8375 | | |
| 292000 | 2.0625 | | | 294000 | 1.9125 | | |
| 294000 | 2.1375 | | | 296000 | 2.1 | | |
| 296000 | 2.25 | | | 298000 | 2.175 | | |
| 298000 | 2.325 | | | 300000 | 2.2125 | | |
| 300000 | 2.3625 | | | 302000 | 2.25 | | |

# APPENDIX D

# ADDITIONAL SEM MICROGRAPHS

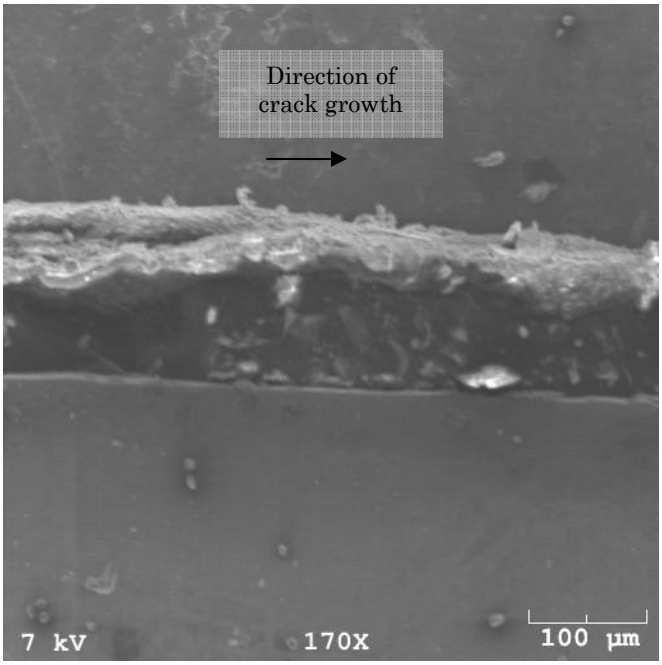


**Monotonic tensile fracture surface of 30 µm thick Al/Mg foil**

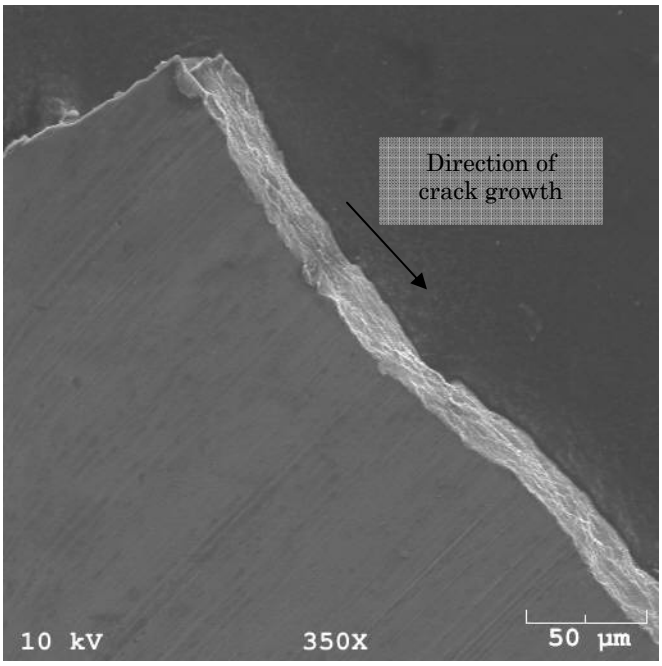


**Fracture toughness test fracture surface of 30 µm thick Al/Mg foil**

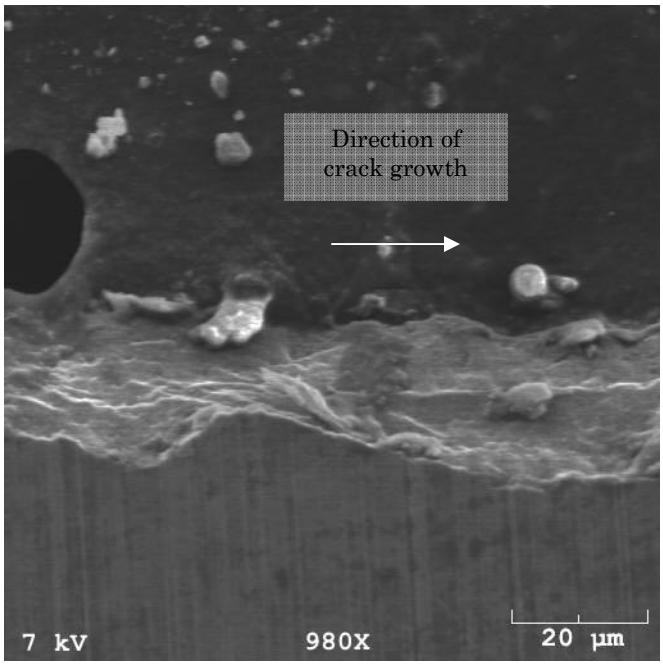


**Fatigue test fracture surface near notch of 30 µm thick Al/Mg foil**

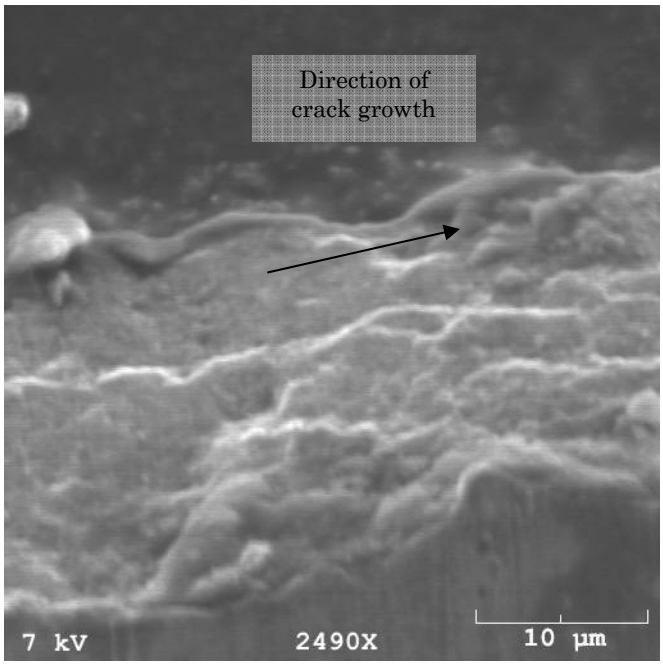


**Fatigue test fracture surface near notch of 30 µm thick Al/Mg foil**

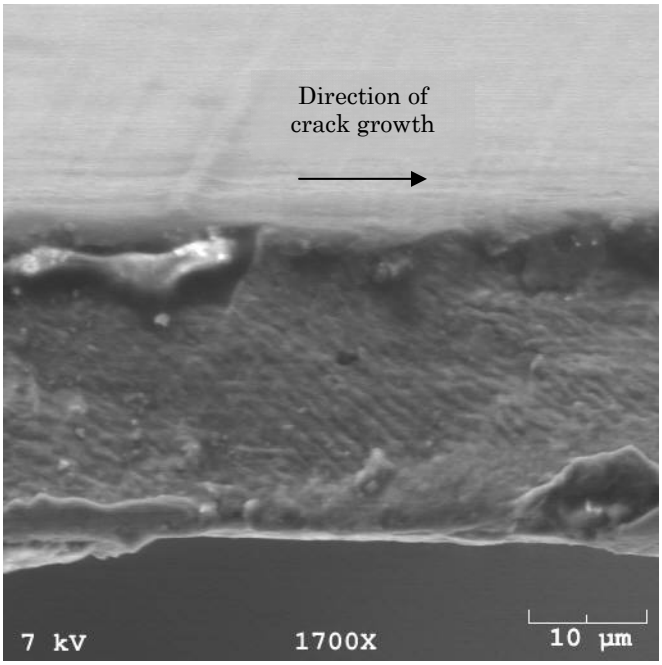


**Fatigue test fracture surface near notch of 30 µm thick Al/Mg foil, possible striation markings**

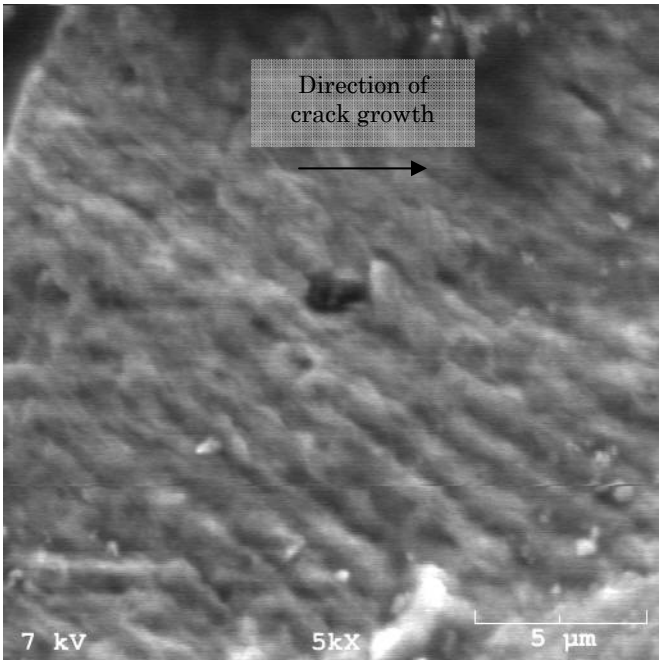


**Fatigue test fracture surface near notch of 30 µm thick Al/Mg foil, possible striation markings**

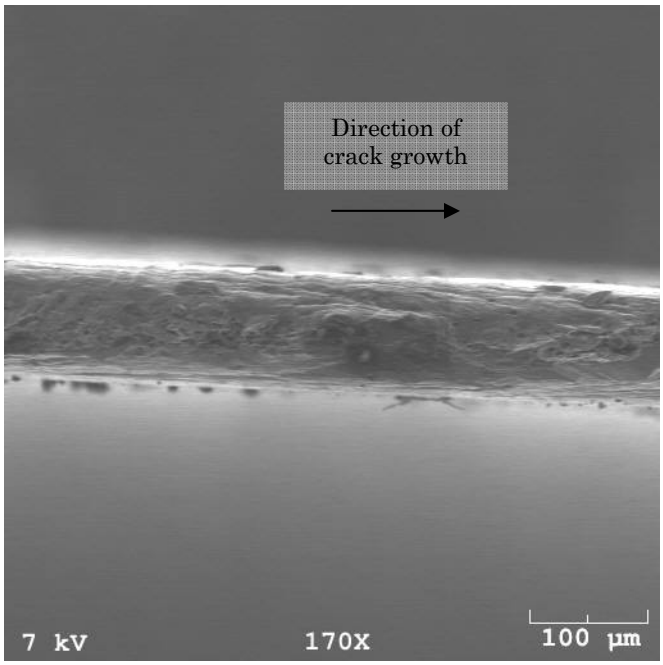


**Monotonic tensile test fracture surface of 100 µm thick Al/Mg foil**

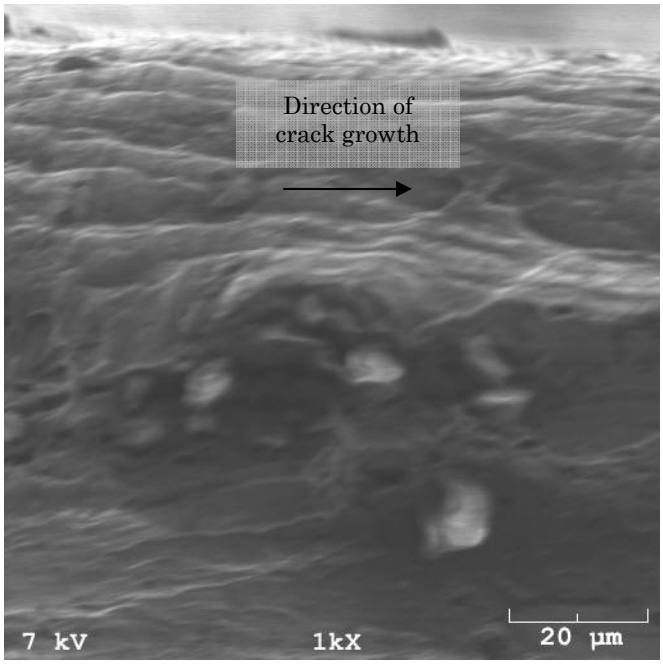


**Monotonic tensile test fracture surface of 100 µm thick Al/Mg foil**

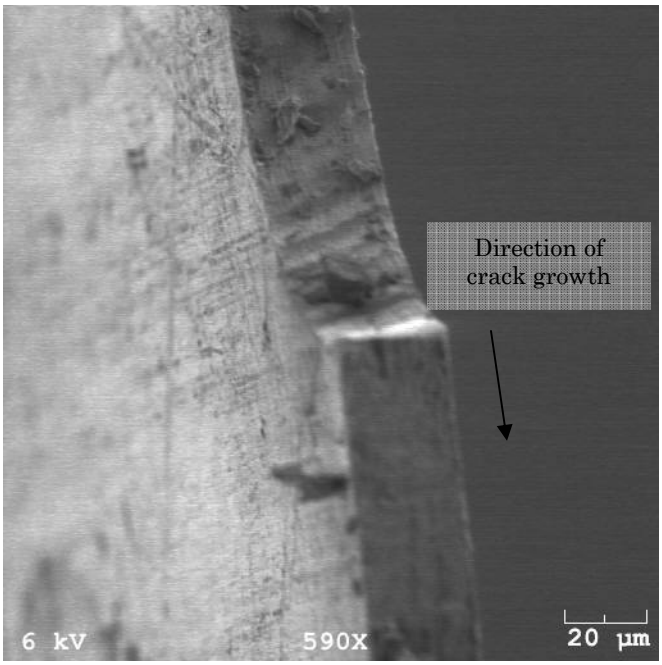


**Fatigue test fracture surface at notch edge of 30 µm thick Al/Mg foil**

# REFERENCES


[1] [Anon], Thermal Material Solutions, Aerospace Engineering 22 (2002) 27-29.

[2] C. Belhomme, M. Cassir, J. Devynck and G. Gregoire, Synthesis by a soft chemistry route and characterization of LixNi1-xO(0<x<0.5) compounds: Behavior in molten carbonates, Journal of Materials Science 35 (2000) 2683-2688.

[3] M. Blosser, Investigation of Fundamental Modeling and Thermal Performance Issues for a Metallic Thermal Protection System Design. 40th Aerospace Sciences Meeting & Exhibit, Reno, Nevada, 2002.

[4] M.L. Blosser, Advanced Metallic Thermal Protection Systems for Reusable Launch Vehicles. Mechanical and Aerospace Engineering, Vol. Doctor of Philosophy, University of Virginia, Charlottesville, 2000, p. 151.

[5] M.L. Blosser, R.R. Chen, I.H. Schmidt, J.T. Dorsey, C.C. Poteet and R.K. Bird, Advanced Metallic Thermal Protection System Development. 40th Aerospace Sciences Meeting & Exhibit, Reno, Nevada, 2002.

[6] D. Broek and J. Schijve, The Influence of Sheet Thickness on Crack Propagation, Aircraft Engineering 38 (1966) 31-33.

[7] J.R. Davis (Ed.), Metals Handbook, 2 edn., Vol. 2, ASM International, Materials Park, OH, 1998.

[8] J.T. Dorsey, C.C. Poteet, R.R. Chen and K.E. Wurster, Metallic Thermal Protection System Technology Development: Concepts, Requirements And Assessment Overview. 40th Aerospace Sciences Meeting & Exhibit, Reno, Nevada, 2002.

[9] J.T. Dorsey, C.C. Poteet, K.E. Wurster and R.R. Chen, Metallic Thermal Protection System Requirements, Environments, and Integrated Concepts, Journal of Spacecraft and Rockets 41 (2004) 162-172.

[10] N.E. Dowling, Mechanical Behavior of Materials, 2nd edn. Prentice-Hall, Inc., Upper Saddle River, 1999.

[11] H. Goldstein, W. Hoffman, W. Johnson and M. Smith, High-temperature Materials Go the Distance, Aerospace America 33 (1995) 32-35.

[12] Goodfellow, Al/Mg Technical Data, Material Properties. Goodfellow Corporation, www.goodfellow.com, March 5, 2005.

[13] W. Guo, C.H. Wang and L.R.F. Rose, The influence of cross-sectional thickness on fatigue crack growth, Fatigue & Fracture of Engineering Materials & Structures 22 (1999) 437-444.

[14] A. Hadrboletz, B. Weiss and G. Khatibi, Fatigue and fracture properties of thin metallic foils, International Journal of Fracture 107 (2000) 307-327.

[15] R. Hahn, S. Wagner, A. Schmitz and H. Reichl, Development of a planar micro fuel cell with thin film and micro patterning technologies, Journal of Power Sources 131 (2004) 73-78.

[16] K. Huang, P.Y. Hou and J.B. Goodenough, Characterization of iron-based alloy interconnect for reduced temperature solid oxide fuel cells, Solid State Ionics 129 (2000) 237-250.

[17] L.A. James, J.L. Straalsund and R.E. Bauer, Optimization of Fatigue-Crack Growth Testing for First Wall Materials Development Evaluations, Journal of Nuclear Materials 85 & 86 (1979) 851-854.

[18] J.-J. Jiang, An electrochemical investigation of sintered thick metal hydride electrodes for oxygen-metal hydride semi-fuel cell applications, Journal of Applied Electrochemistry 33 (2003) 101-106.

[19] M. Klein, A. Hadrboletz, B. Weiss and G. Khatibi, The 'size effect' on the stress-strain, fatigue and fracture properties of thin metallic foils, Materials Science and Engineering A319-321 (2001) 924-928.

[20] L. Liu and J.W. Holmes, An Experimental Technique for Elevated Temperature Mode I Fatigue Crack Growth Testing of Ni-Base Metal Foils, Journal Materials and Technology [Accepted] (2006).

[21] Q. Liu, J. Ding, F.K. Mante, S.L. Wunder and G.R. Baran, The role of surface functional groups in calcium phosphate nucleation on titanium foil: a self-assembled monolayer technique, Biomaterials 23 (2002) 3103-3111.

[22] M. Morra and C. Cassinelli, Organic surface chemistry on titanium surfaces via thin film deposition, Journal of Biomedical Materials Research 37 (1997) 198-206.

[23] D.E. Myers, C.J. Martin and M.L. Blosser, Parametric Weight Comparison of Advanced Metallic, Ceramic Tile, and Ceramic Blanket Thermal Protection Systems. National Aeronautics and Space Administration, Hampton, 2000, pp. 1-44.

[24] D.E. Myers, C.J. Martin and M.L. Blosser, Parametric Weight Comparison of Current and Proposed Thermal Protection System (TPS) Concepts. 33rd Thermophysics Conference, Norfolk, VA, 1999.

[25] C.C. Poteet, H. Abu-Khajeel and S.-Y. Hsu, Preliminary Thermal-Mechanical Sizing of Metallic TPS: Process Development and Sensitivity Studies. 40th Aerospace Sciences Meeting & Exhibit, Reno, Nevada, 2002.

[26] R.J. Puigh, R.E. Bauer, A.M. Ermi and B.A. Chin, Miniturized Fatigue Crack Growth Specimen Technology and Results, Journal of Nuclear Materials 103 & 104 (1981) 1501-1504.

[27] D.J. Rasky, F.S. Milos and T.H. Squire, Thermal Protection System Materials and Costs for Future Reusable Launch Vehicles, Journal of Spacecraft and Rockets 38 (2001) 294-296.

[28] N.J. Simms, R. Newton, J.F. Norton, A. Encinas-Oropesa, J.E. Oakey, J.R. Nicholls and J. Wilber, Degradtion of Fe-Cr-Al-RE and Ni-Cr-Al-RE foils in air and combustion gas atmospheres, Materials at High Temperatures 20 (2003) 439-451.

[29] D. Son, J.J. Kim, J.Y. Kim and D. Kwon, Tensile properties and fatigue crack growth in LIGA nickel MEMS structures, Materials Science and Engineering 406 (2005) 274-278.

[30] E. Vanswijgenhoven and J.W. Holmes, Fatigue Crack Growth in Inconel 718 Superalloy Foil at Elevated Temperature. Fifth International Special Emphasis Symposium on Superalloys 718, 25, 706, and Derivatives, Pittsburgh, PA, 2001.

[31] J. Williamsen, K. Mahrer, W. Bohl, J. Galbraith and R. Ahmed, Meteoroid/Orbital Debris Risk Assessment for Resuseable Launch Vehicles Using Metallic TPS. 44th AIAA Structures, Structural Dynamics and Materials Conference, Norfolk, Virgina, 2003.

[32] H. Zhu, S.V. Bhavani, R.T. Haftka and M. Blosser, Evaluation of Integrated Sandwich TPS design with Metal Foam Core for Launch Vehicles. 46th AIAA Structures, Structural Dynamics & Materials Conference, Austin, Texas, 2005.